

**A Precision Search for Exotic Scalar and Tensor Couplings in
the Beta Decay of Polarized ^{37}K**

by

Melissa Anholm

A Thesis submitted to the Faculty of Graduate Studies of
The University of Manitoba
in partial fulfillment of the requirements of the degree of

DOCTOR OF PHILOSOPHY

Department of Physics and Astronomy
University of Manitoba
Winnipeg

Abstract

The nuclear weak interaction is known to feature both vector and axial-vector couplings in a dominant role, however the presence of scalar and tensor couplings cannot be ruled out entirely. In beta decay physics, the Fierz interference, b_{Fierz} , is an observable comprised of a linear combination of scalar and tensor couplings, and can be measured as an adjustment to the shape of the resultant beta energy spectrum. A precision measurement experiment is conducted to observe the β^+ decay of spin-polarized ^{37}K from an atom cloud intermittently confined by a magneto-optical trap, and the beta energy spectra are observed in two detectors on opposing sides of the cloud, along the axis of polarization. This geometry, combined with a knowledge of the polarization, allows the superratio asymmetry to be constructed, providing an observable which is particularly sensitive to the value of b_{Fierz} , while simultaneously eliminating contributions from a variety of systematic effects. Geant4 simulations are used to model scattering effects that could mimic the signal being searched for. The resulting measurement gives $b_{\text{Fierz}} = +0.033 \pm 0.084(\text{stat}) \pm 0.039(\text{syst})$, consistent with the Standard Model.

Needs a more general sentence to start, and then needs to say what space these are 'vectors, ...tensors' in.

Georg's item 8:

The abstract in its current form comprises 186 words or so. The FGS regulations allow for 350 words maximum; I would encourage the author to make better use of that space – not the least in light of my earlier comments regarding the “big picture” and such.

Needs a sentence on why that's interesting.

Acknowledgements

People to acknowledge here include: John Behr, Gerald Gwinner, Dan Melconian.
Also: Spencer Behling, Ben Fenker, Alexandre Gorelov, James McNeil, Danny Ashery.

Contents

Abstract	ii
Acknowledgements	iii
Contents	vi
List of Figures	vii
List of Tables	ix
List of Abbreviations	x
Shit To Do	x
Note Color Legend	xi
Long Comments	xii
1 Background	1
1.1 Introduction	1
1.2 A Historical Look at Beta Decay	4
1.3 Draft of Intro Section	8
1.3.1 bullet points.	8
1.3.2 paragraphs	8
1.4 Beta Decay within the Standard Model	12
1.5 A Generalized Description of the Weak Interaction	14
1.6 Mathematical Formalism	16
1.7 Our Decay	18
1.8 The Shake-off Electron Spectrum	19
1.9 Fierz Interference – The Physical Signature	21

2 Considerations and Implementation of Atomic Techniques	25
2.1 An Overview of Magneto-Optical Traps	25
2.1.1 Zeeman Splitting	26
2.1.2 Doppler Cooling	27
2.1.3 Atom Trapping with a MOT	28
2.2 Optical Pumping	29
2.3 An Overview of the Double MOT System and Duty Cycle	30
2.4 The AC-MOT and Polarization Setup	33
2.5 Measurement Geometry and Detectors	36
2.5.1 Microchannel Plates and Electrostatic Hoops	37
2.5.2 Beta Detectors	39
2.5.3 The Photoionization Laser	40
3 Calibrations and Data Selection	43
3.1 An Overview of Available Data	43
3.2 Preliminary Data Selection with the rMCP	45
3.3 Calibrations with the rMCP	49
3.4 Measurements of the Atom Cloud	54
3.5 Electron Run Data Selection and Preliminary Cuts	57
3.6 Further Cuts Using the DSSD	59
3.7 Further Cuts Using the Scintillators	61
3.8 Timing Improvements with the Leading Edge and Scintillator Walk Correction	62
4 Simulations	66
4.1 Considerations for Software Upgrade Implementation	66
4.2 Simulations for the Ninety-eight Percent Branch and the Two Percent Branch	69
4.3 The Simple Monte Carlo and Response Function	70
4.4 Modeling the Scattering Effects from the Cloud	85
4.5 Simulating the Background and Time of Flight	88
5 Analysis and Estimates of Systematic Effects	93
5.1 Comparing Simulations to Experimental Data: The General Methodology	94
5.2 Evaluation of Systematic Effects	101
5.2.1 Beta Scattering	101
5.2.2 Detector Calibrations and Thresholds	102
5.2.3 The Atomic Cloud	105
5.2.4 The Response Function's Low Energy Tail	109
5.2.5 Background Events	109
5.2.6 Material Thicknesses	110

6 Results and Conclusions	111
6.1 Measured Limits on b_{Fierz} and A_β	111
6.2 Other Possible Future Work for the Collaboration: R_{slow}	115
6.2.1 Motivation	115
6.2.2 The Decay Process	116
6.2.3 Status of the R_{slow} Measurement	117
6.3 Conclusions	118
Bibliography	119
Appendices	126
A Statement of Contributions	126
A.1 Chapter 1	126
A.2 Chapter 2	126
A.3 Chapter 3	127
A.4 Chapter 4	127
A.5 Chapter 5	127
A.6 Chapter 6	127
B Notable Differences in Data Selection between this and the Previous Result	128
B.1 Polarization Cycle Selection	128
B.2 Leading Edge / Trailing Edge and Walk Correction	129
B.3 TOF Cut + Background Modelling	129
B.4 BB1 Energy Threshold	129
C Derivation of the Probability Density Function	130
C.1 JTW Formalism	130
C.2 Holstein Formalism	135
C.3 Qualitative Parameter Descriptions and Convention Compatibility .	141
D Notation	142
E SuperRatio	146

List of Figures

0.1	That exclusion plot from John	xv
0.2	New ^{37}K decay scheme	xix
0.3	A Fit From John	xxiv
0.4	A Slide From John	xxv
1.1	An exhaustive list of weak vertices	2
1.2	Beta Decay Feynman Diagrams	3
1.3	A level diagram for the decay of ^{37}K	19
1.4	Naive Beta Energy Spectrum and Superratio Asymmetry to Measure b_{Fierz}	22
2.1	Components of a Magneto-Optical Trap	29
2.2	The TRINAT experimental set-up, viewed from above	31
2.3	The 2014 duty cycle for transferring, cooling, trapping, and optically pumping ^{37}K	33
2.4	The AC-MOT and Optical Pumping Cycle	34
2.5	Diagram of the TRINAT Detection Chamber	38
2.6	A Photo from Inside the TRINAT Detection Chamber	42
3.1	Timing sums for the rMCP, run 447.	47
3.2	Cloud Position for run 447 for various rMCP timing sum cuts	49
3.3	rMCP Calibration	52
3.4	Photoion Hit Positions in 2D	53
3.5	Photoion Hit Positions at 535 V/cm, as a function of AC-MOT Time	56
3.6	LE and TE Timing Peaks	63
3.7	SOE TOF Walk and Correction	64
3.8	Experimental Scintillator Spectra	65
4.1	Fit to Mono-Energetic Spectrum, 5000 keV	76
4.2	Fit to Mono-Energetic Spectrum, 3000 keV	77
4.3	Fit to Mono-Energetic Spectrum, 1500 keV	78
4.4	Fit to Mono-Energetic Spectrum, 1000 keV	79
4.5	Fit to Mono-Energetic Spectrum, 750 keV	80

4.6	Lineshape Parameter Fits (Part 1)	81
4.7	Lineshape Parameter Fits (Part 2)	82
4.8	Lineshape Parameter Fits (Part 3)	83
4.9	Lineshape Parameter Fits (Part 4)	83
4.10	Goodness of Fit for Modeled Response Functions	84
4.11	Simulated Beta emission angle w.r.t. the detector vs adjusted SOE–Beta TOF	88
4.12	(SOE–Beta) TOF	91
4.13	Averaged Superratio Asymmetry by TOF	92
5.1	SetB Superratio Asymmetry	95
5.2	SetC Superratio Asymmetry	96
5.3	SetD Superratio Asymmetry	97
5.4	χ^2 Map for Runset B	98
5.5	χ^2 Map for Runset C	99
5.6	χ^2 Map for Runset D	100
5.7	Scattering Effects in the Asymmetry	102
5.8	Response Function Comparison	106
5.9	A_β Position Error	107
5.10	b_{Fierz} Position Error	108
6.1	χ^2 Map for All Data	112

List of Tables

1.1	Dirac Matrix Operators	10
3.1	List of Electron Runs	44
3.2	List of Recoil Runs	44
3.3	Cloud Position and Size	55
5.1	Scintillator Calibrations	103
6.1	Error Budget	113
D.1	Kinematic Terms Guide	143
D.2	Angular Momentum Notation	143
D.3	Multipole Notation	144
D.4	Selected Integrals from Holstein's Eq. (51)	145

List of Abbreviations

AC-MOT	alternating current magneto-optical trap	xviii
BSM	beyond the standard model (of particle physics)	
DC-MOT	direct current magneto-optical trap	
JTW	Jackson–Treiman–Wyld [1][2]	130, 134
MOT	the regular-est trap	xviii
OP	optical pumping	
PDF	probability density function	130
SM	standard model of particle physics	1
SOE	shake-off electron	

9. The thesis would benefit from a list of abbreviations.

Must refine this list of abbreviations before I hand it in!

A Note Color Legend!

A Note Color Legend!

Tag for stuff that has to be made to at least *look* presentable before submitting.

Default notes to self.

Organizational comments.

Stuff I don't actually understand.

Round 1 comments from John.

Comments from John – new round!

Comments from Gerald.

Comments from Georg.

Stuff that's fucking done.

Notes that may have started here, but aren't relevant here, so their content has been moved elsewhere, where I'll actually pay attention to it.

End Legend

...

Long Comments

Do everything in the giant list of giant-comments.

From Gerald:

...

Hi Melissa,

...

Attached is the report by Georg. It contains many valid points, and even for those where I'm not fully on board, it's clear that this has to be addressed. To be clear: This is not really that big of a deal. The actual work is not questioned in any way, and that's of course the really relevant part in the end. But it does have to be framed within a context, especially for the non-experts. I should have probably called off things like the handwritten appendix earlier, but thought that the committee members would ask for that in passing (on the basis that everything in the thesis must stand on its own, which those personal notes arguably don't; if this is relevant, it should be typed up).

...

I will write to the other committee members and call off their effort on this version, because Georg already won't sign off on it, so there is not point for them to go through it, as they most likely will agree with his points.

...

The course of action will now be for you to address these issues and then we'll resubmit.

...

I'm not entirely sold myself on a full "Standard Model intro" in the sense that the beta decay work stands on its own, and can be told as its own story. This is reflected by the fact that JTW predates the SM and is still fully relevant. So I'd go a somewhat light SM exposure. The most important goal is to make the non-experts comfortable in introducing what this is all about.

...

This will also bolster the citation count, which indeed looks suspiciously low (even though I'm not keen on such bean counting arguments).

...

Gerald

John's suggestions for fixing the stuff that Georg wanted fixed – that giant email. Moved to somewhere in Chapter 1.

...

hi Melissa,

Gerald will soon send good clear corrections from a committee member. It will be clear you need to address those, and it will be clear what to do.

Please read those first, and start answering them. Maybe then (and only then!) you will find two suggestions useful:

From John, moved to the beginning of Ch. 1

i) Among the necessary technical corrections, there's a solid request for more background info. I think you know what to do.

...

A large thing is some kind of extra qualitative description of what the SM is. You could do that qualitatively without any trouble.

...

You might point out some part of this:

- the charged weak interaction you're writing down predates the Weinberg-Salam model by more than a decade. The version you've written down assumes protons and neutrons are fundamental particles.
- The exchange boson is much heavier in mass than the energy and momentum in the decay, so it can be approximated by an interaction with zero range.
 - Fermi did that very early on,
 - and Gamow and Teller added a process that change the nucleon spin.
 - Lee and Yang, which you cite, added the possible currents with different Lorentz transformations (do you mention that since any further combination of Dirac matrices can be reduced to these, so they span the space), and the possibility of parity violation by writing out helicity projections for the leptons. I.e. Lee and Yang assumed some fields (the nucleons and leptons) and a general interaction preserving the symmetries of the theory, which by definition is then an effective field theory.
- Feynman and Gell-Mann's 1958 paper is the one that postulated V-A, again a decade before Weinberg-Salam, and they did this by making analogies between the boson exchanged and the photon, i.e. an analogy between the charged weak interaction and the electromagnetic current, so you could cite them instead of saying "SM predicts everything"

People had assumed there was a massive boson exchanged for a very long time.

What Weinberg (and, independently, Salam) did was come up with a consistent mathematical theory of massive bosons, incorporating Yang Mills gauge theory (looks like E&M but with non-abelian operators) to do that, and the result was the weak neutral interaction prediction.

ii) Similarly, answering how the results fit into the bigger picture is what you wanted to do.

...

I'm convinced that you don't want to do a full review of all beta decay experiments.

...

But you could say the Fierz term has been constrained by the energy spectrum and by the energy dependence of the beta asymmetry, cite the best paper in the neutron and maybe the UCNA one as well, and use that figure I sent (I'm sending the improved version).

...

It is a good approximation to linearize the situation, i.e. this figure is good for small Cs and Ct. (A similar approach is being used in a letter coming out soon, and 3 referees did not nag them about it.)

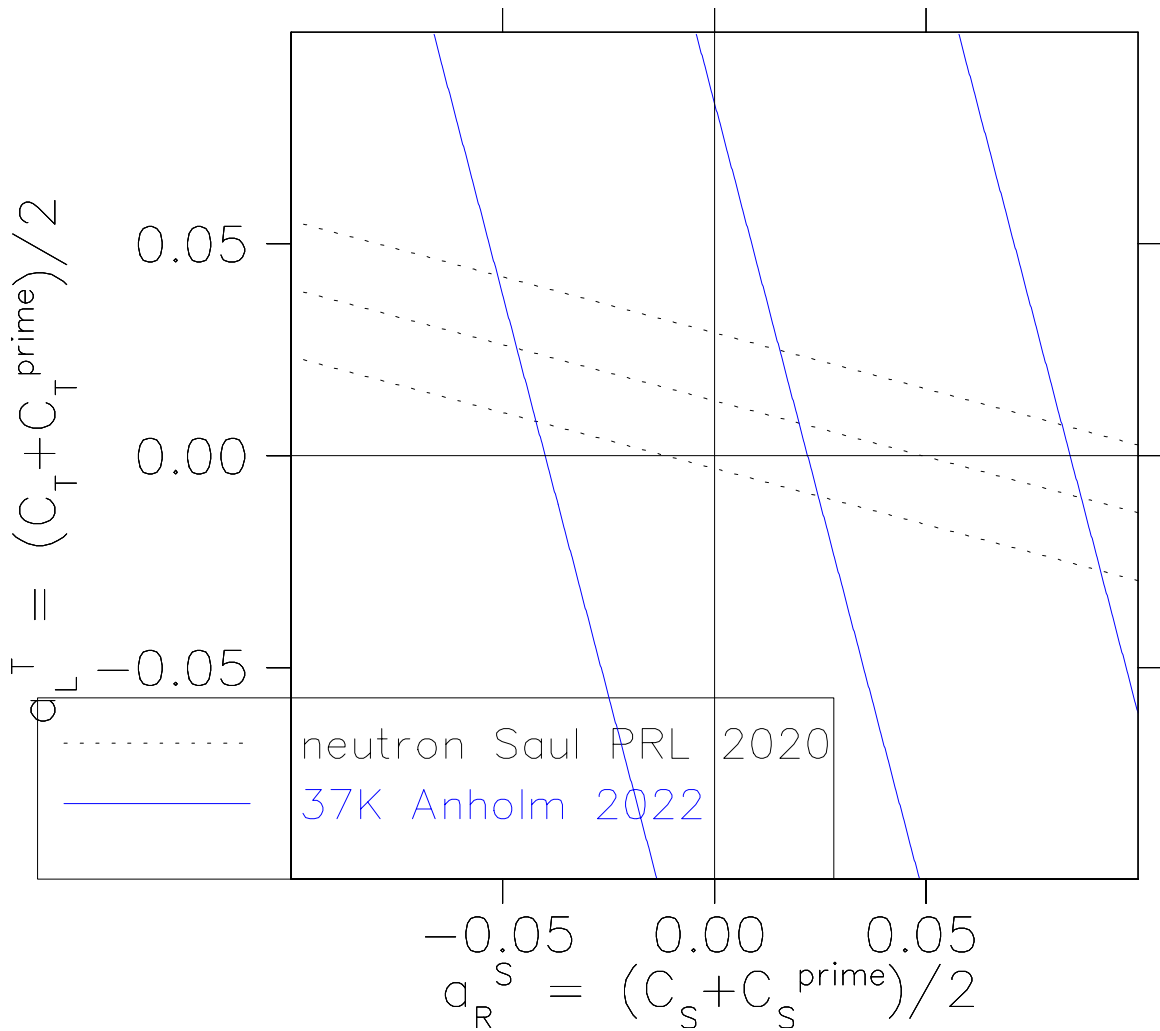


Figure 0.1: That exclusion plot from John. I think he means " $C_S - C'_S$ ", etc.

Immediate follow-up email from John:

...

another basic big point. What would it mean if there were nonzero Cs, Ct?

In the context of the more elegant SM, a theory of quarks and leptons and mathematically consistent interactions, that would imply the existence of at least one extra unknown exchange boson. The mass would not be measured, just its coupling strengths to the particles participating in the beta decay.

...

Maybe background to understand that includes:

If one were to write the SM weak interaction, C_A and C_V and C_A and $C_V g_A$ would all be constants with abs value 1. The (1+- gamma_5)'s are projection operators– in the SM, the W boson only couples to left-handed nu's and right-handed antinu's

('more will be said in the forward-looking Ch. 6.2 about tests of that part.)

So all the known information about Ca and Cv is accounted for.

($g_A = 1.26$ for the neutron... it's not equal to 1 because of strong interactions between the quarks in the neutron.)

From Georg Schreckenbach:

Re: Melissa Anholm, Ph.D. thesis, version April 18, 2022

In response to your request for pre-evaluation of Melissa Anholm's Ph.D. thesis, dated April 18, 2022, I believe that the thesis in its current form is *not* ready for distribution.

In my view, the following are critical problems:

1. 1. The thesis in its current form is completely missing any embedding into a “bigger picture”. This would be the task of the Introduction chapter primarily, but should also significantly permeate other parts such as, notably, the conclusions. One could phrase this in the form of questions, including – but certainly not limited to – the following:

- - What is the Standard Model?
- - Why are we even searching for “physics beyond the standard model”? Why is there a need or desire to do so?
- - What other efforts have been or are being made to search for physics beyond the standard model? Have any of them been successful? If so – or if not, what does this mean?
- - Closely related to the previous question, how does the current work fit into this overall effort? What is the unique contribution here?

Etc.

2. 2. These aspects should be picked up in the Conclusions. What do the results mean for the “big picture”? Again, how do the fit in with the other efforts, prior, concurrent, or planned? Etc.

3. 3. As an outsider, it is my understanding that the author worked as part of a larger collaboration. It would be beneficial to clearly lay out what her unique contributions are. This could be done, for instance, in the Introduction, and/or the Conclusions.

4. 4. Formulas and symbols contained in these need to be defined, as do symbols that appear in the text. Currently, this is only done partly. It starts right at the beginning with Eq. 1.4 (formerly 1.1) and continues throughout. Sure, one can of course guess the meaning of the symbols in Eq. 1.4 – but one should not have to guess! – and this is certainly not true for later equations. (For instance, I have no idea about the meaning of most of the symbols in Eq. 1.12 (formerly 1.9), to give but one example.)

5. 5. Similarly, several figures need better explanations, starting with Fig. 1.1. Which, btw., also needs a source attribution (unless it was created by the author) and, presumably, a copyright note. Similar comments apply to various other figures as well.

6. 6. At first glance, I find a bibliography that contains only 28 entries to be problematic for a Ph.D. thesis. This goes, to some degree, back to my earlier points about embedding the work in the “bigger picture” – doing so would necessarily lead to several additional references – but it might be more than that.

7. 7. Appendix C, adding scanned pictures of handwritten notes as figures that, moreover, seem not to be referenced at all, is – well – problematic. I don’t think that it conforms to the instructions as per Supplemental Regulations either (though I did not explicitly check).

...

Given these various issues, I have not fully read the thesis in detail; I have instead focused on the question at hand: what is needed for the thesis to be in a form that can be distributed? I will provide a more formal report on the version of the thesis that I will receive from FGS.

...

Besides, there are some additional points that I would suggest for modification but that do not, in my mind, prevent distribution. These include:

See: the abstract, which I apparently can’t link to directly.

8. 8. The abstract in its current form comprises 186 words or so. The FGS regulations allow for 350 words maximum; I would encourage the author to make better use of that space – not the least in light of my earlier comments regarding the “big picture” and such.

9. 9. The thesis would benefit from a list of abbreviations.

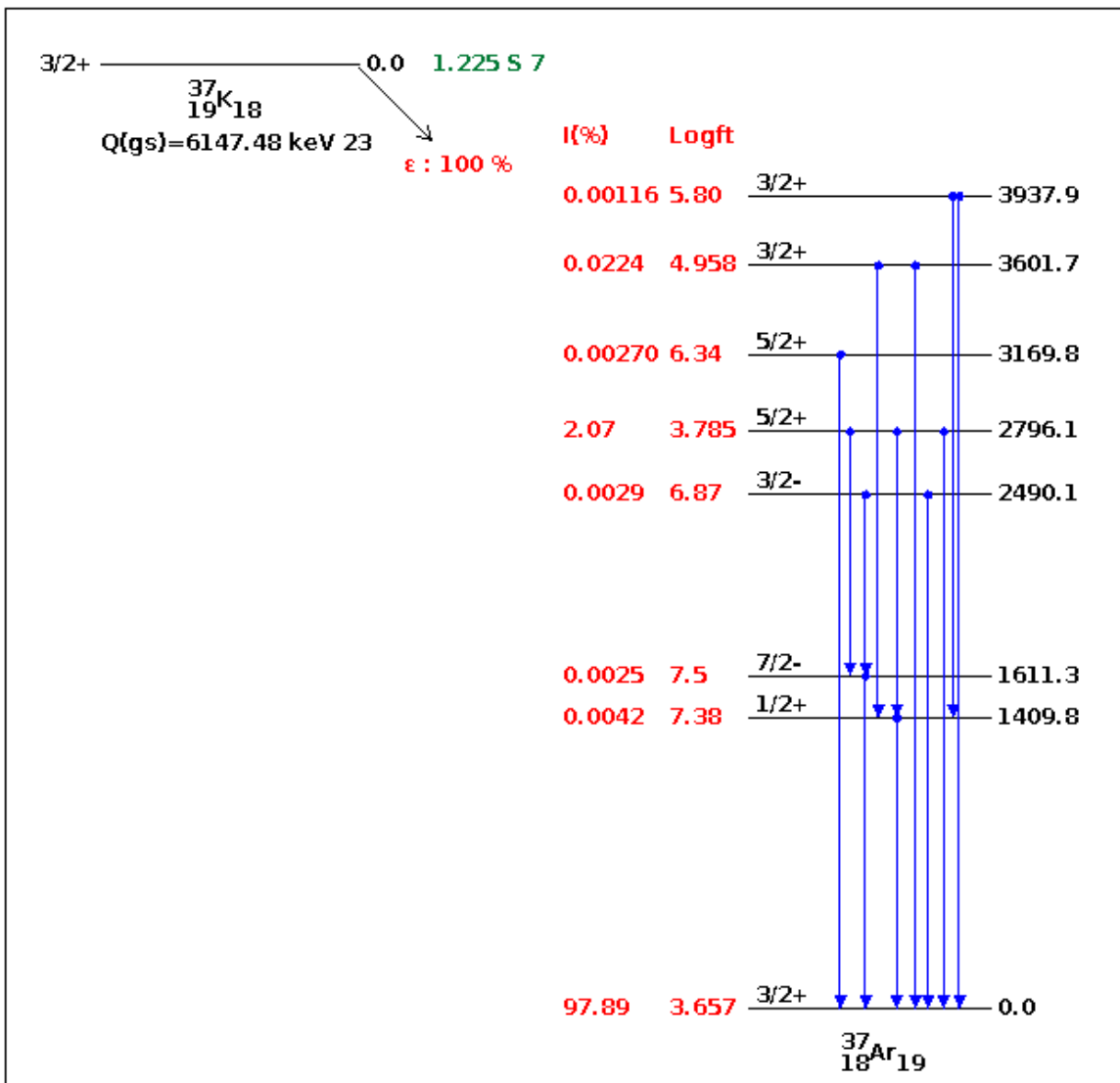
Consider the magneto-optical trap (MOT). Consider, next, the alternating current magneto-optical trap (AC-MOT). But wait, what was a MOT again?

10. 10. P. 93 contains a reference to “Figure ??”

11. 11. Likewise, p. 98, a reference to “Ch. ??”, as well as a reference to “our recent PRL article” – the latter needs to be referenced properly!

See over here: ??

12. 12. I have no idea what the title of Appendix B means. It is for sure original and even funny though ... Also, the actual appendix title in the thesis is not the same as that listed in the TOC.



Authors: John Cameron, Jun Chen and Balraj Singh, Ninel Nica.

Citation:Nuclear Data Sheets 113, 365 (2012)

...

Also, it's generated by the page from: National Nuclear Data Center (NNDC) at Brookhaven National Laboratory. Possibly from the NuDat3 database.

Figure 0.2: A newer, better, less generated-by-Dan level diagram for the decay of ^{37}K .

Suggestions from John on listing my contributions that need to be mentioned and/or general stuff that needs to be mentioned:

Georg wants you to list your contributions in the intro, good.

...

First, in Section 2.4 the sentence after Harvey and Murray are referenced could be "There are some details of the present implementation of the AC MOT in Ref. [3], done with a separate MOT geometry from this beta decay work."

(Presently your thesis is Ref. 14, which is only cited so far for Fig. 2.1)

...

*you need a subsection in Section 2.4 "The AC-MOT and Polarization" on your field trimming.

...

Time-constant ambient fields were trimmed in all dimensions using two horizontal pairs of Helmholtz coils and the AC MOT coils for the vertical direction. These ambient B fields were first trimmed to be near zero using a giant magnetoresistance 3-axis probe at the trap center, with the MCP assembly removed and the vacuum chamber up to air.

...

Final trimming was done by optimizing polarization of stable ^{41}K atoms with the apparatus assembled (cite[Fenker PRL Suppl Mat] has some details).

...

The AC MOT and polarization B fields were generated by SRS DS345 arbitrary waveform generators, amplified by Matsusada bipolar 20 KHz bandwidth 80A 20V amplifiers. The waveforms were carefully trimmed in amplitude and time to minimize B fields from eddy currents during the optical pumping cycle, again with the MCP assembly removed and the vacuum chamber up to air.

...

The bipolar amplifier bandwidth was inadequate when using current control mode, so voltage control had to be used, a much more time-exacting process requiring empirical iteration. These waveforms are not the same for the top and bottom coils, as during the optical pumping cycle one coil had to be flipped with respect to the MOT cycle to create the uniform vertical field for optical pumping by a Helmholtz rather than antiHelmholtz configuration.

The beta detector full assemblies were in place during the field trimming.

...

All materials near the trap cloud are chosen to minimize both magnetic permeability to suppress time-constant B field gradients and conductivity to suppress eddy currents. E.g., the E field electrodes are made from either glassy carbon semiconductor or titanium alloy. A copper ring (not pictured in Fig. 2.5) with a slit mounted on each beta detector stainless steel reentrant flange suppresses the worst eddy currents fighting the B field along the z-axis. These designs were all confirmed by finite element calculations of another collaboration member.

I think you've neglected where the fT value and prediction for Abeta come from, entirely, and still don't have an equation for b_Fierz in terms of Cs and Ct.

...

You had a note to do this, and in desperation I encouraged you to leave it out. I was wrong and Georg is right– the whole SM prediction for Abeta makes no sense this way, and something about it needs to be there.

...

there are two ways to add a dedicated section in ch 1:

- i) by writing the equation for the rate in terms of Vud and rho (the G-T matrix element over Fermi squared), and saying Shidling et al. gets rho from that by assuming Vud from the 0+ to 0+ decays. (You had a note "Do the master equation!" which I think I said you needed to leave out, but I was probably wrong.) But then you have to define all the small corrections, which is a lot of physics.
- ii) Write the SM equation for Abeta in terms of rho, to give you the SM prediction for Abeta. State that recoil order corrections are in Appendix X. (If that's now a collaboration note? cite that there are recoil corrections considered in Appendix X-1 and a collaboration note).
- iii) Such a section would then naturally end with b_Fierz in terms of Cs and Ct, a natural followup to what you've written.

"JTW does the Dirac matrix traces necessary to write down the decay rates in term of the Lee-Yang Lagrangian's parameters. The prediction for b_Fierz is " " which is zero in the SM." **even with recoil-order corrections** (there is no recoil order correction with the same m/Ebeta dependence).

Then and only then will the final addition of the bFierz plot will make sense.

OR, more likely:

leave out i).

Say in text that Shidling et al. (I've added the reference in a sticky note for the figure) hands you rho (the M_{GT}/M_F ratio prediction) using as input the absolute rate, Vud from the 0+ to 0+ beta decays, and calculations of isospin mixing and radiative corrections (cite[shidling]) for details beyond the scope of this thesis. The sign of rho comes both from a shell model by Ian and by if it were flipped Abeta would be off by an enormous factor.

...

Then you would just need **ii and iii**.

As a reward for reading this far, I'll admit I wrote the bFierz m/E dependence wrong in the sticky notes in ch 1, sorry.

first, actually, Ben writes a good summary of F_t mirror equation in terms of F_{t0+} to $0+$ in the PRL, you could just use that in Ch. 1 and it would help enormously. (Of course now I'm scared because it doesn't mention isospin mixing is different for 37K and the others, and that should be in the numerator as (F_{t0+}/F_{t37K}) well as in rho, shouldn't it? I would need to compare to Shidling's expressions to sort this out.)

I said F_t wrong. I think you must know what to do.

F is the lepton phase space integral.

$(\text{Decay rate})/F$ is then a dimensionless quantity proportional to $|\text{matrix element}|^2$, which you could call the intrinsic strength of the transition.

People instead consider the inverse quantity denoted F_t defined as $F^* t_{1/2}$, so if $\log_{10}(F_t)$ is smaller, the strength is larger.

...

So e.g. $t_{1/2}$ is wildly different for the $0+$ to $0+$ decays ($t_{1/2}$ for ^{14}O is a minute, not a second like 38mK) but once you correct for the wildly different phase space (the Coulomb energies and therefore the decay Q-value smoothly grow, and phase space goes like Q^5) the F_t rates are close (closer once percent corrections from isospin mixing and nucleus-dependent radiative corrections are applied).

...

(That equation is fine— I was confused earlier.) You can mention that $\text{script}F_t$ has isospin-breaking and other theory corrections beyond the scope of the thesis, and cite Shidling for those. This equation, along with the Abeta equation in terms of rho (you should not include the right-handed currents in Ben's Abeta equation and re-state that your thesis is working on scalar and tensor in your title) then sets up the inputs you need for the Abeta prediction.

Chapter 2 corrections from John:

all of these are trivial except the last, which counts as a glaring omission.

- *section 2.1.3 "using a Helmholtz coil" add "but with currents in opposite direction." (saying it correctly here then implicitly defines anti-Helmholtz which you use correctly later for the AC MOT)
- *It would be simplest to write down what you mean by a quadrupole field. You could say: "approximately in our geometry near the trap center
$$\vec{B} = 2B_o z\hat{z} - (B_0 x\hat{x} + B_0 y\hat{y})$$
- *section 2.4 near end "divergencelessness" is not a word. It's obvious how to fix it "since del dot B =0 in a current-free region..."
- 2.5.1 "roughly" -> "approximately" The Efield is not rough at all, it's pretty good really. Is the rMCP really just a 2-plate chevron in 2014? I don't remember. Why can't I find Ben's thesis?
- *2.5.1 state clearly in an extra paragraph at the end that the polarization-determining data was taken with the rMCP, while the Abeta and bFierz data were taken with the eMCP. The polarization was assumed to be the same during the Abeta+bFierz data. This is backed up by constant 41K polarization data for weeks of optimization, with all optical pumping and B field switching parameters kept constant. Ambient magnetic field changes of 50 milliGauss could cause some polarization perturbations at the precision achieved, yet the stray fields are under control at that level. The TRINAT lab is in a basement well-shielded from the experimental hall by concrete with rebar, and though 50 mG fields are seen in that Hall from an open Helmholtz ion trap, they and the 5-ton crane produce negligible fields when measured at the atom trap. The cyclotron field makes 0.5 Gauss, predominantly vertical, and a smaller horizontal component, but trim Helmholtz coils at TRINAT are adjusted during calibrations with cyclotron on vs. off, and of course the cyclotron is on with constant field during the 37K delivery.
- ***You don't state the polarization achieved 99.1 ± 0.1 percent anywhere that I can see., citing the publication.** You might also state that's important for Abeta but has much more precision than needed for the near-zero bFierz term.

...

You mention the polarization is different by approximately 0.3% in Section 6.1 from the cut, but never say what P is.

...

Appendix A has ?? for a discussion of the changes of the polarization cut, so you need to clean up that ???. It is presently in Section 6.1.

Another Round of Thoughts from John!

...

Fitting Ben's data (using for the bFierz function my convolution of 1/E with a Clifford tail) as I've shown before, compare what happens if I let Abeta float, or if I then fix Abeta arbitrarily to that floated value.

That's not a well-motivated thing to do on its own, but it's not that much different than using Abeta[Cs²,Ct²] constrained by Ft[Cs²,Ct²] since that's only dependent on squares of small quantities.

...

So I would expect the ability to extract Cs and Ct from the 37K data to have more sensitivity if Abeta[Cs²,Ct²] and Ft[Cs²,Ct²] and bFierz[Cs,Ct] are floated together in a 2d fit rather than floating Abeta and bFierz without any theoretical constraints and then considering getting linear combinations of Cs and Ct from the bFierz value.

...

Note that my simply fixing Abeta lowers bFierz uncertainty by a factor of 3. I expect similar improvement in sensitivity to Cs and Ct.

...

(Here I'm using Cs as a stand-in for (Cs+Cs')/2 for simplicity)

```
ASYMNORM          0.98878          8.03416E-03  8.01756E-03
BFIERZ           -6.36573E-02    4.35364E-02  4.34464E-02
Iter&      BFIERZFIX Residual   Step Size
 1  -6.366E-02  40.8     1.00
 2  -6.366E-02  40.8     1.00
number of degrees of freedom = 42
total CHISQ = 40.8306557
sqrt( CHISQ/point ) = 9.7444863E-01
CHISQ/(degrees of freedom) = 9.72158468E-01
confidence level = 52.224923%
PARAMETER          VALUE          E1          E2
BFIERZFIX        -6.36573E-02  1.24867E-02  1.23117E-02
*** ERROR in expression evaluator
```

Figure 0.3: A Fit From John, or something. idk, it goes with the text immediately previous.

More thoughts from John:

...

hi Melissa,

...

I think you should keep Section 6.2, but I think it would be clearer to point out the observable manifests as a dip in the raw TOF spectrum, not going all the way to zero as in the ideal on-axis situation you describe for simplicity. I.e., I would say you need to qualify this "exactly" word (emphasis mine below), and since it ends up as a $\cos(\theta)$ distribution like in my attached slide on the subject, your figure of the TOF spectrum would be a good way to do that.

...

"Henceforth, daughter nuclei from a back-to-back decay as shown in Figure ?? will be described as 'slow' recoils. In terms of observables, this means that if the electric field is configured to point along one of the axes perpendicular to the polarization direction, then when the recoiling ion is swept away into a detector, the slow recoil's hit position should be **exactly** along the projection of the polarization axis. Furthermore, the slow recoil's time of flight should be in the middle of the time of flight spectrum, since other recoils will be emitted with momentum towards or away from the detector"

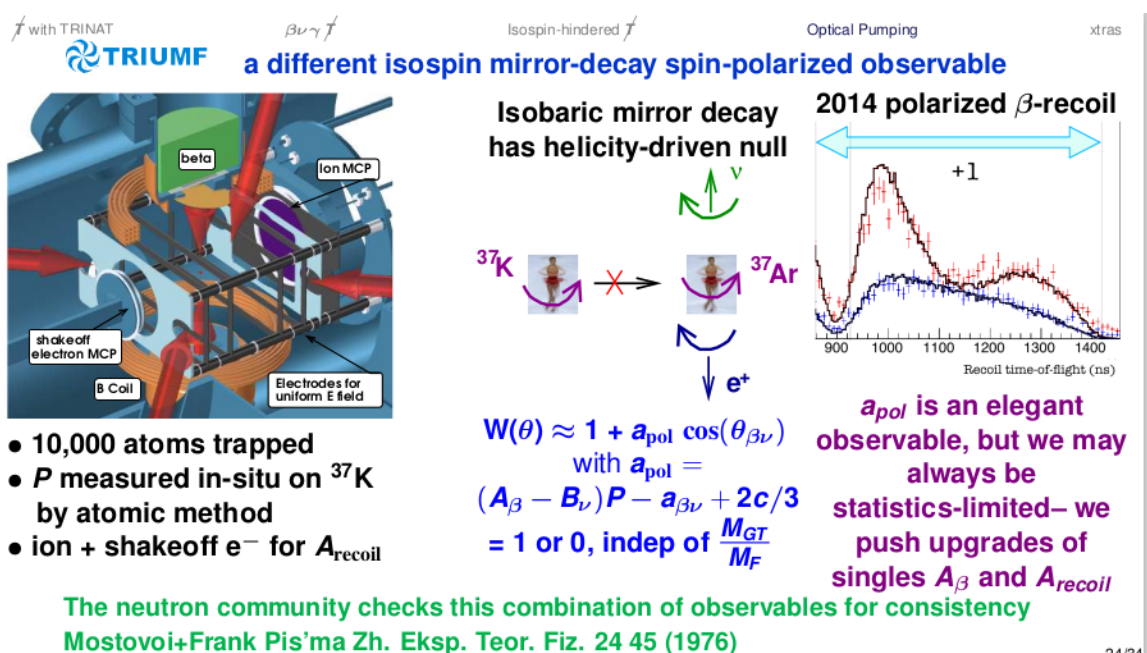


Figure 0.4: A Slide From John, or something. idk, it goes with the text immediately previous.

Old Notes!

JB on intuitive concepts that are missing (are they *still* missing?!?):

The SM couples to left-handed neutrinos and right-handed antineutrinos. Since the neutrinos only have weak interactions, there are no right-handed nu's nor left-handed antinu's in nature. The neutrino asymmetry B_ν is a number with no energy dependence.

Similarly, the SM weak interaction only couples to right-handed positrons and left-handed electrons. Since these are massive particles, the average helicity of positrons is not 1, but instead v/c . One can always boost to a frame where the positron keeps its circulation but is moving in the opposite direction. This is why the beta asymmetry is $A v/c$, not just A .

The Fierz term's additional energy dependence of m/E also comes from helicity arguments, stemming from the fact that it still is coupling to SM nu's and antinu's only, so the beta's are generated with wrong handedness.

The details are built at 4th-year undergrad level in Garcia's paper with his student and post-doc [4].

I have legit just deleted a section in Ch.6: "Relation to Other Measurements and New Overall Limits". It's gone now. Because it was stupid. Only John's comments about what it might do in the future remain.

JB on Ch. ??: "Relation to Other Measurements and New Overall Limits"

6.3 might be better left to a collaboration memo. You have to decide what to do here, and decide it quickly.

...

I already gave you the latest Perkeo Fierz paper, and the info that we are relatively less sensitive to tensor by by the ratio of $Mgt^2 = 3/0.6 = 5$.

...

so if you make a linearized exclusion plot of tensor vs. scalar as straight lines with the uncertainty of bFierz, using Perkeo and your result, you will see even with 0.09 uncertainty you compete with them on the scalar limit.

...

(However, see attached figure from my article with Alexandre on 38mK's beta-nu scalar limit. I think the constraints on Lorentz scalars are hard to compete with.)

JB says: To put your work in context, please add at the end of that minimal S,T section, or at the end of "Our Decay" section

...

The best existing measurement of b_{Fierz} is in the decay of the neutron [5], $b_{\text{Fierz}} = 0.017 \pm 0.021$, consistent with the Standard Model prediction of zero. Our measurement is strongly related, yet complementary. In terms on non-Standard Model Lorentz current structures, to lowest order in the non-SM currents the same equation applies:

$$b_{\text{Fierz}} = \pm (C_S + C'_S + (C_T - C'_T)\lambda^2)/(1 + \lambda^2)$$

(the plus is for β^- decay and the - for β^+ decay) [1]. [to be continued...]

[...continued from prev.]

In our ^{37}K case, $\lambda^2 = |M_{\text{GT}}|^2/|M_F|^2$ is close to 3/5 (the expected value $j/(j+1)$ for a single $j=3/2$ d3/2 nucleon) [6], while for the neutron λ^2 is close to 3 (the expected value for an $(j+1)/j$ $j=1/2$ s1/2 nucleon). $|M_F|$, the Fermi matrix element, is nearly the same for both of these isospin = 1/2 decays (the largest correction is the larger isospin mixing of ~ 0.01 in ^{37}K). So our observable is relatively less sensitive to Lorentz tensor currents, and will predominantly constrain or discover Lorentz scalar currents.

...

Full considerations would require a weighted fit of b_{Fierz} experiments and similar observables [7], and are beyond the scope of this thesis. The info from this thesis, values of A_β and b_{Fierz} with their uncertainties, can together with the known fT value (lifetime and branching ratio) allow the community and/or the collaboration to include the results in a future constraint or discovery of scalar and tensor Lorentz currents contributing to β decay.

End of John's comments on the section I deleted.

Chapter 1

Background

1.1 Introduction

Within our present understanding of physics, there are four fundamental forces governing the interactions of particles with one another: electromagnetism, the nuclear weak force, the nuclear strong force, and gravity. These forces are considered to be distinct from one another by virtue of their differing behaviours, however attempting to unify them within a single theoretical framework has been a major focus of later 20th- and early 21st century physics to date. The effort has been met with only partial success, and the resulting theoretical framework is collectively known as the standard model of particle physics (SM).

The standard model provides a quantum mechanical description for the behaviour of three of the four fundamental forces: electromagnetism, the nuclear weak force, and the nuclear strong force. The SM notably does not describe gravitational processes — despite extensive efforts, the gravitational force has thus far defied all attempts to describe it in a fully quantum mechanical way, though this remains an active field of research.

Each force has its own specific mediating particle(s) which couple only to a particular type of (generalized) charge, and therefore interact only with particles that possess that charge. For example, the gravitational charge is *mass*, and (at least within a simplified particle physics model) gravity acts only on objects that possess mass. With only a single type of charge and no negative masses, the gravitational force can only ever be attractive. By contrast, the electromagnetic force couples

Can I turn this into a footnote? It's not true because the curvature of spacetime also affects photon trajectories, and there even exist (unstable) (quasi-?) bound states comprised *only* of photons, as in e.g. Aichelburg-Sexl.

to both positive and negative electric charges, and can produce both attractive and repulsive forces. Both the electromagnetic and gravitational forces are mediated by massless force-carrying particles (the photon and still-theoretical graviton, respectively), a property which implies that the amount of flux per unit solid angle is constant over all distance scales, and Gauss's Law holds true.

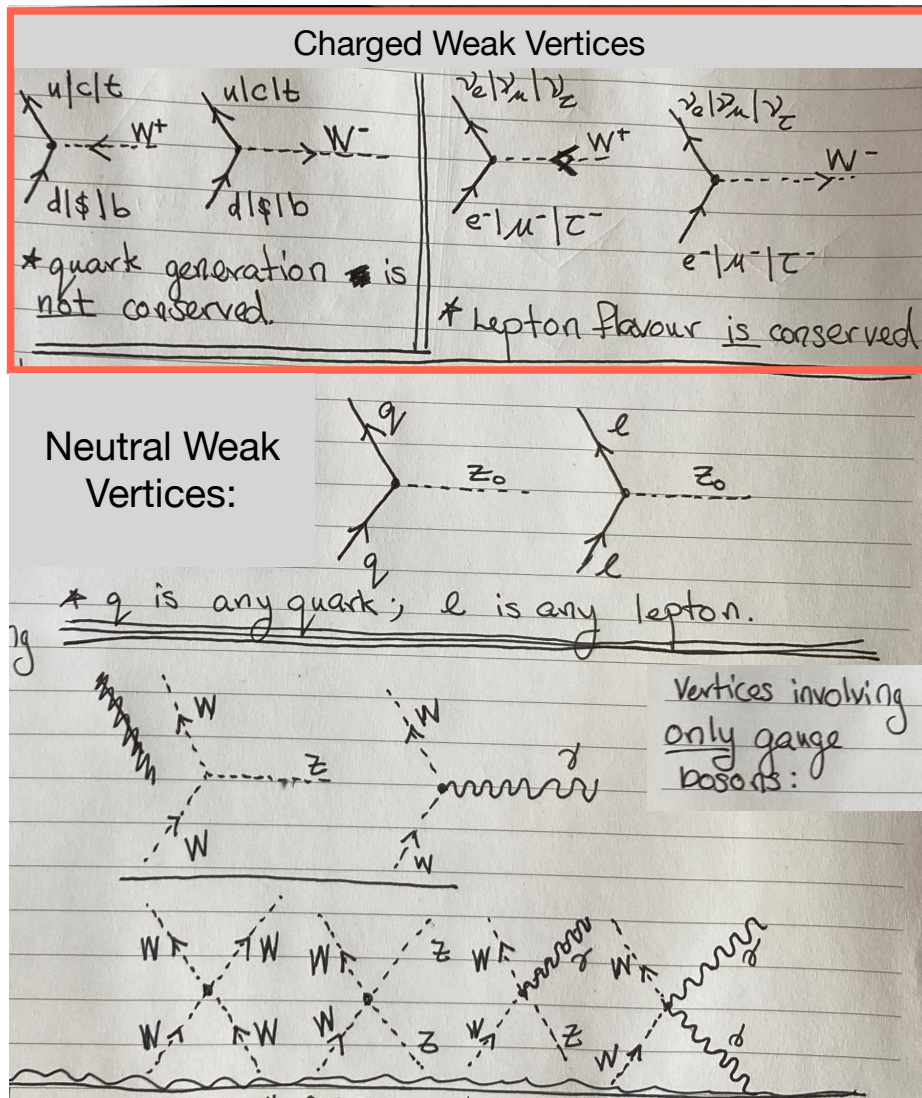
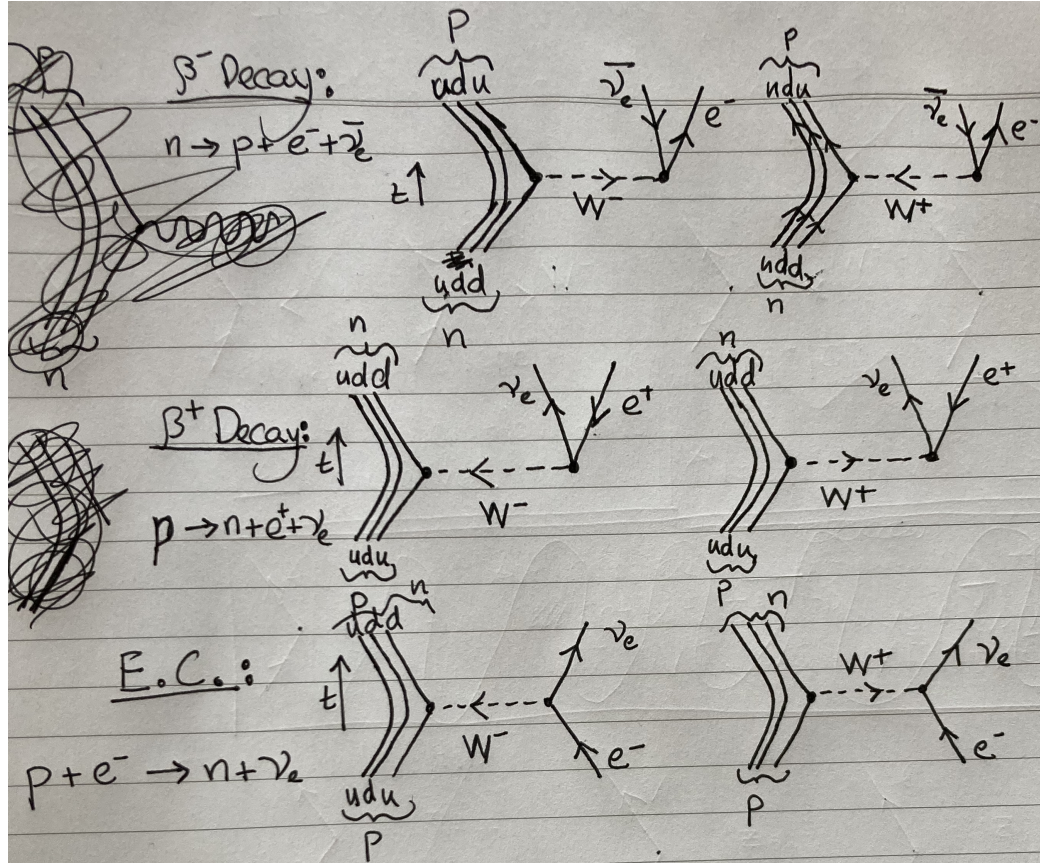


Figure 1.1: An exhaustive list of weak vertices. All possible Feynman diagram vertices involving W^+ , W^- , or Z^0 bosons are shown. Time goes up. The usual rules for Feynman diagram vertices apply.

In the case of the nuclear weak force, which will be the primary concern within this thesis, the notion of generalized charge is no longer entirely straightforward to apply. We must rely instead on a list of allowed Feynman diagram vertices to describe the types of interaction that are possible (see Fig. 1.1). We note that the weak force involves three mediating particles — W^+ , W^- , and Z^0 bosons — and these mediators can interact with both (anti-)quarks and (anti-)leptons. The W^+ and W^- particles also carry electric charge, which must be separately conserved in any interaction, but the Z^0 is electrically neutral. All three are massive, which implies that the strength of the weak force falls off more rapidly as distance increases, and Gauss's Law does not apply.

(wait, is that true?
what about with the
photon vertex?I
think it's fine.....)



Fix beta decay Feynman diagram placeholder figure.

Figure 1.2: Beta decay Feynman diagrams are shown here at the nucleon(?) sort of level.

With a comparatively large number of possible vertex types, it can be challenging

to develop an intuition about the behaviour of the weak force. Perhaps the most well known physical behaviour that arises from the weak force is nuclear beta decay. In Fig. 1.2 the tree-level Feynman diagrams pertaining to the most common beta decay processes are shown. It is these beta decay processes which present what is arguably the most accessible experimental window on the workings of the nuclear weak force.

Although beta decay is generally well understood, it presents a unique opportunity for precision measurements to search for physics beyond the Standard Model within the Weak coupling. By observing the kinematics and angular correlations involved in the decay process, one gains access to a wealth of information about the form of the operators mediating the decay.

- (we're not proposing a new feynman diagram. Just, a new vertex factor thingy, I guess.)
- Weak force lagrangian! I think possibly it's only for the *charged* weak force??
- ...then we demand that the Lagrangian must be Lorentz invariant, otherwise we break physics.
- within this thesis, we will focus primarily on the *charged* weak interactions (using W^\pm as mediators rather than Z^0), with first-generation normal matter quarks (*i.e.* up (u) and down (d) quarks, but not charm (c), strange (s), top (t), or bottom (b) quarks; no anti-quarks (\bar{q} for $q = \{u, d, c, s, t, b\}$)) and first-generation leptons (*i.e.* electrons, positrons, electron neutrinos and electron anti-neutrinos, but not positive or negative muons or taus, nor muon or tau neutrinos or anti-neutrinos)).
- Really, we'll only be looking at weak force interactions involving the two most common nucleons – protons and neutrons. ...each of which is a (meta-)stable bound state involving three quarks.
- masses of W and Z bosons?

Standard Model ->
standard model of
particle physics (often
denoted here "SM").
The standard model is
...
...
Weak -> weak.
...
This of course is the
place where Georg
wants more for orientation.

Something something
... it's so well under-
stood that all that's
left to do is the preci-
sion measurements.

1.2 A Historical Look at Beta Decay

History section needs *all* the citations.

We consider the historical development of our scientific understanding of beta decay and the nuclear weak force. This is a historically rich topic, and a full discussion is beyond the scope of this document, however we shall attempt to touch on some highlights.

Radioactivity was first observed in 1896 by Henri Becquerel in uranium, and this

landmark discovery set off a flurry of activity in the field [8]. Ernest Rutherford noted in 1899 that the particles emitted by a sample of uranium could be classified into two groups based on how readily they were absorbed in materials – alpha particles are easily absorbed, while beta particles are more penetrating [9]. A third and even more penetrating type of radioactive emission was observed in 1900 by Paul Villard, who made no attempt to give it a name – but within a few years, Rutherford’s naming convention had been applied and this third type of particle became known as a gamma ray [10][11].

When, in 1900, Becquerel measured the charge-to-mass ratio of emitted beta (β^-) radiation and found that it was the same as that of the electron, he proposed that these must be the same particle [12], and in 1901 Rutherford and Soddy demonstrated that the processes of alpha and beta decay both transmute the original chemical element into another.

Despite these early successes, in 1911 Lise Meitner and Otto Hahn noticed that beta particles are emitted with a variety of different kinetic energies, and in 1914 James Chadwick demonstrated that energies of emitted beta particles formed a continuous distribution. The physics community was baffled for years by the fact that it seemed impossible to predict the energy of a beta particle emitted by a particular process; if the emitted beta simply took on the difference in energy between the initial and final states, then surely that energy should be a fixed, unchanging value for a particular transition. Finally, in 1931, a frustrated Wolfgang Pauli famously proposed that if an additional small, neutral, difficult to detect particle were emitted simultaneously with the beta and allowed to carry away a varying amount of energy, then this accounting trick could account for the continuous beta energy spectrum. He named this particle a “neutron” – though today we refer to that same particle as a(n) “(anti-)neutrino,” and use the name “neutron” for an entirely different particle.

Pauli’s 1931 insight paved the way for Enrico Fermi to propose a quantitative description of the beta decay process. Now known as Fermi’s Golden Rule, the introduction of this model in 1933 arguably marks the beginning of our modern understanding of beta decay. Fermi’s Golden Rule is both remarkably general in its approach, as well as powerful in its predictive power, approaching the matter from a fully quantum mechanical perspective (see Section ??).

On the experimental front, 1934 marks the first discovery of β^+ radiation, for which Irène and Frédéric Joliot-Curie later received a Nobel prize. This was also

I think. Also, I think that's the right citation..

or possibly 1903?

That arxiv rando claims that the half-life thing was developed or hinted at by 1900 Rutherford, but who the fuck knows?

Fermi renamed it, because Italian.

1933 in Italian, 1934 in German.after being rejected by Nature. Citation is: Pais, Abraham (1986). Inward Bound. Oxford: Oxford University Press. p. 418. ISBN 0-19-851997-4.

add link

Rephrase.

the year when the electron capture mechanism for beta decay was first proposed by Gian-Carlo Wick. The theory was fleshed out over 1935-1936 by Yukawa and Sakata, and first observed in 1937 by Luis Alvarez.

Over the next few years, developments within the field of nuclear physics were largely directed elsewhere, but beta decay returned to scientific prominence with Lee and Yang's 1956 suggestion that, contrary to the community's prior expectation, parity may not be conserved within beta decay processes. The proposition was rapidly put to the test by C.S. Wu's landmark 1957 measurement of ^{60}Co , confirming that beta decay violates parity conservation [31].

...

OK, how/when did they do electroweak unification, and who did it?—
Glashow+Weinberg+Salam, 1968.

What about the full SM, incorporating the strong force too?

Schwinger does renormalization, which makes QED go. Glashow [13] extends it to the Z boson. But now it's not renormalizable. Salam and Ward [14] did a similar thing, but independently. Then Weinberg (1967) did it but didn't know what to do with Z bosons [15]. Until later. Or something. Then, 't Hooft (1971) proved that this thing was normalizable even with massive gauge bosons [16]. Or at least, that's how Wikipedia describes it. Also, in the end, electroweak unification was based on Yang-Mills (1954) [17], but their theory didn't really get that much attention initially because it was just a lot of boring math, and they couldn't figure out how to something something symmetry breaking.

Halliday doesn't remember Meitner+Hahn, and says Pauli's thing is 1927, but doesn't give a reference for it.

...

Also from Halliday: Yukawa and Sakata first proposed the possibility of (orbital) electron capture in 1935-1936. (What about Wick in 1934?)

...

Also-also: Fermi in 1934 drew an analogy between emission of electrons and neutrinos from nuclei and emission of photons from excited atomic states.... (probably this gets us one step closer to isospin?)

I could totes add a reference to Halliday's 1955 textbook (v2).

Other references to add include that one letter to the collaboration giving values of *things* from Ian Towner, 2011.

omg, I can't just give first names for only the non-Asian people...

their hamiltonian operates at the nucleon level, because they hadn't discovered quarks yet. also, this is the basis for where we're going with this experiment. shows all possible Lorentz-invariant contributions to the thingy. V,A,S,T,P. I don't think they knew about W and Z bosons either.

For a while everyone thought it was S,T. But it turns out it's V,A.

How do I reference a grant proposal?

separate ref. for the PRL's supp. mat.

...
I should probably cite Dan's thesis. And Alexandre's too.

...
More references to add, for some of the numbers in that text file:

...
The Branching Ratio from Severijns 2008 [18]
The Probability of electron capture from Severijns 2008
The halflife from Shidling PRC 2014 [19]
statistical rate function from Severijns 2008
Axial to Vector Ratio from Severijns 2008
Nucleus Dependent Radiative Correction from Severijns 2008
Nuclear Structure Dependent Corrections and isospin symmetry breaking correction from Severijns 2008
Isospin symmetry breaking correction ($\delta_{C1} + \delta_{C2}$) from Severijns 2008
FT from 0plus to 0plus decay Hardy PRC 2015 (eq. 5) [20] (Hardy+Towner)
Weak Magnetism from Naviliat-Cuncic 2009
Sign of Rho determined by shell model from Severijns 2008
Average Mass need to calculate parameters as a function of energy Naviliat-Cuncic 2009 (is it [21], or [22]?? No way to know.)
Parent Magnetic Moment from von Platen Z. Phys. 244 (1971) [23]
daughter magnetic moment from M. Pitt Ph.D. (1992) [24]
Parent quadrupole moment Minamisono PLB 662 (2008) [25]
daughter quadrupole moment Klein NPA 607 (1996) [26]
??? for electron mass (wikipedia)
mass of parent 37K taken out of Dan's code mass of 37K
daughter mass from ???
Average kinetic energy from Severijns 2008 (is this thing even used??)
"ALPHA", whatever that is: CODATA 2018 (It's what I think it is.) []
things from Ian Towner 2013: all the (reduced) matrix elements and all the coupling constants with quenching corrections. [27]
...
Really, this shit can probably can be an appendix.

alpha and beta decay:

Rutherford, Ernest (1899). "Uranium radiation and the electrical conduction produced by it," Philosophical Magazine 47, 109-163.

...

half-life:

Rutherford, Ernest (1900). "A radio-active substance emitted from thorium compounds," Philosophical Magazine 49, 1-14. Or, possibly:

Rutherford, Ernest (1906). Radioactive Transformations. London: Constable & Co.

...

Transmutations?: 1902, 1903 — rutherford and soddy.

1.3 Draft of Intro Section

1.3.1 bullet points.

Standard Model:

- ???? - Schwinger
- 1959 - Glashow
- 1964 - Salam and Ward
- 1967 - Weinberg
- 1971 - 't Hooft
- ...
- 1954 - Yang + Mills huh?

1.3.2 paragraphs

OK. This stuff is basically yoinked from Ben's thesis. And Dan's. I'll need to re-organize and rephrase the content – but I want to make sure I get the important points down.

In 1931, Pauli figured out about neutrinos, because beta decay produced a whole spectrum of beta energies, so there had to be a third body available to carry off some of the energy. (Dan doesn't cite anyone here)

There's the matrix element, \mathcal{M}_{fi} , which connects the initial and final nuclear states, before and after an interaction (decay).

$$\mathcal{M}_{fi} = \int \psi_f^* \mathcal{O} \psi_i dV \quad (\text{What is } V?? \text{ Pretty sure it's phase space volume.}) \quad (1.1)$$

which goes with Fermi's Golden Rule (or at least one of them):

$$\Gamma = \frac{1}{\tau} = \frac{2\pi}{\hbar} |\mathcal{M}_{fi}|^2 \rho(E_f) \quad (\text{Why is this formatted weird??}), \quad (1.2)$$

where, as Ben puts it, $\rho(E_f)$ is "the thermodynamic density of states available at a final energy". Then he writes down the differential decay rate and cites [28] for it, which is in German:

$$\frac{d^5W}{dE_\beta d\Omega_\beta d\Omega_\nu} = \frac{G_F^2}{(2\pi)^5} p_\beta E_\beta (E_0 - E_\beta)^2 F_\pm(E_\beta, Z') |\mathcal{M}_{fi}|^2 \quad (1.3)$$

Anyway, that thing was published in 1934 ! And he assumed the interaction only worked at 0 distance. Also, he postulated that the weak force was a vector interaction, and some of it is!

Later, we collectively learned that a better model is to suppose that the interaction is mediated by a massive, charged W^+ or W^- particle. Also, it's pretty heavy, and Ben totally gives the mass so he can cite the dudes who compile that stuff, but there's a new version now. As of 2018, we have $m_W = 80.379(12) \text{ GeV}/c^2$ [29]. The point is, the fact that it's so massive means that the approximation of 0 distance was pretty good, since the larger mass implies that the interaction can only occur at short range.

So we're going to require that \mathcal{O} must behave under a Lorentz transformation. You can construct operators with the correct form out of Dirac γ -matrices, and you get scalar, pseudoscalar, vector, axial vector, and tensor couplings. potentially. Anything else would just reduce to linear combinations of those, so those ones span the space. Some of those respect parity, and some don't.

Up until 1956, it was common wisdom that weak interactions should respect parity, but there was really no evidence for it. Lee and Yang formulate a more general description of beta decay, with all the Lorentz symmetry respecting operators, and

Lorentz Invariant Operators	
Name	Form
Scalar	1
Pseudoscalar	γ_5
Vector	γ_μ
Axial-vector	$\gamma_\mu \gamma_5$
Tensor	$\gamma_\mu \gamma_\nu - \gamma_\nu \gamma_\mu$

Table 1.1: Dirac Matrix Operators. I need to reference this table somewhere. Also, these are dirac matrices in 4D. More D, different Dirac matrices.

only some of those obey parity [30]. It was an open question, then, whether parity should be respected in the nuclear weak interaction – but not for long, because C.S. Wu tested it out in 1957 [31]. The result of the experiment is that not only is parity *not* conserved, it's (sometimes) *maximally* not conserved! Neat! Nobody would have expected it.

Ben points out that they thought it was scalars and tensors at first, and cites some people([32][33]), but frankly, I can't access those articles and I thought there was more evidence for it than that. Also, the one article is published before Madame Wu's, so idk what to make of that.

Ben points out that the $V - A$ form of the interaction means that parity is *maximally* violated, however he also says that A has + and V has - parity.

Anyway. We're maximally parity violating, and when we describe this in modern terminology, we would say that the W^\pm particles only couple to negative helicity (left-handed) leptons, or positive helicity antimatter leptons (anti-leptons).

Also, chirality as a concept. It's an intuitively straightforward concept when your particle is going at the speed of light. So, for a massless neutrino, if it has a negative chirality, that means that its spin vector is pointed opposite to its direction of motion.

Also-also, the fundamental property is chirality, not helicity. Helicity can be flipped by a simple Lorentz boost. But because we're talking about an interaction, there is some sense in which this defines a rest frame for us.is this even the correct way to think about it? I think it has to be fine.

So anyway, we have lots of evidence for the $V - A$ form of interactions. (Ben doesn't cite anyone for this). But other forms of the interaction could be in there too. And at this point, Ben just assumes the Standard Model and goes with it.

JB says: Chapters 1.1 and 1.2 look fine.

My only comment is to ask where the Fermi "singlet" and "triplet" came from, referring to coupling of the lepton spins. I have not seen this– it could be fine, yes, I don't know.

JB: The Gamow-Teller operator sigma dot tau refers to nucleon spins, not lepton spins, i.e. the nucleon spin can flip, but that doesn't tell me about this lepton rule either way. You correctly state the lepton and antilepton chirality farther down.

John's suggestions for fixing the stuff that Georg wanted fixed – that giant email. i) Among the necessary technical corrections, there's a solid request for more background info. I think you know what to do.

...

A large thing is some kind of extra qualitative description of what the SM is. You could do that qualitatively without any trouble.

You might point out some part of this:

- the charged weak interaction you're writing down predates the Weinberg-Salam model by more than a decade. The version you've written down assumes protons and neutrons are fundamental particles.
- The exchange boson is much heavier in mass than the energy and momentum in the decay, so it can be approximated by an interaction with zero range.
 - Fermi did that very early on,
 - and Gamow and Teller added a process that change the nucleon spin.
 - Lee and Yang, which you cite, added the possible currents with different Lorentz transformations (do you mention that since any further combination of Dirac matrices can be reduced to these, so they span the space), and the possibility of parity violation by writing out helicity projections for the leptons. I.e. Lee and Yang assumed some fields (the nucleons and leptons) and a general interaction preserving the symmetries of the theory, which by definition is then an effective field theory.
- Feynman and Gell-Mann's 1958 paper is the one that postulated V-A, again a decade before Weinberg-Salam, and they did this by making analogies between the boson exchanged and the photon, i.e. an analogy between the charged weak interaction and the electromagnetic current, so you could cite them instead of saying "SM predicts everything"

People had assumed there was a massive boson exchanged for a very long time.

What Weinberg (and, independently, Salam) did was come up with a consistent mathematical theory of massive bosons, incorporating Yang Mills gauge theory (looks like E&M but with non-abelian operators) to do that, and the result was the weak neutral interaction prediction.

1.4 Beta Decay within the Standard Model

A nucleus undergoing beta decay converts one of its protons (neutrons) into a neutron (proton), and simultaneously emits a lepton and anti-lepton. The daughter nucleon remains bound in place of its parent, and the overall electric charge of the nucleus is changed by -1 (+1), with the extra charge being carried away by the anti-lepton (lepton). In particular, at the nucleon level, three beta decay processes are

possible:

$$p \rightarrow n + e^+ + \nu_e \quad (1.4)$$

$$n \rightarrow p + e^- + \bar{\nu}_e, \quad (1.5)$$

$$p + e^- \rightarrow n + \nu_e \quad (1.6)$$

where the processes described in Eqs. 1.4 and 1.6 are energetically disallowed for an unbound proton, however there is no similar requirement for Eq. 1.5.

Electron capture decay of Eq. 1.3 is calculated to be an 0.080% branch compared to positron decay in 37K decay (Table VII of N. Severijns, M. Tandecki, T. Phalet, and I.S. Towner) [18], an important correction when interpreting the total decay rate of 37K to determine the theoretical prediction for 37K Abeta (P.D. Shidling, R.S. Behling, B. Fenker, J.C. Hardy, V.E. Iacob, M. Mehlman, H.I. Park, B.T. Roeder, D. Melconian Phys Rev C 98 015502 (2018) [34]; A. Ozmetin, D.G. Melconian, V.E. Iacob, P. Shidling, V.S. Kolhinin, D.J. McClain, M. Nassar, B. Schroeder, B. Roeder, H. Park, M. Anholm, A.J. Saastamoinen, APS DNP Abstract KF.00005 2020 “Improving the ft value of 37K via a precision measurement of the branching ratio”) [35].

Eqs. 1.4 and 1.6 are energetically disallowed for an unbound proton, but allowed energetically when bound in nuclei as in 37K decay.

Limiting the focus of this discussion to Eq. 1.4, we note that this expression provides no information at all about the momenta or spin of the outgoing daughter particles. This behaviour is governed by the form of the Weak coupling that mediates the decay.

Within the field of nuclear physics, it is common to classify beta decay processes as being either “Allowed” or “Forbidden” (sometimes with an associated number to describe the extent to which it is Forbidden), where Forbidden processes are generally suppressed but not truly forbidden. In an Allowed transition, the positron and anti-neutrino are treated as being created at the nuclear centre, and as a result they may not carry away any *orbital* angular momentum. However, since the outgoing leptons both have spin $S = 1/2$, it is still possible for the total nuclear angular momentum, J , to be changed in an Allowed decay. This implies that an Allowed transition must *always* change the total nuclear angular momentum by either 0 or ± 1 .

don't capatalize "Allowed" and "Forbidden." The quotes are justified.

First forbidden decay emits leptons with total orbital angular momentum 1, changing the nuclear parity- suppressed in a long-wavelength approximation $((\beta \text{ momentum})/(\hbar c))^2$ or about two orders of magnitude. This is one reason decays to negative-parity excited states of 37K are so small (Fig. 1.3).

The Allowed decays traditionally are further separated into a “Fermi” singlet in which there is no change to nuclear angular momentum ($\Delta J = 0$) and therefore the

singlet in lepton spin

two leptons are required to have anti-parallel spins, and a “Gamow-Teller” triplet [36], where the projection of the nuclear angular momentum is changed by ± 1 .

This implies that the total nuclear angular momentum is changed by $\Delta J = \{0, \pm 1\}$ during a Gamow-Teller transition. A mixed transition is also possible, however we note that the $J_i = J_f = 0$ decays must always be pure Fermi transitions, because there is no way to produce this result from two outgoing leptons with parallel spins. [37] [38] [36].

Given the differing behaviour within the angular momenta of the daughters in Fermi and Gamow-Teller transitions, it is perhaps not surprising that that the *linear* momenta of the outgoing particles should also follow a different set of distributions in these two cases. At the level of the Weak coupling, Fermi- and Gamow-Teller transitions are governed by different operators, with the Fermi interaction mediated by a so-called “vector” (V) coupling, and the Gamow-Teller interaction mediated by an “axial-vector” (A) coupling.

The vector and axial-vector couplings refer to Lorentz transformation of the Lagrangian terms involved, which we come to next.

Don't capitalize Weak anywhere, either. You can keep quotes around the first "weak", I guess.

you should indeed capitalize Fermi and Gamow-Teller because these are people.

1.5 A Generalized Description of the Weak Interaction

According to the predictions of the Standard Model (SM), the Weak force involves only vector (V) and axial-vector (A) couplings, where a relative sign within the quark-lepton Lagrangian produces the left-handed “($V - A$)” form of the interaction in maximal violation of parity. In terms of physical behaviour, one consequence of this model is that “regular matter” leptons emerge from a Weak interaction with left-handed chirality, while antimatter leptons emerge with right-handed chirality. Any deviation from this behavior would be indicative of “new” or “exotic” (i.e., not previously discovered) physics.

standard model

There exists an extensive body of experimental evidence to demonstrate that the above model is overall a very good description of the beta decay process [31]. Despite the success of the ($V - A$) model, there are still certain lingering questions that must be addressed by precision measurements. Any deviation from maximal parity violation (i.e., a “($V + A$)” contribution to the Weak force) would be of great

"new" -> new
"exotic" -> exotic.
...
You define them right away. There is no need for air quotes. You should seriously think about never using air quotes, but use them as an indication to you that you need to write down more clarifying words instead.

interest to the community, as would the presence of certain other exotic couplings, such as the so-called Scalar (S) and Tensor (T) interactions. Any such behaviour beyond the Standard Model (BSM) would represent a non-dominant contribution to the interaction, however the possibility cannot be entirely ruled out.

This is where I'm suggesting a little more explanation of Lee and Yang, and V-A from Feynman and Gell-Mann

The generalized nucleon-level Lagrangian to describe the Weak interaction including BSM behaviour is given by:

$$\begin{aligned} \mathcal{L} = & -\bar{p}\gamma^\mu n \left(C_V^+ \bar{e} \gamma_\mu \nu_L + C_V^- \bar{e} \gamma_\mu \nu_R \right) - \bar{p}\gamma^\mu \gamma_5 n \left(C_A^+ \bar{e} \gamma_\mu \nu_L - C_A^- \bar{e} \gamma_\mu \nu_R \right) \\ & - \bar{p}n \left(C_S^+ \bar{e} \nu_L + C_S^- \bar{e} \nu_R \right) - \frac{1}{2} \bar{p} \sigma^{\mu\nu} n \left(C_T^+ \bar{e} \sigma_{\mu\nu} \nu_L + C_T^- \bar{e} \sigma_{\mu\nu} \nu_R \right) \\ & + \bar{p}\gamma_5 n \left(C_P^+ \bar{e} \nu_L - C_P^- \bar{e} \nu_R \right) + \text{H.C.}, \end{aligned} \quad (1.7)$$

where the coupling constants C_X^\pm (with $X = \{V, A, S, T, P\}$) are written in such a way as to separate out the left-handed (C_X^+) and right-handed (C_X^-) components from one another, and the neutrino fields $\nu_{L,R}$ are given a similar treatment. A simple variable transform relates Eq. 1.7 to expressions that are potentially more familiar from the older literature, much of which was written before it had been determined that the Weak force is primarily or entirely left-handed:

$$\nu_L = \frac{1}{2} \nu (1 + \gamma_5) \quad (1.8)$$

$$\nu_R = \frac{1}{2} \nu (1 - \gamma_5) \quad (1.9)$$

$$C_X = \frac{1}{2} (C_X^+ + C_X^-) \quad (1.10)$$

$$C'_X = \frac{1}{2} (C_X^+ - C_X^-) \quad (1.11)$$

Can you please provide a reference for Eq. 1.7? I'm now confused about how you can get pure $1+\gamma_5$ projections without assuming $C_V=C_V'$ and $C_A=+/-C_A'$ (I forget the convention) so I really think you need to reference this expression rather than derive it.

It can be seen from the form of the Lagrangian that the V, A, S, T, P couplings within are described as such because they *behave* as vectors, axial-vectors, scalars, tensors, and pseudoscalars (respectively) under a Lorentz transform, where the La-

grangian itself must be a scalar both before and after a Lorentz transform [30] [7] [4].

(Any quark-lepton pseudoscalar couplings have usually been ignored in beta decay, because they are suppressed by (beta momentum)/(nucleon mass). Note that more recently it's been pointed out that C_P is naturally quite large in the nucleon (M. Gonzalez-Alonso and J. Martin Camalich Phys Rev Lett 112 042501 (2014)) and allows for significant constraints from allowed beta decay.)

1.6 Mathematical Formalism

In a beta decay event, conservation of energy and momentum are of course required, but those conditions alone cannot provide a full description of the kinematics of emitted particles.

Although momentum and energy conservation determine all kinematics event-by-event. the actual distributions include complications.

The distribution of energy and momenta is probabilistic rather than deterministic with three bodies involved, and the full probability distribution for the momenta of outgoing particles cannot be written in closed form.

"probabilistic rather than deterministic with three bodies involved, and the full probability distribution for the momenta of outgoing particles cannot be written in closed form."

→

If terms including the tiny kinetic energy of the recoil are neglected, then the distribution of energy and momenta comes from a simple integral over final momentum states $d^3 p$ of the leptons. But the outgoing beta sees a large correction from the Coulomb field of the nucleus, written as a Fermi function F(Z,E_{beta}). The result is in Eq. 1.12 (provide a reference for it).

"cannot" is very misleading. The delta function for all 4 particles is a nontrivial mathematical object, but people do deal with it. I'm trying to suggest rephrasings.

Because the nucleus is significantly more massive than either of the other two outgoing particles, the great majority of the released kinetic energy is distributed between the leptons, while the nucleus receives only a tiny fraction of the total. This feature lends itself to an approximation in which the energy of the recoiling nucleus (the "recoil") is neglected entirely, and the decay may be described only in terms of the momenta of the outgoing positron(electron) and neutrino(anti-neutrino), as in the description from Jackson, Treiman, and Wyld (JTW) [1] [2]. The terms that have been neglected in this treatment are sometimes called 'recoil-order corrections'.

In order to proceed with a measurement, we must find an equation to describe the probability of beta decay events with any given distribution of energy and momenta

among the daughter particles, as a function of the strength of the specific couplings of interest to us. To do this, two sets of formalisms are combined – the older formalism of JTW, which describes the effects of all types of Standard Model and exotic couplings of interest to us here, but which truncates its expression at first order in the (small) parameter of transferred nuclear recoil energy, and a newer formalism from Holstein [39], which includes terms up to several orders higher in recoil energy, but which does not include any description of the exotic couplings of particular interest to us. We note that because any exotic couplings present in nature have already been determined to be either small or nonexistent, it is sufficient to describe these parameters with expressions truncated at first order, despite the fact that it is still necessary to describe the larger Standard Model couplings with higher-order terms.

Unfortunately, the outgoing (anti-)neutrino is very difficult to detect directly, and we make no attempt to do so in this experiment. Instead, we might look for coincidences between an outgoing beta and a recoiling nucleus, and use that information to reconstruct the kinematics of the neutrino.

The procedure for combining the two formalisms is described in detail in Appendix C. Integrating the JTW expression over neutrino direction, we find:

$$\begin{aligned} d^3\Gamma dE_\beta d^2\hat{\Omega}_\beta &= \frac{2}{(2\pi)^4} F_{\mp}(Z, E_\beta) p_\beta E_\beta (E_0 - E_\beta)^2 dE_\beta d^2\hat{\Omega}_\beta \xi \\ &\times \left[1 + b_{\text{Fierz}} \frac{m_e c^2}{E_\beta} + A_\beta \left(\frac{\vec{J}}{J} \cdot \frac{\vec{p}_\beta}{E_\beta} \right) \right], \end{aligned} \quad (1.12)$$

Do it! Do the master equation!

JB: cut "so we will simply provide the combined master equation here"
Don't. The equation you have is all you need.

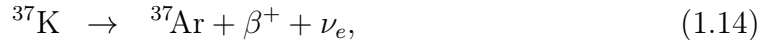
where a comparison with Holstein's treatment yields the relation,

$$\xi = G_v^2 \cos \theta_C f_1(E). \quad (1.13)$$

...and $f_1(E)$ has both Fermi and Gamow-Teller contributions (? I hope; otherwise it can't be the total rate that it strives to be?)

1.7 Our Decay

Here, we will focus on the decay,



which is extremely well suited to the type of experiment to be discussed in this thesis. The parent, ^{37}K , is an isotope of potassium—an alkali. Though this fact may initially seem unremarkable, it is their ‘hydrogen-like’ single valence electron which allows alkalis to be readily trapped within a magneto-optical trap, a critical component of our experimental design (see Chapter 2).

hydrogen-like does not
need quotes

A potential concern in any experiment concerned with the angular correlations resulting from one particular decay branch is the background from competing decay branches. As can be seen in Fig. 1.3, the decay of ^{37}K is dominated by a single branch which contributes nearly 98% of ^{37}K decay events, and the remaining events nearly all arise from a single branch contributing around 2% of the decay events. The other branches combined account for only around 0.04% of decays. Taken all together, this means that the background events which must be accounted for are both infrequent and well understood.

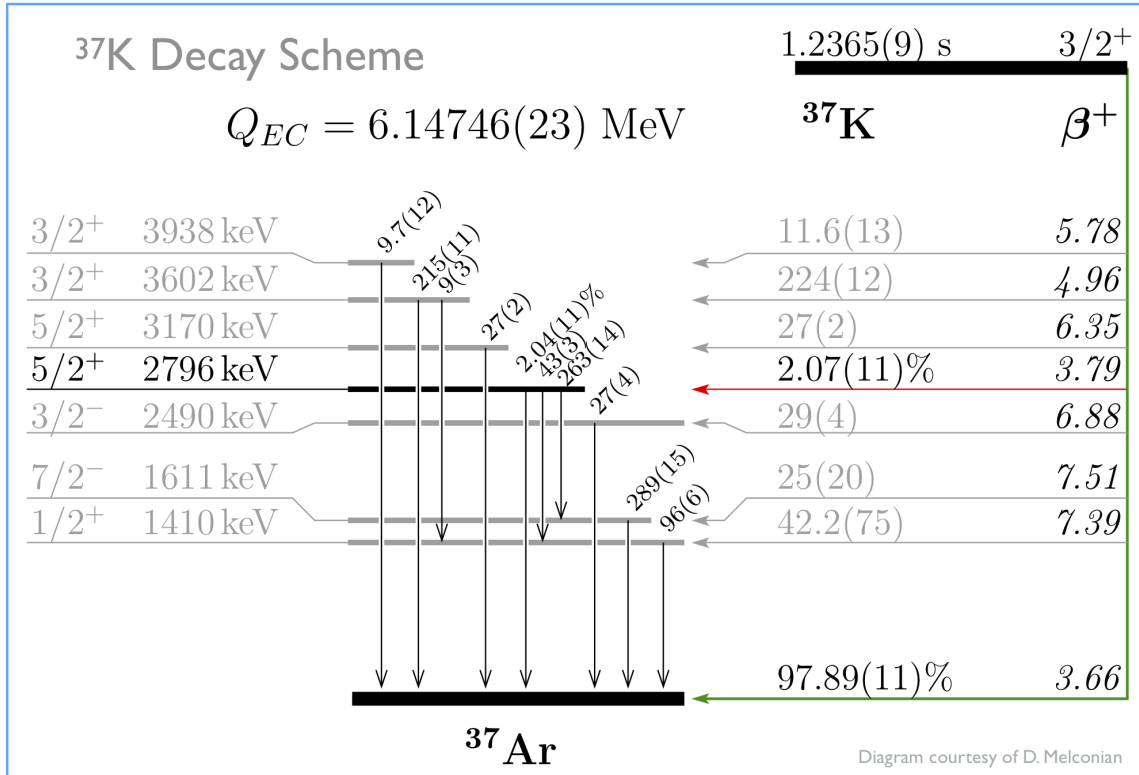
As in any decay, the angular correlations between the emerging daughter particles provide a rich source of information about the type of interaction that produced the decay. This particular decay involves a set of ‘mirror’ nuclei, meaning that the nuclear wavefunctions of the parent and daughter are identical up to their isospin quantum number and corresponding electrical charge. Because the two wavefunctions are so similar, effects to the decay from nuclear structure corrections can be kept to a minimum, and it is therefore possible to place especially strong constraints on the size of the theoretical uncertainties associated with the decay.

Also, ^{37}K is a really nice isotope for this, because its big A_β value means we have a big thing to multiply any b_{Fierz} value there might be when we construct the superratio asymmetry to eliminate systematics.

no one will let you
publish air quotes,
ever. Have mercy on
your committee, take
them all out. Use the
opportunity to make
sure you've defined
them.

...
Here, just say isobaric
mirror nuclei. You
define it right there
in text. It's fine to
use textbook terms
as long as you define
them immediately.

Is it definitely true
that the nuclear struc-
ture corrections are
smaller? Or is it
just that they're bet-
ter understood?



The caption should include that the right-hand column is $\log_{10}(fT)$, a measure of the absolute decay rate (ref. Krane e.g.). The left-hand column has I^π where I is spin and π is parity. This should not only include Dan's thesis for a reference, but the most recent paper with the branches- it should work to reference P.D. Shidling et al. Phys Rev C 98 015502 (2018) which re-did the half-life and summarized the fT value extraction. I see no publication of your branching ratio work, so I referenced Ozmetin's DNP talk in an earlier note.

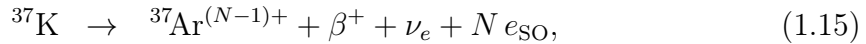
Figure 1.3: A level diagram for the decay of ^{37}K .

1.8 The Shake-off Electron Spectrum

Although the beta decay process is primarily concerned with the emission of beta particles (electrons or positrons) from a Weak interaction that occurs within the nucleus, it is common for one or more *orbital* electrons to also be lost in the process. Although beta particles are emitted over a continuous energy spectrum, they commonly carry several MeV of kinetic energy. By contrast, an atomic electron that becomes unbound in this process is likely to only carry a few eV of kinetic energy, and we say that they are ‘shaken’ off.

These are referred to as shakeoff electrons (SOEs), since they are in some sense shaken off.

We will amend Eq. 1.14 to reflect the presence of N such ‘shake-off electrons’ (SOEs) within each decay event, as



where it is clear that, since the parent ${}^{37}\text{K}$ atom was electrically neutral before its decay by β^+ emission, the daughter ${}^{37}\text{Ar}$ will initially have an ‘extra’ orbital electron (and therefore a negative net charge) if no electrons are shaken off. We also note that it is common for multiple SOEs to be created in a given decay event.

A further consideration is that the outer electron in an ${}^{37}\text{Ar}^-$ ion is *not bound*, and in an electric field such as is present within our experimental chamber, this outer electron is removed immediately to be accelerated through the field, leaving behind a neutral ${}^{37}\text{Ar}$ atom. Although this is in principle a different physical loss mechanism, we will refer to unbound electrons resulting from either process as SOEs.

It is useful to consider the energy spectrum of these shake-off electrons. The most straightforward component of the SOE energy spectrum arises from the electrons that are lost immediately following decay, and we take these to initially have 0eV in kinetic energy.

For the shake-off electrons arising from the Weak process itself, the initial energy spectra for SOEs originating in a particular orbital shell can be estimated according to the procedure outlined by Levinger [40].

→“by Levinger, who credits Feynman for the suggestion [40].”

...

(Since this is a true story that is not embellished by Feynman in someone else’s joke book, but is in a footnote in the Physical Review, I like to mention it.)

‘extra’ -> extra.
You’re not breaking
charge conservation
here, you don’t need
to define the word.

cite someone!! I don’t
know who.

The strategy is to assume that the sudden approximation holds, and simply calculate the overlap in electron wavefunctions between the initial and final states, where the final state may be either an outgoing electron or one bound within the atom. Analytic expressions can be obtained if the atom is treated as being hydrogenic – an excellent approximation here, as ${}^{37}\text{K}$ is an alkali.

Unfortunately, this treatment cannot determine the fractional contribution of each orbital to the total, nor can it determine the *number* of electrons likely to be removed in a single decay event. The implications of the SOE energy spectrum to the present experiment are discussed further in Section 4.5.

In the end, we used $(0.09) * (0\text{eV}) + (0.91) * (0.85 * (4S) + 0.15 * (3P))$. But I say that in the other section. Also, John used Eq.20 for the 4S, and Eq.24 for the 3P.

Comment on how well this matches our data? Somehow?

A picture of the SOE spectrum for the intro was here. It's gone now, but it's important that we remember!

1.9 Fierz Interference – The Physical Signature

The physical effects resulting from the presence of scalar or tensor couplings include a small perturbation to the energy spectrum of betas produced by radioactive decay, labeled b_{Fierz} in Eq. C.13. Within the Standard Model, the parameter b_{Fierz} is identically zero, and a departure from that would be indicative of (BSM) scalar or tensor couplings.

The measured value of b_{Fierz} can be evaluated by using a simple beta energy spectrum, as in the top plot of Fig. 1.4, but by constructing a so-called “superratio asymmetry” instead (bottom plot in Fig. 1.4), these small changes to the overall spectrum are amplified, and many systematic effects cancel out entirely. This result comes at the cost of an increased statistical uncertainty.

→ not only by.... but also by...

By normalizing Eq. 1.12 to have a conventional angular distribution $1 + (\text{term}) * A_\beta$, we can write $W(\theta) = 1 + A_\beta / (1 + b_{\text{Fierz}} E_\beta / m_e) \cos(\theta) \approx 1 + A_\beta \cos(\theta) - b_{\text{Fierz}} E_\beta / m_e A_\beta \cos(\theta)$ for small b_{Fierz} . Our superratio observable measures directly the coefficient of the $\cos(\theta)$ term., and its distortion with energy is multiplied by $b_{\text{Fierz}} A_\beta$.

...

The 37K A_β is much larger than the neutron’s A_β , so we gain in sensitivity compared to the neutron.

The superratio and superratio asymmetry are discussed in detail in Appendix E. The discussion includes details on which sort of systematic errors will cancel out entirely, or to leading order, with this treatment – however it must be noted that for this project, higher-order corrections are included in all simulations, and the effects are propagated through to the end of the analysis. Therefore, measured values of A_β (and b_{Fierz} , though that is trivial) may be directly compared to theoretical predictions.
the "Physical Signature" section probably needs more work, but it's not getting it tonight.

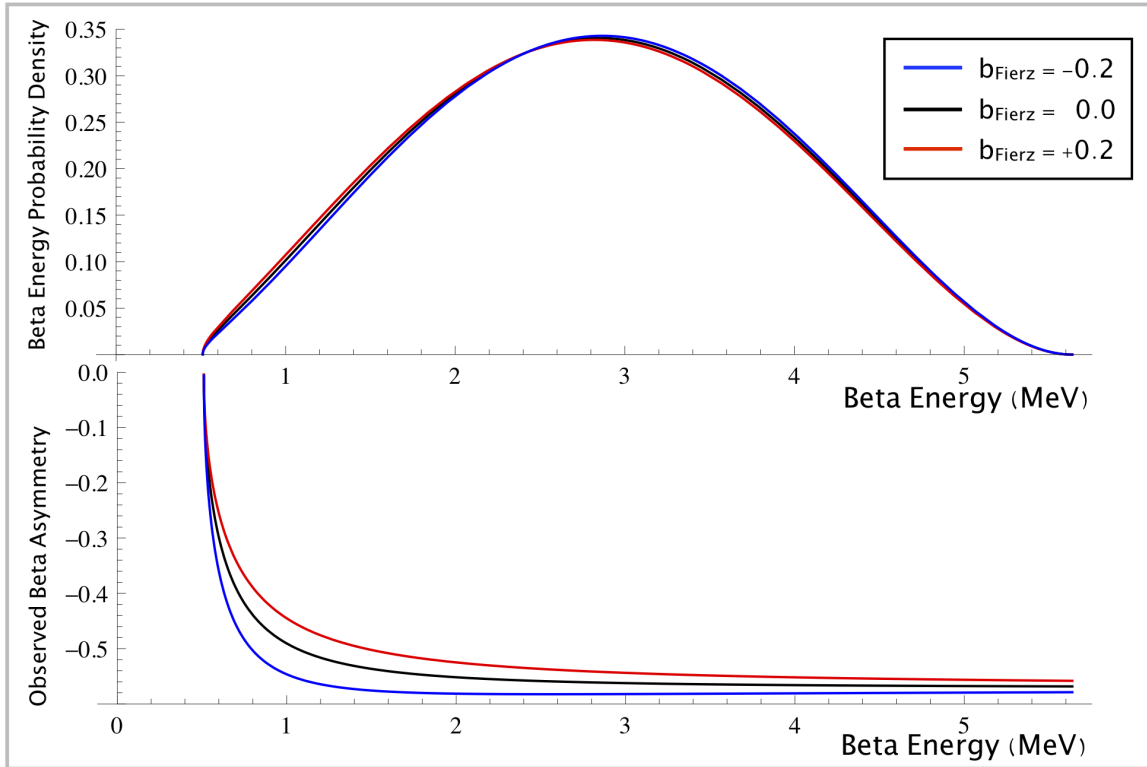


Figure 1.4: A naive beta energy spectrum (top) and superratio asymmetry (bottom) are constructed to measure b_{Fierz} .

JB on simple things still missing:

Intro or theory section:

...

$$P(\cos(\theta)) = 1 + b_m/E + P \text{Abeta} v/c \cos(\theta)$$

where theta is the angle between beta and polarization direction

...

Higher-order corrections to this equation (citing your appendices and/or chapters) are included in the simulation, so you are extracting b and Abeta in this equation to be compared with theory

...

{This is a simple but vital statement– some people actually extract Abeta(Ebeta=0) without recoil-order corrections, which is not the same parameter.}

...

The theory prediction for Abeta (citing Fenker PRL) is X.

The theory prediction for bFierz is 0 (maybe you have that already).

JB on that missing figure that I've now put in: "A dependence of Abeta on beta energy is also introduced.

UCNA fits energy spectrum and Abeta[Ebeta] simultaneously now."

The point is, the presence of either scalar or tensor interactions will produce a b_{Fierz} term in the decay PDF. It has other effects on the PDF, but those come in at higher-order in the tiny scalar and tensor couplings. So, the Fierz term would be by far the biggest thing that changes in the PDF. The PDF describes the energy and momentum of the outgoing beta w.r.t. a variety of other things. Notably, we can write an elegant-ish description of beta momentum w.r.t. nuclear polarization direction, and ignore the neutrino completely after integrating over it. We have a PDF in beta *direction* (w.r.t. polarization), and beta *energy*. To lowest order (and lowest order is best order) the distribution w.r.t. polarization direction doesn't change, but the distribution w.r.t. energy does change. Or ... something? The point is, it makes a change in the beta energy spectrum. This change is most pronounced at low energies, because the Fierz term is scaled by $(1/E_\beta)$. However, the asymmetry is also a function of E_β . A different function of E_β . In fact, it is scaled by (p_β/E_β) within the PDF, which is distinctly different than b_{Fierz} . So, one might ask what effect a b_{Fierz} term would produce on a constructed asymmetry spectrum.This explanation has gone way off track.

Here's a reference to the picture that shows the result of a non-zero b_{Fierz} term. It's Fig. 1.4.

Kludge-deleted section: "On the Superratio, the Supersum, and the Constructed Asymmetry"

Clean Superratio,Supersum,Super-Asymmetry section. Prolly merge w/ bFierz section.

JB: You need to at some point say that the supersum is the beta energy spectrum. There are experiments trying to do this method better, but they are very difficult. UCNA published a combined energy spectrum and Abeta[Ebeta] analysis on the neutron in March 2020 [41].

...

MJA: I can't help but also notice the follow-up article from September 2020 [5]. Ugh.

The data can be combined into a superratio asymmetry. This has the benefit of causing many systematics to cancel themselves out at leading order. It also will increase the fractional size of the effects we're looking for. This can be shown by using math.

Not all systematics effects are eliminated. We'll want to be careful to propagate through any effects that are relevant. Using the superratio asymmetry as our physical observable makes this process a bit messier for the things that don't cancel out, but it's all just math. Some other groups have performed similar measurements using the supersum as the physical observable. There are pros and cons to both methods. I can show, using a back-of-the-envelope calculation, that for this particular dataset, the superratio asymmetry method produces a better result.

"This is shown in full detail in Appendix E."

You really need a literature reference to the superratio method here. I know you have one. Danny gave us one a long time ago.

If you're not going to do this back-of-envelope calculation here, you need to just reference Appendix D and likely eliminate this paragraph?

Chapter 2

Considerations and Implementation of Atomic Techniques

2.1 An Overview of Magneto-Optical Traps

Since its initial description by Raab et. al. in 1987 [42], the magneto-optical trap (MOT) has become a widely used technique in many atomic physics laboratories. The MOT produces confined samples of cold, electrically neutral and isotopically pure atoms confined within a small spatial region. It is these properties that make the MOT a valuable tool not only in atomic physics, but for precision measurements in nuclear physics as well, and the TRIUMF Neutral Atom Trap (TRINAT) collaboration has adopted the technique wholeheartedly.

The technique is used predominantly with alkalis due to their simple orbital electron structure, and once set up it is quite robust. The MOT's trapping force is specific to the isotope for which the trap has been tuned. This feature makes it ideal for use in precision radioactive decay experiments, since the daughters are unaffected by the trapping forces keeping the parent confined.

A typical MOT can be created from relatively simple components: a quadrupole-shaped magnetic field, typically generated by two current-carrying coils of wire, and a circularly polarized laser tuned to match one or more atomic transitions in the isotope of interest. Because a MOT is easily disrupted by interactions with untrapped atoms, the trap must be created within a vacuum system. Finally, a source of atoms to be trapped is required. See Fig. 2.1.

In order to understand the mechanism by which a MOT is able to confine atoms, we must first introduce the Zeeman effect (Section 2.1.1) and a description of an optical molasses (Section 2.1.2). A functional MOT combines the forces resulting from these two physical effects to trap and cool atoms.

2.1.1 Zeeman Splitting

In the presence of an external magnetic field \vec{B} , the Hamiltonian associated with an atom's orbital electrons will acquire an additional "Zeeman Shift" term, given by [43]

$$H_{\text{Zeeman}} = -\vec{\mu} \cdot \vec{B}, \quad (2.1)$$

where $\vec{\mu}$ is the magnetic moment associated with the orbital under consideration. In the limit where the magnetic field is too weak to significantly disrupt the coupling between the electron's spin- and orbital angular momenta, $\vec{\mu}$ may be treated as being fixed with respect to changes in the magnetic field. It is this weak field regime which will be primarily of interest to us in work with magneto-optical traps.

With $\vec{\mu}$ fixed, it is clear that the magnitude of the energy shift must scale linearly with the strength of the magnetic field. In considering the perturbation to the energy of a particular *transition*, the perturbations to the initial and final states must of course be subtracted:

$$\Delta E_{\text{transition}} = -(\vec{\mu}_f - \vec{\mu}_i) \cdot \vec{B}. \quad (2.2)$$

When this is combined with a circularly polarized laser beam, the effect is to move the atomic resonance closer to- or farther from- the frequency of the laser. The circular polarization, combined with some selection rules, means a circularly polarized laser will only couple to one particular transition, w.r.t. angular momentum. ie, for a σ_+ polarized laser, the atom's overall angular momentum projection (along some axis) will be incremented by +1. The Zeeman shift means that in a magnetic field, this transition ($M+=1$) not be the same as the $M=1$ transition. So, if you have a magnetic field that changes linearly across space, you can make it so that in $+B_z$ regions, the laser beam with one certain polarization is closer to resonance and therefore more likely to be absorbed – and similarly, in $-B_z$ regions, a different laser with the opposite polarization will be more likely to be absorbed. Again, if the B-field is linear in space, you can do it so that as the atoms get further and further from the ‘centre’ region, the effect gets progressively stronger. So, if you’ve done this right, you can make it so that the atoms get a stronger “push” back towards the center the farther away they’ve drifted.

They still get the optical molasses cooling effect for free.

2.1.2 Doppler Cooling

We consider a setup in which a cloud of two-level atoms lies along the path of two counter-propagating laser beams, both tuned to resonance. For simplicity, we treat this cloud as being one dimensional along the axis of laser propagation. With two counter-propagating laser beams of equal intensity and detuning, the “push” from interaction with one beam is, on average within the lab frame, perfectly counteracted by the push from the opposite-propagating beam, so there is no net velocity transfer to a cloud initially at rest. These pushes, however, are applied on the level of the individual atom, and are the result of individual photons being absorbed and emitted. Because this process is probabilistic rather than deterministic, each individual atom will undergo a random walk.

...and opposite polarization. Or something. I have to talk about the selection rules somewhere else.

We now consider the effect of detuning on this process. We will suppose that both lasers are equally detuned slightly to the red of resonance. This will obviously decrease absorption by atoms at rest within the lasers’ path – however the atoms within the cloud are not at rest, but rather are undergoing thermal motion. As such, within the rest frame of each individual atom, the two laser beams will appear to be Doppler shifted in opposite directions, with the sign dependent on atomic motion. In particular, atoms moving against a laser’s direction of propagation will see that laser beam as being blueshifted within their own rest frame. Since the laser was redshifted relative to resonance within the lab frame, adding an additional blueshift will serve

to bring the photons' energy back towards resonance, making them more likely to be absorbed. For this same atom, the laser propagating in the same (lab frame) direction as the atom itself will appear further redshifted, and its photons are less likely to be absorbed.

The result of many such atom-photon interactions is that an individual atom, no matter which way it's moving at any given time, will absorb more photons from the direction where the momentum transfer slows them down, and fewer from the direction where the momentum transfer speeds them up. In short, each individual atom is *greatly* slowed down. At the macroscopic level, this translates to a decrease in the *temperature* of the atom cloud. Such a setup is sometimes referred to as a (one-dimensional) "optical molasses" due to the viscous drag force induced on atomic motion, and it is straightforward to extend this model to three dimensions.

Although this setup will decrease atomic velocity, it does not create a confining force, so (eg, in three dimensions) the atoms are still free to move out of the lasers' path, albeit at a decreased speed.

...This will slow the atom down, at least up to a limit related to the linewidth of the atomic transition and/or the laser. There's something to look up.

2.1.3 Atom Trapping with a MOT

A Magneto-optical trap (MOT) combines the slowing features of an optical molasses (Sec. 2.1.2) with the Zeeman splitting (Sec. 2.1.1) arising from a quadrupolar magnetic field, to produce a robust and isotope-specific trapping force in all three dimensions. The quadrupolar magnetic field is typically generated using a Helmholtz coil surrounding the space in which the trap is formed. The quadrupole shape of the field implies that it must be zero at some central point between the two coils, and in the space nearby, the magnitude of the magnetic field increases linearly in every direction as one moves away from the centre.

The retroreflecting lasers are red-detuned and circularly polarized in a direction selected to couple to the Zeeman shifted energy level which will push a given atom towards the centre. This provides a restoring force in all three dimensions to atoms that have moved too far from the centre. See Fig. 2.1.

Upon decay, atoms literally aren't trapped anymore by the trap. No trapping forces, no slowing forces, because it's all isotope-specific. This is super useful for us.

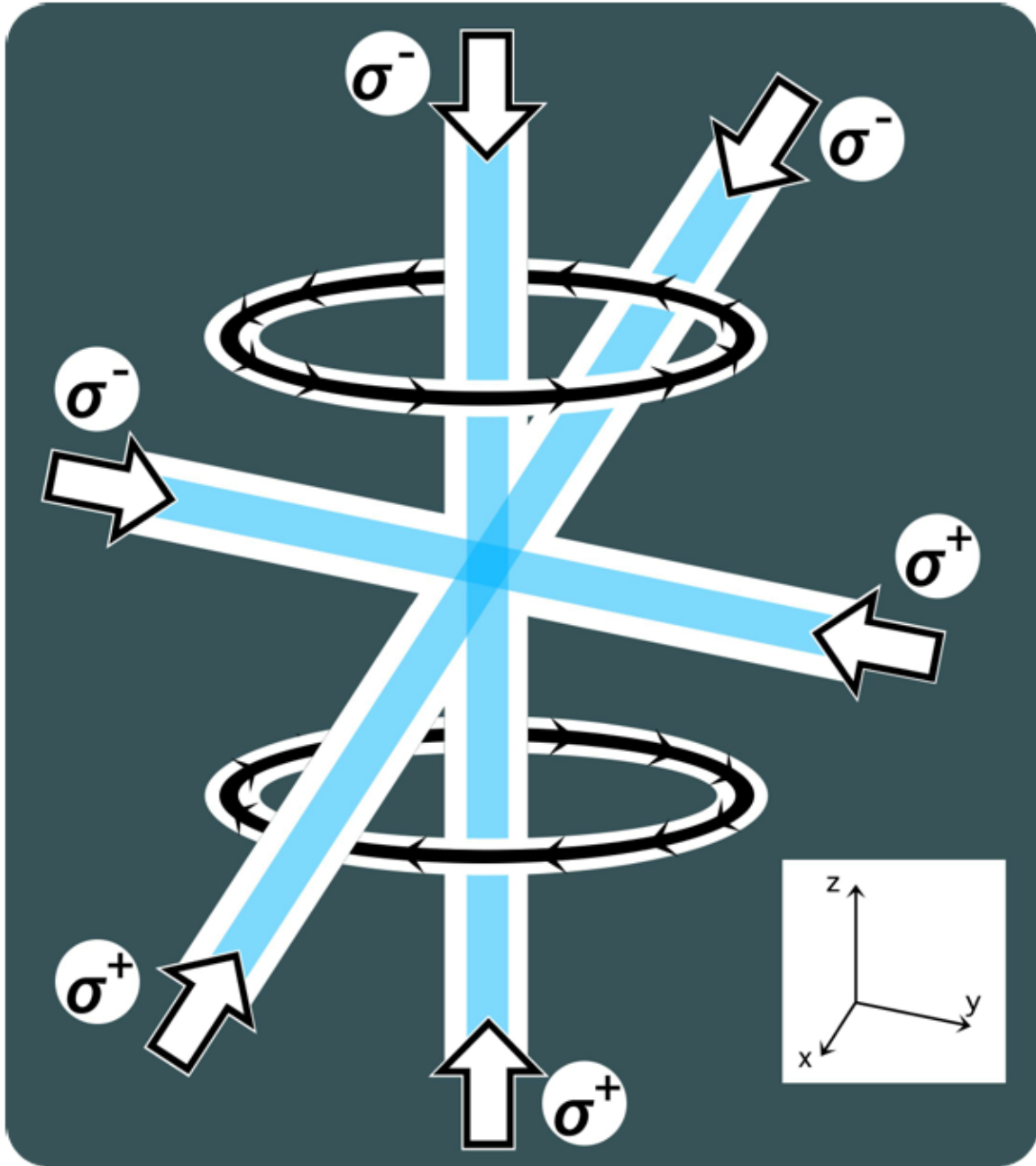


Figure 2.1: Components of a magneto-optical trap, including current-carrying magnetic field coils and counterpropagating circularly polarized laser beams. Diagram taken from [3]

2.2 Optical Pumping

Direct quote from John follows below:

The optical pumping process is described in detail within our collaboration's Ref. [44]. The primary detail described here is that the optical pumping is disturbed by any component of magnetic field not along the quantization axis. (Ours is the vertical axis, defined by the direction of the optical pumping light, and along which the detectors are placed.) This required sophistication with an AC-MOT described in Section 2.4 below.

End quote from John.

JB says: "I would say you don't need an atomic level diagram. You could just describe in words the semiclassical picture of atoms absorbing photons until they are nearly fully polarized, then they stop absorbing. The optical pumping + photoionization is then an *in situ* probe of the polarization. ... You would need to add in words that quantum mechanical corrections to this picture are in the optical Bloch equation approach in B. Fenker et al. The depolarized states still have high nuclear polarization (1/2 for $F = 2, M_F = 1$, 5/6 for $F = 1, M_F = 1$) and determining the ratio of those two populations provides most of the info we need – we model with the O.B.E, measure the optical pumping light polarization, and float an average transverse magnetic field. This is adequate to determine the depolarized fraction to 10% accuracy, which is all that is needed."

2.3 An Overview of the Double MOT System and Duty Cycle

put this in! "...and is designed to operate at ultra-high vacuum (UHV) to minimize trap losses from collisions." Also, I think it helps prevent sparking?

Remember the pulser LED! To evaluate the stability of the scintillator gain!

We obtain a sample of neutral, cold, nuclear spin-polarized ^{37}K atoms with a known spatial position, via the TRIUMF accelerator facility, by intermittently running a magneto-optical trap (MOT) to confine and cool the atoms, then cycling the trap off to polarize the atoms. With β detectors placed opposite each other along the axis of polarization, we are able to directly observe the momenta of β^+ particles emitted into 1.4% of the total solid angle nearest this axis. We also are able to extract a great deal of information about the momentum of the recoiling ^{37}Ar daughters by measuring their times of flight and hit positions on a microchannel plate detector with a delay line. Because the nuclear polarization is known to within < 0.1% [44], and we are able to account for many systematic effects by periodically reversing the polarization and by collecting unpolarized decay data while the atoms are trapped within the MOT, we expect to be well equipped to implement a test of 'handedness' within the nuclear weak force.

The experimental subject matter of this thesis was conducted at TRIUMF using

the apparatus of the TRIUMF Neutral Atom Trap (TRINAT) collaboration. The TRINAT laboratory offers an experimental set-up which is uniquely suited to precision tests of Standard Model beta decay physics, by virtue of its ability to produce highly localized samples of cold, isotopically pure atoms within an open detector geometry. Although the discussion in this chapter will focus on the methodologies used to collect one particular dataset, taken over approximately 7 days of beamtime in June 2014, the full apparatus and the techniques used are fairly versatile, and can be (and have been) applied to several related experiments using other isotopes.

Surely most of this paragraph goes in an intro chapter somewhere.

Cite a bunch of papers here.

TRINAT DOUBLE MOT TRAPPING SYSTEM

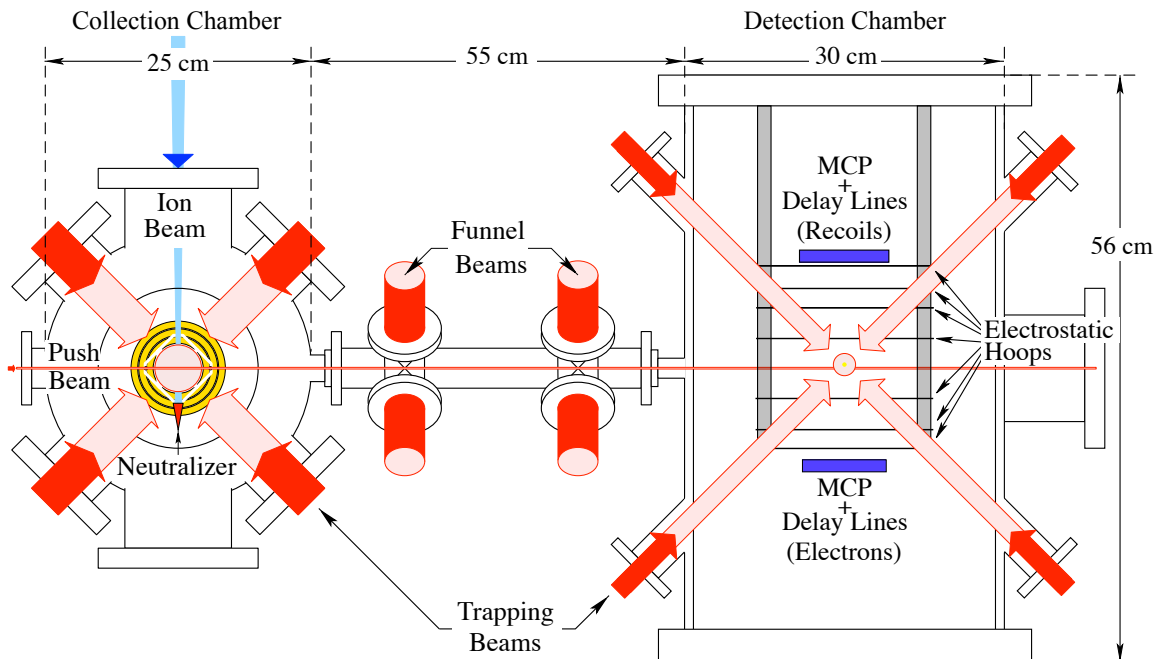


Figure 2.2: The TRINAT experimental set-up, viewed from above. The two MOT system reduces background in the detection chamber. Funnel beams along the atom transfer path keep the atoms focused.

Figure was originally created by Alexandre, modified by ... someone else? Or Alexandre? And I got it from ... probably an experimental proposal? I should figure out how to cite a proposal...

The TRINAT lab accepts radioactive ions delivered by the ISAC beamline at TRIUMF. These ions are collected on the surface of a hot zirconium foil where they are electrically neutralized, and subsequently escape from the foil into the first of two experimental chambers (the “collection chamber”). Further details on the neutral-

ization process are presented in a previous publication [45]. Within the collection chamber, atoms of one specific isotope – for the purposes of this thesis, ^{37}K – are continuously collected into a magneto-optical trap from the tail end of the thermal distribution. Although this procedure preferentially traps only the slowest atoms, once trapped, atoms will be cooled further as a side-effect of the MOT's trapping mechanism. The result is a small (~ 1 mm diameter), cold (~ 1 mK) cloud of atoms of a particular isotope.

made possible by UHV!

These properties of the atomic cloud allow for a relatively clean transfer of linear momentum from an appropriately tuned laser beam to the atoms within the cloud, and we use this mechanism to “push” the atoms out of the collection MOT and into the “detection chamber”, where they are loaded into a second MOT (see Fig. 2.2). During regular operation, atoms are transferred approximately once per second.

There is no need to release previously trapped atoms in the second MOT when a new group of atoms is loaded. Although the trap loses atoms over time as a result of a variety of physical processes, during typical operation the majority of atoms loaded in a given transfer will still be trapped at the time the next set of atoms is loaded, and after several transfer cycles, something like a steady state is obtained.

discussed ... idk, somewhere else.

Because the transfer and trapping mechanisms rely on tuning laser frequencies to specific atomic resonances, these mechanisms act on only a single isotope, and all others remain unaffected. The result is a significant reduction of background contaminants within the detection chamber relative to initial beamline output. The transfer methodology is discussed in some detail within another publication [46].

We now turn our attention to what happens to the atom cloud in the detection chamber between loading phases (see Fig. 2.3). One of the goals for the 2014 ^{37}K beamtime required that the atom cloud must be spin-polarized, as well as being cold and spatially confined. Although the MOT makes it straightforward to produce a cold and well confined cloud of atoms, it is fundamentally incompatible with techniques to polarize these atoms. The physical reasons behind this are discussed in Section 2.4.

Once the newly transferred set of ^{37}K atoms has been collected into the cloud, the entire MOT apparatus cycles 100 times between a state where it is ‘on’ and actively confining atoms, and a state where it is ‘off’ and instead the atoms are spin-polarized by optical pumping while the atom cloud expands ballistically before being re-trapped. These 100 on/off cycles take a combined total of 488 ms. The laser components of the trap are straightforward to cycle on and off on these timescales, but the magnetic

I *do* discuss this, right? Right??

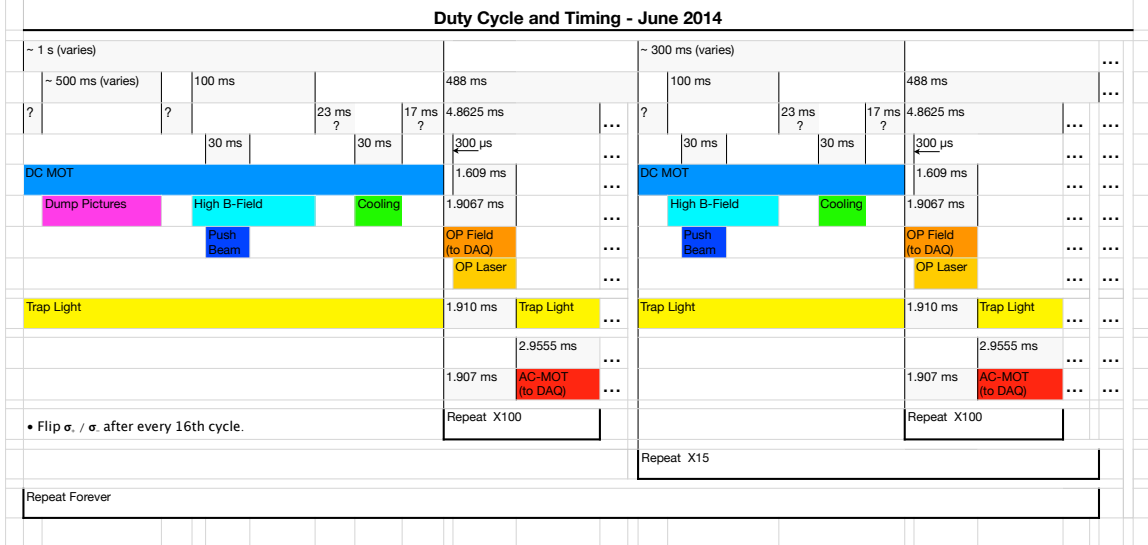


Figure 2.3: The duty cycle used for transferring, cooling, trapping, and optically pumping ^{37}K during the June 2014 experiment. Not drawn to scale. Question marks indicate timings that varied either as a result of electronic jitter or as a result of variable times to execute the control code. Atoms are transferred during operation of the DC-MOT. Though the push beam laser itself is only on for 30 ms, the bulk of the DC-MOT's operation time afterwards is needed to collect and cool the transferred atoms. After 100 on/off cycles of optical pumping and the AC-MOT, the DC-MOT resumes and the next group of atoms is transferred in. After 16 atom transfers, the polarization of the optical pumping laser is flipped to spin-polarize the atoms in the opposite direction, in order to minimize systematic errors.

field is much more challenging to cycle in this manner.

Immediately following each set of 100 optical pumping cycles, another set of atoms is transferred in from the collection chamber to the detection chamber, joining the atoms that remain in the trap (see Fig. 2.3). The details of the trapping and optical pumping cycles are described further in Section 2.4, and the optical pumping technique and its results for this beamtime are the subject of a recent publication [44].

2.4 The AC-MOT and Polarization Setup

Fix the phrasing of AC-MOT/OP experimental section. It's not passable, but still kind-of a mess.

The AC-MOT was first described by Harvey and Murray [47], but the TRINAT

collaboration has adopted its use because it enables the polarization-destroying magnetic field to be eliminated quickly after the MOT is shut off. [3]. A diagram of showing the operation phases of several key components in our AC-MOT/optical pumping duty cycle is shown in Fig. 2.4.

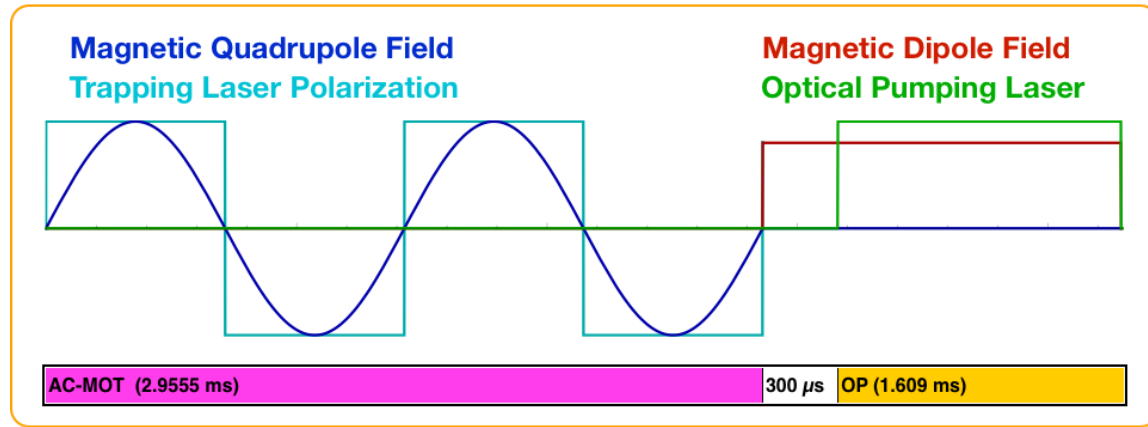


Figure 2.4: One cycle of trapping with the AC-MOT, followed by optical pumping to spin-polarize the atoms. After atoms are transferred into the science chamber, this cycle is repeated 100 times before the next transfer. The magnetic dipole field is created by running parallel (rather than anti-parallel as is needed for the MOT) currents through the two coils.

A standard DC-MOT operates continuously, and in the presence of electrically conductive materials especially, the magnetic field can take a (comparatively) long time to dissipate. This is problematic for an experiment such as this one, because the atoms do not remain confined while the magnetic field dissipates due to potential anomalies in the magnetic field shape arising from induced eddy currents, and for similar reasons, they cannot be successfully optically pumped during this time period either. Therefore, it is important to waste as little time as possible switching between the MOT and the optical pumping phases in the duty cycle. For optical pumping, a weak, dipole-shaped magnetic field is preferred, and this is not possible while the quadrupole field has not dissipated.

The principle behind the AC-MOT is to simply run a sinusoidal current through one's anti-Helmholtz coils while flipping the laser polarization to remain in sync.

Eddy currents in your nearby metal objects will still be produced, and these changing eddy currents will *also* create a sinusoidally oscillating magnetic field. If correctly timed, it is possible to eliminate the current in the anti-Helmholtz coils at the precise time when the eddy currents are also eliminated. This process can easily reduce the size of any eddy currents still produced by around an order of magnitude or more, and these remaining eddy currents decay more rapidly as well.

This content *came from* that other section, and needs to go in here somewhere: “Many laser ports to make the MOT functional, and for optical pumping. Fancy mirror geometry to combine optical pumping and trapping light along the vertical axis. Water-cooled (anti-)Helmholz coils within the chamber for the AC-MOT, fast switching to produce an optical pumping field.”

... Sadly, this also removes our trapping mechanism. We could keep the optical molasses after the field is off if we wanted to, but we don’t, because we wouldn’t be able to optically pump the atoms then. But at least the atoms are cold-ish (we can measure! I think it’s done indirectly in that one table, or for realgies in Ben’s thesis), so we can let them just chill for a little while before we have to re-trap them. Don’t lose too much. (How much do we lose? Have we quantified that somewhere? Probably.). ...

begin content of the historical other AC-MOT+Polarization section.

Probably document things about the waveform and frequency used for the beamtime, since I don’t think it’s in my MSc.

As alluded to in the previous section (2.3), the measurements in question required a spin-polarized sample of atoms, and a precise knowledge of what that polarization was. This is needed in order to make best use of the superratio asymmetry for both A_β and b_{Fierz} measurements. [48][44].

A MOT requires a quadrupolar magnetic field, and we generate ours with two current-carrying anti-Helmholtz coils located within the vacuum chamber itself. Since these coils are expected to run an alternating current, heat is produced and cannot be dissipated in the vacuum. Therefore the coils themselves are hollow copper tubes, and they are continuously cooled by pumping temperature-controlled water through them.

Note that because the atoms within a MOT can be treated as following a thermal distribution, some fraction of the fastest atoms continuously escape from the trap’s potential well. Even with the most carefully-tuned apparatus, the AC-MOT cannot quite match a similar standard MOT in terms of retaining atoms. The TRINAT AC-MOT has a ‘trapping half-life’ of around 6 seconds, and although that may not be particularly impressive by the standards of other MOTs, it is more than adequate for our purposes. ^{37}K itself has a radioactive half-life of only 1.6 seconds (cite someone), so our dominant loss mechanism is radioactive decay rather than thermal escape.

We spin-polarize ^{37}K atoms within the trapping region by optical pumping [44]. A circularly polarized laser is tuned to match the relevant atomic resonances, and is directed through the trapping region along the vertical axis in both directions. When a photon is absorbed by an atom, the atom transitions to an excited state and its total angular momentum (electron spin + orbital + nuclear spin) along the vertical axis is incremented by one unit. When the atom is de-excited a photon is emitted isotropically, so it follows that if there are available states of higher and lower angular momentum, the *average* change in the angular momentum projection is zero. If the atom is not yet spin-polarized, it can absorb and re-emit another photon, following a biased random walk towards complete polarization.

In order to optimally polarize a sample of atoms by this method, it is necessary to have precise control over the magnetic field. This is because absent other forces, a spin will undergo Larmor precession about the magnetic field lines. In particular, the magnetic field must be aligned along the polarization axis (otherwise the tendency will be to actually depolarize the atoms), and it must be uniform in magnitude over the region of interest (otherwise its divergencelessness will result in the field also having a non-uniform direction, which results in a spatially-dependent depolarization mechanism). Note that this type of magnetic field is not compatible with the MOT, which requires a linear magnetic field gradient in all directions (characteristic of a quadrupolar field shape), and has necessitated our use of the AC-MOT.

2.5 Measurement Geometry and Detectors

The TRINAT detection chamber operates at ultra-high vacuum (UHV) and provides not only the apparatus necessary to intermittently confine and then spin-polarize atoms, but also the variety of detectors and implements required to quantify their position, temperature, and polarization. The detection chamber further boasts an array of electrostatic hoops to collect both positively and negatively charged low energy particles into two opposing microchannel plate (MCP) detectors, each backed by a set of delay lines to measure hit position, and a further set of two beta detectors positioned across from each other along the polarization axis, each of which consists of a 40x40 pixel double-sided silicon strip detector (DSSD) and a scintillator coupled to a photomultiplier tube (PMT) (see Fig. 2.5). The chamber also includes 6 view-

ports specifically designed to be used for the trapping and optical pumping lasers (see Fig. 2.6.).

2.5.1 Microchannel Plates and Electrostatic Hoops

Two stacks of microchannel plates (MCPs) have been placed on opposing sides of the chamber, and perpendicular to the axis of polarization. Each stack of MCPs is a relatively large detector backed by a series of delay lines for position sensitivity. These two MCP detectors are designed to operate in conjunction with a series of seven electrostatic ‘hoops’ positioned within the chamber and connected to a series of high voltage power supplies. The hoops are designed in such a way as to maintain a constant and (roughly) uniform electric field across the space between the two MCP detectors, without blocking either the path of particles originating from the central cloud, or necessary laser beams. The resulting electric field acts to pull positively charged ions towards one MCP detector and negatively charged electrons towards the other (see Figs. 2.5 and 2.6).

The detector intended to collect the negatively charged electrons (the “eMCP”) has an active area of 75.0 mm, and is positioned 100.0 mm from the chamber centre. It features a Z-stack configuration of three plates, and it is backed by a set of three separate delay lines in a “hexagonal” arrangement for redundant position sensitivity (the “HEX75”). The detector used to collect positively charged ions (the “iMCP,” or equivalently the “rMCP” since many of the ions collected are recoils from decay) is 80.0 mm in diameter and positioned 101.4 mm from the chamber centre. It features only two plates arranged in a chevron configuration, and it is backed by a set of two separate delay lines (the “DLD80”) for position sensitivity. In the context of the present work, the rMCP data is used primarily in conjunction with the photoionization laser to characterize the atom cloud (Section 2.5.3), while the eMCP data is used, together with the beta detectors, as a ‘tag’ for decay events originating from the cloud.

Due to an unfortunate interaction between the two MCP detectors, during the 2014 beamtime it was not possible to run both the eMCP and the rMCP simultaneously without producing a large background on at least one detector (there seemed to be no consistency as to which detector was most affected at a given time). As a result, data was instead collected with only one MCP detector biased at a time, and

Do I talk about how this works somewhere? Probably in that section on cuts.

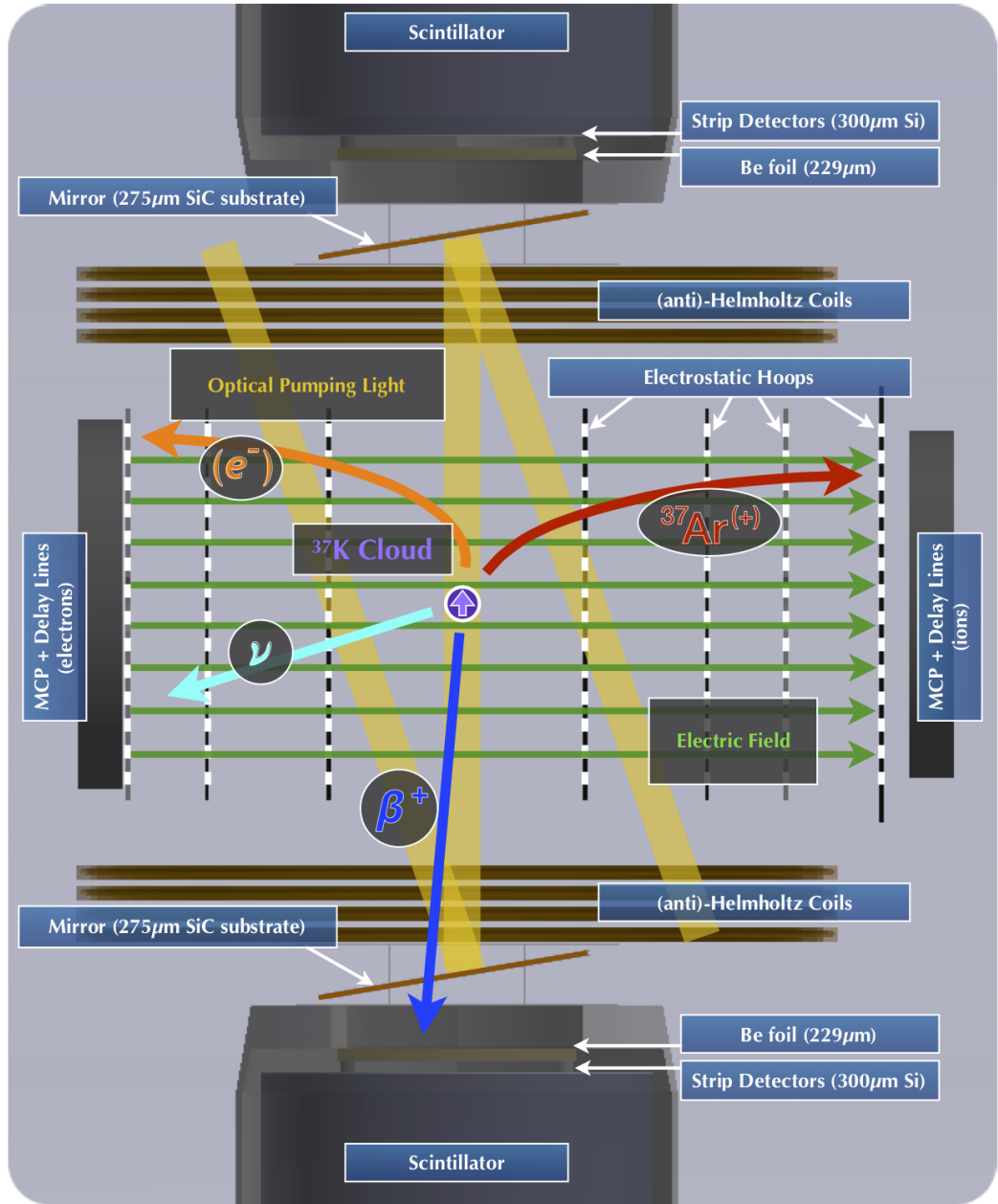


Figure 2.5: A scale diagram of the interior of the TRINAT detection chamber, shown edge-on with a decay event. After a decay, the daughter will be unaffected by forces from the MOT. Positively charged recoils and negatively charged shake-off electrons are pulled towards detectors in opposite directions. Although the β^+ is charged, it is also highly relativistic and escapes the electric field with minimal perturbation.

rMCP is 101.4 mm from center, eMCP is 100 mm from center. Do I say this somewhere else?

the active detector was alternated every few hours to spend approximately equal time collecting data with the eMCP and rMCP. Online scientific data has been collected with the eMCP at electric field strengths of 66.7 V/cm and 150. V/cm, while rMCP data has been collected at 395. V/cm, 415. V/cm, and 535. V/cm. Note that these field strengths are all too low to significantly perturb any but the least energetic of the (positively charged) betas originating from decay, and those betas already lack the energy that would be needed to travel through the SiC mirror and Be foil vacuum seal into a beta detector.

Reference that one table.

2.5.2 Beta Detectors

The beta detectors, located above and below the atom cloud along the axis of polarization (Fig. 2.5), are each the combination of a plastic scintillator and a set of silicon strip detectors. Using all of the available information, these detectors are able to reconstruct the energy of an incident beta, as well as its hit position, and provide a timestamp for the hit's arrival. Together the upper and lower beta detectors subtend approximately 1.4% of the total solid angle as measured with respect to the cloud position.

The two sets of beta detectors were positioned directly along the axis of polarization. Each beta detector consists of a plastic scintillator and photo-multiplier tube (PMT) placed directly behind a 40×40-pixel double-sided silicon strip detector (DSSD). The scintillator is used to measure the overall energy of the incoming particles, as well as to assign a timestamp to these events, while the DSSD is used both to localize the hit position to one (or in some cases, two) individual pixel(s), and also to discriminate between different types of incoming particles. In particular, though the scintillator will measure the energy of an incoming beta or an incoming gamma with similar efficiency, the beta will lose a portion of its kinetic energy as it passes through the DSSD into the scintillator. By contrast, an incident gamma will deposit only a very small amount of energy in the DSSD layer, making it possible to reject events with insufficient energy deposited in the DSSD as likely gamma ray events. Given that the decay of interest to us emits positrons, we expect a persistent background 511 keV gamma rays that are not of interest to us, so it is extremely important that we are able to clean these background events from our spectrum.

There's gotta be a better way to describe it

what's the open area of the detector? how big is each pixel?

It must be noted that the path between the cloud of trapped atoms and either

beta detector is blocked by two objects: a $275\text{ }\mu\text{m}$ silicon carbide mirror (necessary for both trapping and optical pumping), and a $229\text{ }\mu\text{m}$ beryllium foil (separating the UHV vacuum within the chamber from the outside world). In order to minimize beta scattering and energy attenuation, these objects have had their materials selected to use the lightest nuclei with the desired material properties, and have been manufactured to be as thin as possible without compromising the experiment. As the $^{37}\text{K} \rightarrow ^{37}\text{Ar} + \beta^+ + \nu_e$ decay process releases $Q = 5.125\text{ MeV}$ of kinetic energy [49], the great majority of betas are energetic enough to punch through both obstacles without significant energy loss before being collected by the beta detectors.

2.5.3 The Photoionization Laser

In order to measure properties of the trapped ^{37}K cloud, a 10 kHz pulsed laser at 355 nm is directed towards the cloud. These photons have sufficient energy to photoionize neutral ^{37}K from its excited atomic state, which is populated by the trapping laser when the MOT is active, releasing 0.77 eV of kinetic energy, but do not interact with ground state ^{37}K atoms. The laser is of sufficiently low intensity that only $\sim 1\%$ of excited state atoms are photoionized, so the technique is only very minimally destructive.

Probably worth mentioning that we test this stuff offline on stable ^{41}K . But also, surely it should be mentioned in like the AC-MOT/Polarization section too.

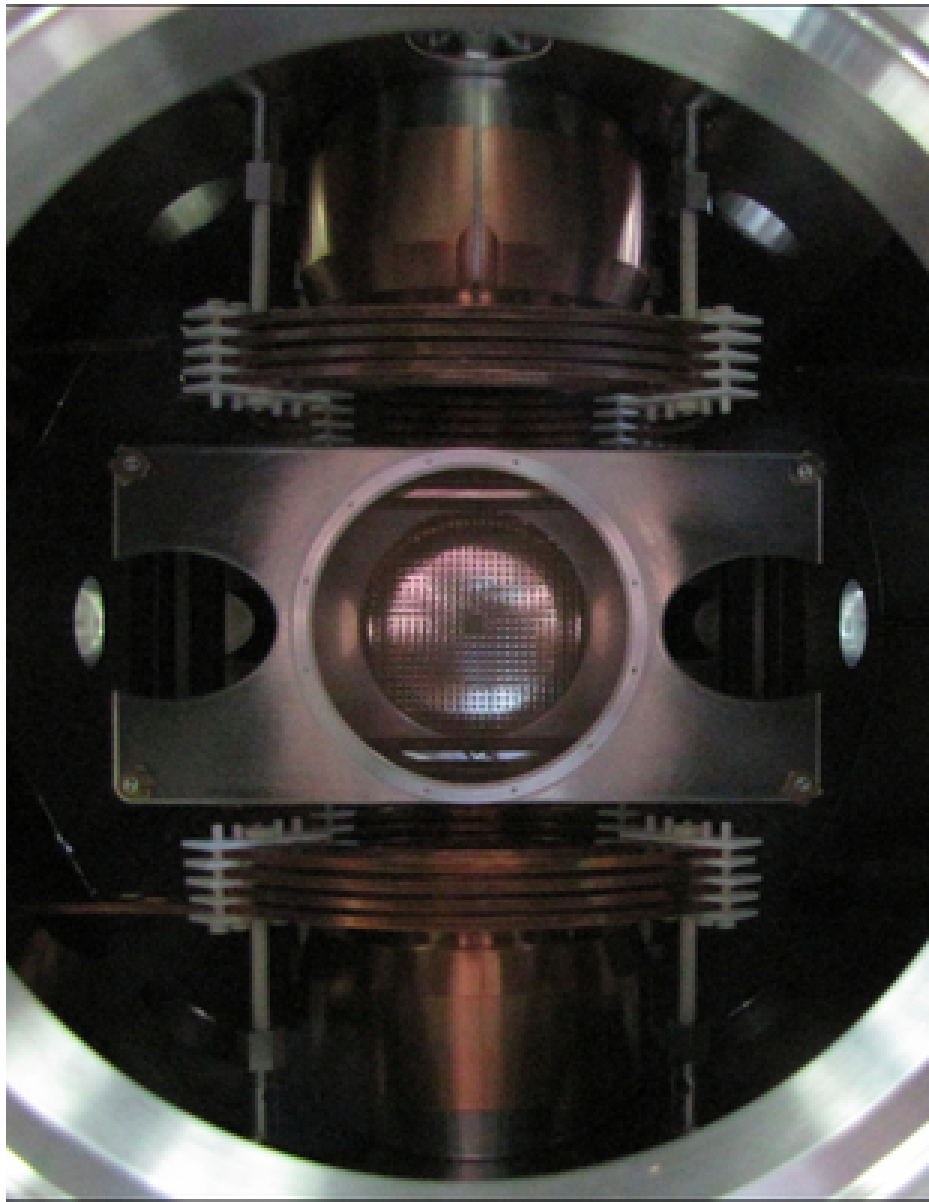
Because an electric field has been applied within this region (Section 2.5.1) the $^{37}\text{K}^+$ ions are immediately pulled into the detector on one side of the chamber, while the freed e^- is pulled towards the detector on the opposite side of the chamber. Because $^{37}\text{K}^+$ is quite heavy relative to its initial energy, it can be treated as moving in a straight line directly to the detector, where its hit position on the microchannel plate is taken as a 2D projection of its position within the cloud. Similarly, given a sufficient understanding of the electric field, the time difference between the laser pulse and the microchannel plate hit allows for a calculation of the ion's initial position along the third axis.

As a check: the camera measurements for photons from de-excitation. It's aimed 35 degrees from vertical, with its horizontal axis the same as one of the other axes. I think it's the TOF axis. I can check this when my computer comes back. Also, there's an unknown additional delay between some of our DAQ channels that can't be explained by accounting for cable lengths, so we really like having the check there.

JB says: “yes, camera x-axis is tof axis.”

With this procedure, it is possible to produce a precise map of the cloud’s position and size, both of which are necessary for the precision measurements of angular correlation parameters that are of interest to us here. However, it also allows us to extract a third measurement: the cloud’s polarization.

The key to the polarization measurement is that only atoms in the excited atomic state can be photoionized via the 355 nm laser. While the MOT runs, atoms are constantly being pushed around and excited by the trapping lasers, so this period of time provides a lot of information for characterizing the trap size and position. When the MOT is shut off, the atoms quickly return to their ground states and are no longer photoionized until the optical pumping laser is turned on. As described in Section 2.2, and in greater detail in [44], the optical pumping process involves repeatedly exciting atoms from their ground states until the atoms finally cannot absorb any further angular momentum and remain in their fully-polarized (ground) state until they are perturbed. Therefore, there is a sharp spike in excited-state atoms (and therefore photoions) when the optical pumping begins, and none if the cloud has been fully polarized. The number of photoion events that occur once the sample has been maximally polarized, in comparison with the size and shape of the initial spike of photoions, provides a very precise characterization of the cloud’s final polarization [44].



Chamber walls are made from 316-L stainless steel, chosen for strength, cost, and minimal eddy currents.

Figure 2.6: Inside the TRINAT detection chamber. This photo is taken from the vantage point of one of the microchannel plates, looking into the chamber towards the second microchannel plate. The current-carrying copper Helmholtz coils and two beta telescopes are visible at the top and bottom. The metallic piece in the foreground is one of the electrostatic hoops used to generate an electric field within the chamber. The hoop's central circular hole allows access to the microchannel plate, and the two elongated holes on the sides allow the MOT's trapping lasers to pass unimpeded at an angle of 45 degrees 'out of the page'.

Chapter 3

Calibrations and Data Selection

In a precision measurement, the bulk of the research is in determining the systematic uncertainties through self-consistent analysis and simulation. Each detector in this experiment is critical and has independent calibrations and cuts, which are described in detail in this chapter. Because this analysis was not blinded, there is an increased importance that the choice of cuts should be clearly justified. The main goal of blinding was nevertheless achieved — to make sure all analysis is done completely with full redundancy of checks wherever possible — so the discipline entailed must be described in full detail.

3.1 An Overview of Available Data

Although the detection chamber was designed to feature two MCP detectors on opposing sides of an applied electric field intended for simultaneous use (see Section 2.5.1), in practice the two detectors produced quite a bit of feedback when operated at the same time. In order to salvage usable data from the beamtime, it was necessary to run only one detector at a time, but switched which detector was in use every few hours, collecting approximately the same amount of data with each detector (see Tables 3.1 and 3.2). Thus, the runs are sorted into ‘electron’ and ‘recoil’ runs, depending on what the detector in use was intended to detect. The data is further split up into several runsets based on when certain settings were adjusted, and the individual runsets have been treated separately for nearly all parts of the analysis.

While the beta asymmetry and Fierz interference are best evaluated using the

Electron Runs

	OP Delay	Events	Electric Field	Runs
Runset EA	$300\ \mu s$	0	66.67 V/cm	314, 362, 363, 383-386, 393.
Runset EB	$300\ \mu s$	173,640	150.0 V/cm	428-437, 440-445.
Runset EC	$700\ \mu s$	18,129	150.0 V/cm	476, 477.
Runset ED	$400\ \mu s$	207,596	150.0 V/cm	478-489, 502-505, 510, 513.

Ben doesn't seem to include Runs 436 and 437 in *any* set of good runs. Is it an oversight? I think they're perfectly legit electron runs. They're fairly long runs...

Table 3.1: A list of 2014 online electron runs with potentially usable data. The “Events” column includes only the number of events that passed all cuts.

Recoil Runs

	OP Delay	Electric Field	Runs
Runset RA	$300\ \mu s$	395.0 V/cm	303, 308-313, 318, 326, 327, 328, 340, 342, 343, 376, 377, 378, 394, 395, 396, 398-402.
Runset RB	$300\ \mu s$	535.0 V/cm	409-419, 421-426, 446, 447, 449.
Runset RC	$700\ \mu s$	395.0 V/cm	450, 454, 455.
Runset RD	$700\ \mu s$	415.0 V/cm	460-466, 473, 474.
Runset RE	$400\ \mu s$	415.0 V/cm	491, 497, 498, 499, 509.

Ben includes 448 as a ‘good’ recoil run. But I don’t. Why? Also 451, 451, 453. ...Also 467,468,469,470,471,472. Also-also, 492, 493, 494, 495, 496.

Table 3.2: A list of 2014 online recoil runs and associated parameters. A count of good events that pass all cuts is not included because different cuts must be used for polarization and trap position data.

electron runs, the polarization (a dominant uncertainty in the beta asymmetry measurement) and cloud position are best evaluated with recoil runs. The polarization measurement is the subject of a recent publication (see [44]), and the evaluation of cloud position is discussed in Section 3.4. The recoil runs may also be analyzed in the future as part of a search for right-handed Weak interactions (described further in Chapter 6.2).

In considering Tables 3.1 and 3.2, we note that Runsets EA and RA were neglected completely during analysis after it was determined that one scintillator had an improperly set hardware threshold such that lower energy betas weren’t being detected

at all. Additionally, there was a QDC module failure before Run 450, resulting in an abrupt change in calibration for the two scintillators. The electric field is larger during recoil runs in an attempt to maximize the fraction of nuclear recoils collected, as well as the separation in TOF between different charge states. For electron runs, although not all SOEs were collected, the lower electric fields were preferred in order to decrease background events and the sparking incidents. Although the final analysis uses only the eMCP runs directly, the result could not have been obtained with the same degree of precision had the rMCP data not been present.

3.2 Preliminary Data Selection with the rMCP

As described in Chapter 2.5.3, the primary function of the rMCP within the context of this experiment is as a probe of the atom cloud, and it provided a critical check of the cloud's position, size, and polarization state over the course of the beamtime. The process of cleaning, calibrating, and analyzing this data is described here.

The two delay lines located just behind the rMCP provide information about hit position. The principle behind a delay line's operation is relatively straightforward. The delay line itself is made from a thin wire wound into a flattened coil that covers the area of the microchannel plate. The second delay line is oriented perpendicular to the first and immediately behind it, but also covers the full area of the microchannel plate. When a charged particle is incident on the stack of microchannel plates, an electron shower is initiated. The shower gains strength as it propagates through the MCPs' microchannels, and emerges on the back side of the stack after having been greatly amplified.

After emerging from the back of the MCP stack, the electron shower is then incident on a delay line, generating an electrical pulse that propagates from the hit point towards both ends of the wire. Although the wire is conductive, the propagation speed is finite, and this fact is key to extracting the hit position. The time of arrival for the electrical pulse is recorded at each end of the delay line wire, and it is the difference between the two times that tells where along the wire the original hit occurred. In general, a single delay line is only precise enough to determine the hit position as projected along the direction perpendicular to its coil's wires. The electron shower continues past the first delay line to hit the delay line immediately

how precise is the rMCP supposed to do? in practice, it wasn't nearly that good.

behind, which again creates an electrical pulse that propagates towards the ends of that wire, and a similar procedure can be used to evaluate the hit position in the perpendicular direction. Therefore, for an event in which the rMCP is hit and an electron shower is triggered, we expect to have five timestamps associated with that hit – one associated with the MCP stack itself, and two from each delay line.

It's not really *every* event...

A diagram of how delay lines work would really help here, but there's no time for that. I'll put it in if someone asks.

Do I want the above section about how delay lines work to go in the other chapter? Maybe.

This understanding of how delay lines work informs the initial stages of data processing for rMCP events. To obtain the cleanest possible rMCP data, the first step is to simply throw out every event which doesn't have a complete set of five timestamps associated with it – even though it would still be possible to make good use of many events which have only partial data. Even though many “real” rMCP hit events came in under threshold in one or more channels, detector noise was plentiful, and that noise varied in both quality and quantity over the course of the beamtime. Therefore, it was decided to be more important for the rMCP data to be as clean as possible, despite the fact that its statistical power would be reduced. (Note that this step is *not* done on the eMCP side – more on that in Section 3.8)

The next stage of rMCP data cleaning is to discard events with an aberrant set of timestamps. A delay line is essentially just a long wire, and the time it takes to propagate a signal from one end of the wire to the other is fixed. This means that no matter where along the delay line a pulse is generated, if one adds rather than subtracts the timestamps at which the pulse arrives at each of the two ends, that sum should be constant after accounting for the time of the original hit – which we can determine from the timestamp associated with the MCP. To that end, we construct delay line sums for the “x” and “z” delay lines,

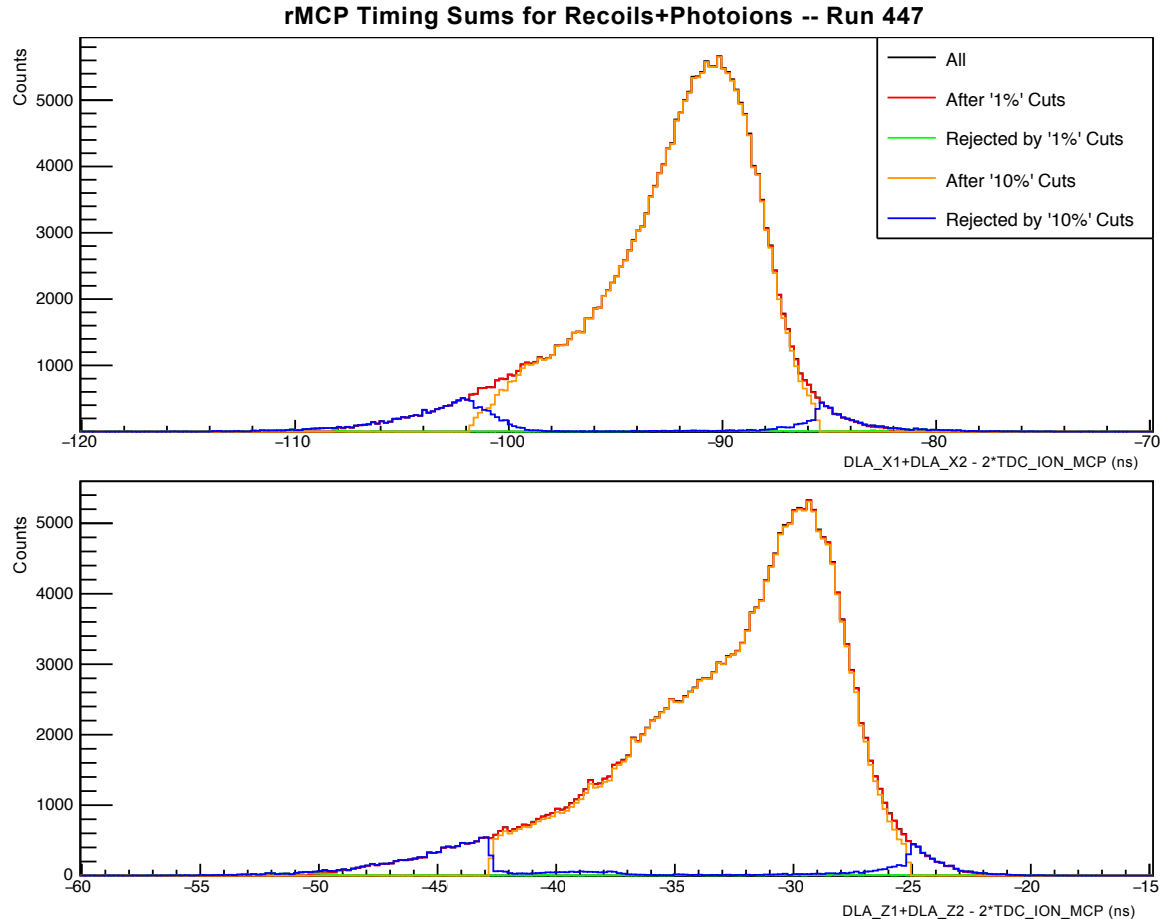
$$\text{DLA_XSUM} = (\text{TDC_DL_X1}) + (\text{TDC_DL_X2}) - 2(\text{TDC_ION_MCP}) \quad (3.1)$$

$$\text{DLA_ZSUM} = (\text{TDC_DL_Z1}) + (\text{TDC_DL_Z2}) - 2(\text{TDC_ION_MCP}). \quad (3.2)$$

OK, I have to *actually* discuss this a bit somewhere though.

For a perfectly operating detector, one would expect for a collection of many measurements of DLA_XSUM and DLA_ZSUM to each look like an isolated delta spike. In practice however, our distributions had a more complex set of features. The shapes, widths, and even positions of these distributions changed from run to run, and not all of these changes could be attributed to a known cause (e.g. a change in

detector settings). Distributions from a single run are shown in Fig. 3.1.



Are these things *definitely* in nanoseconds? Check!

Figure 3.1: Timing sums and associated cuts for the rMCP detector, run 447. The ‘10%’ cuts shown simply eliminate events in which the distribution’s height at that value is less than ‘10%’ of that distribution’s maximum, and the ‘1%’ cuts are performed in a similar manner. Note that this is *not* the equivalent of eliminating 10% (1%) of events. The above distributions each show the results within their own distribution after cuts are taken on the *other* distribution. Only a single run is shown here to avoid washing out features – because the characteristics of these spectra varied significantly over the course of the beamtime, and not all of the changes can be attributed to a change in settings.

Because the characteristics of these timing sum distributions varied from run to run, it didn’t make sense to aggregate all the data before taking cuts, so any cuts had to be chosen on a run-by-run basis. Because of the asymmetry and occasional

bimodality of the distributions, it also didn't make sense to try to fit the distributions to a function such as a gaussian and then cut away some number of sigma from the fit function. The algorithm that was used in the end was to determine the peak's maximum, then discard events from the portion of the distribution in which the distribution's height is less than 10% of the maximum. Fig. 3.2 shows the effect of these cuts on the measured cloud position within a single run.

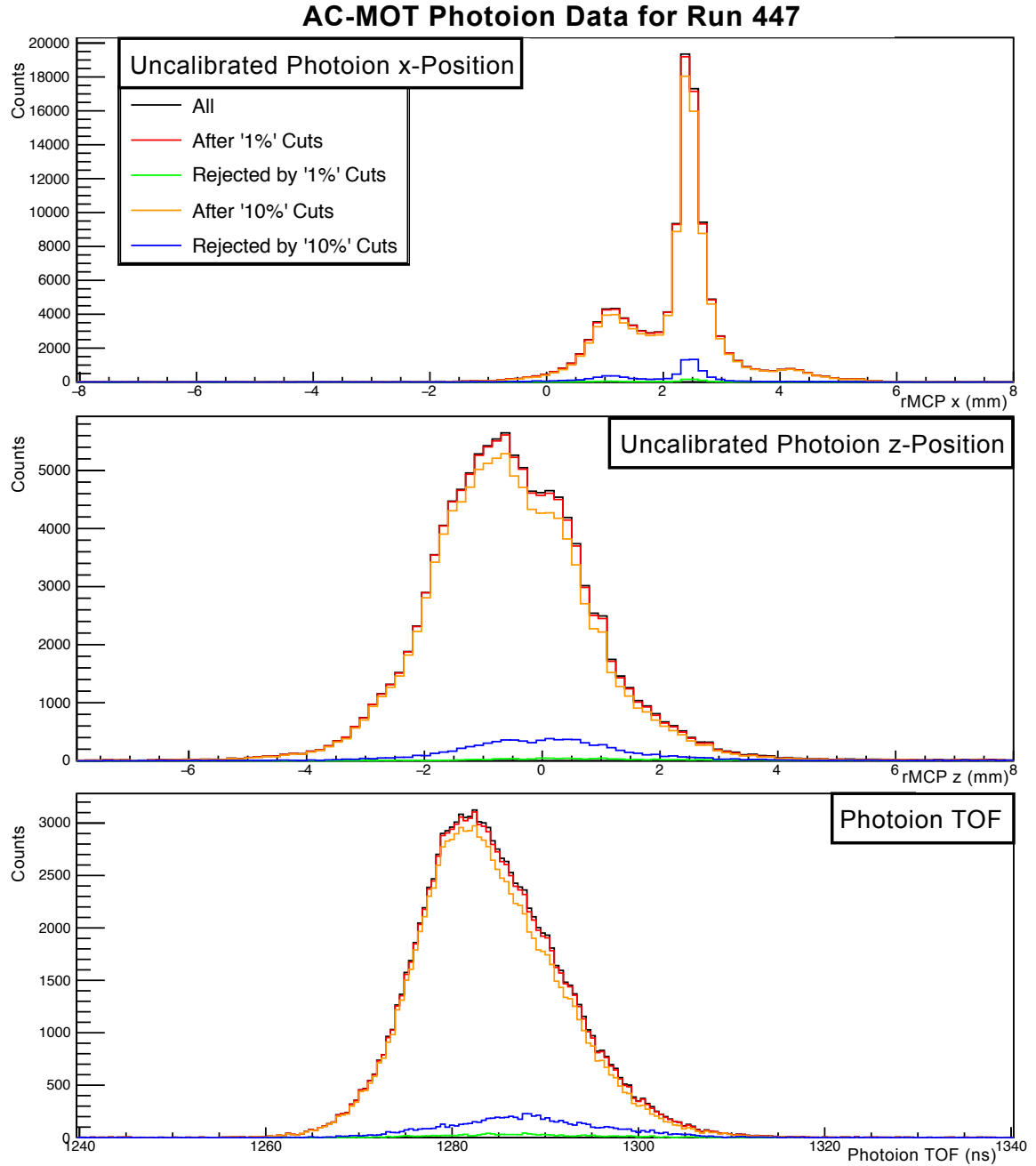


Figure 3.2: Cloud Position for run 447 for rMCP timing sum cuts as shown in Fig. 3.1.

3.3 Calibrations with the rMCP

A calibration mask was created for the rMCP, to eliminate any nonlinearities in the images produced. Several months before the ^{37}K beamtime was to occur, the

mask was attached in front of the rMCP, and a test of the delay lines' ability to produce an image was performed using an alpha source to illuminate the full surface of the detector. The mask was later removed in advance of the beamtime, in order to preserve the highest possible surface area, and calibrations were performed using the older mask data and subsequently applied to the online ^{37}K data.

I *think* we used an alpha source? Not sure what else we could have done, but I better check this!

The calibration to the offline data with a visible mask was performed over a number of steps. The data was given a preliminary rough calibration, performed on each delay line separately, which simply involved taking the difference in pulse arrival times between each end of the delay line, scaling the result by a factor chosen to get the image to be the approximate correct size, and then subtracting an offset to center the image.

With the preliminary calibration providing a visible image to work with, the '10%' cuts as described in Section 3.2 were applied, significantly sharpening the visual mask lines and overall image border. Next, a small rotation was applied, followed by a more precise centering algorithm. Following this, a linear stretching algorithm was applied to adjust the height and width of each row and column individually, while aligning the grid lines to their known position on the detector. Finally, an additional radial stretch was applied to only the outer areas of the image. This last adjustment can be justified by noting that it's expected for the outer parts of the detector to produce a more distorted image, and that appeared to be the case here. See Fig. 3.3.

When the online rMCP data was eventually collected, it was found that the rMCP image appeared offset by several centimeters relative to the previous calibration, which necessarily affected the location of the timing sum peaks (similar to those shown in Fig. 3.1). The most likely cause for this is a change in cable lengths between the readout and data acquisition in the months between the calibration and online data collection, but it meant a new set of '10%' cuts needed to be established for the online data, and also cast some doubt on the validity of the established calibrations. In the end, these cuts were established on a run-by-run basis due to the varying shape of the timing sum peaks.

Our ability to confidently accurately apply the old offline calibration to the new online data depended on our ability to center the image correctly, as different parts of the image are stretched and squeezed differently. The appearance of the plate edge—the only remaining indicator of the quality of the centering or overall calibration—changed shape slightly from run to run. Despite this, images from the online data

were all summed together after applying run-by-run cuts, and the resulting image was centered by eye.

The centering was performed iteratively, because the subsequent steps in the calibration will distort the image differently depending on how accurately it was centered beforehand. These subsequent steps in which the image is stretched and squished will also change the apparent centering of the overall image. Calibrated and uncalibrated images are shown in Fig. 3.3 for both offline and online data.

The lower plots in Fig. 3.3 show an unfortunate pattern of vertical stripes across the full surface of the rMCP. These stripes persisted over many (but not all) of the online runs. They can still be clearly seen in Fig. 3.4, which is a sum of all Runset RB's photoion events. The cause for these stripes could not be determined, and they could not be removed in post-processing analysis.

It is worth mentioning that the mask calibration data was collected without the presence of the magnetic fields involved in trapping and optical pumping, but these were of course present in the online data to which it was being compared. Since a magnetic field can change the trajectory of a charged particle, one might suspect that there could be some effect on the resulting image. There are two stages at which this might occur: while the ion is accelerating through the electric field within the experimental chamber before impacting the rMCP, and while the electron shower is emerging from the back of the MCP stack before it is incident on the delay lines. ... But also, I really don't want to get into this, otherwise somebody will ask me to quantify the size of the effect. Turns out: it's tiny, but it will be really annoying to demonstrate that.

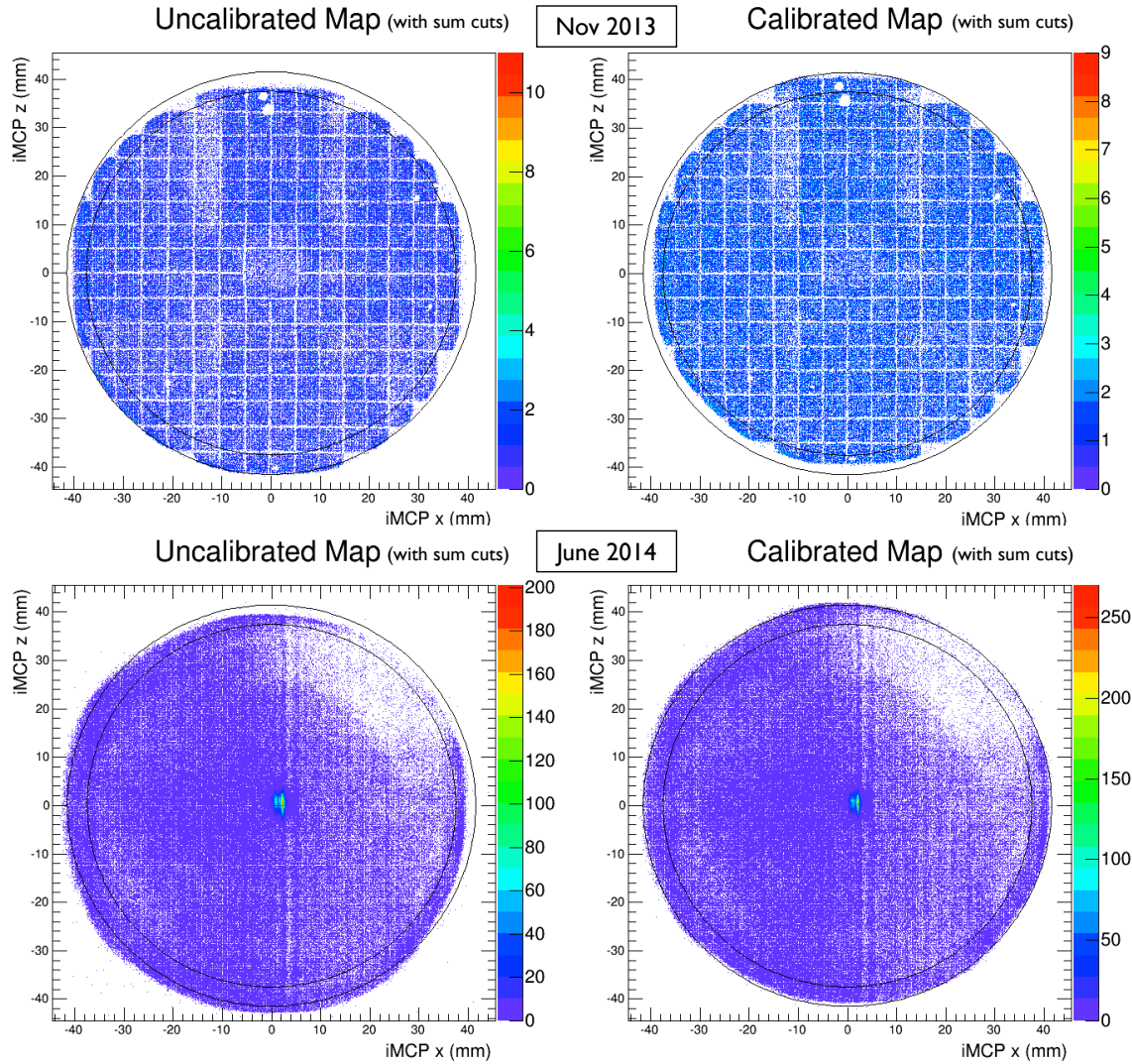
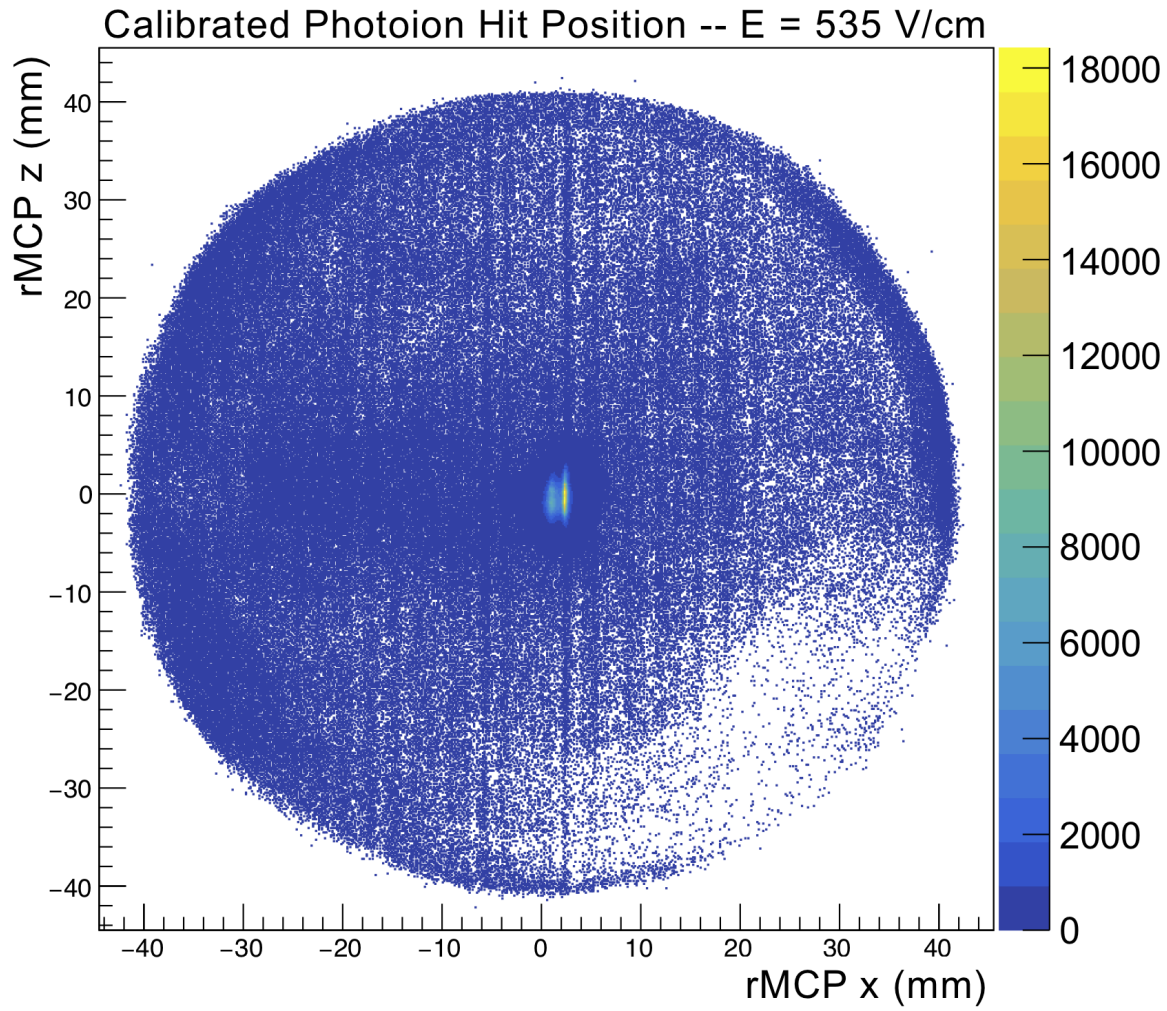


Figure 3.3: rMCP Calibration. The left images show the rMCP hit map with only a basic preliminary calibration; the images on the right are filled with the same hit data, but after the calibration has been performed. The upper two images are from data collected offline in advance of the 2014 beamtime using an alpha source; the shadow from a calibration mask is clearly visible. The lower images show rMCP data taken from a single online run, and includes both photoion and nuclear recoil data, collected over both the polarized and AC-MOT times. The photoion image of the atom cloud visible in the centre of the lower plots.



You know, I think this one is flipped relative to the previous image. Bleh. Probably this one is the correct one, but who wants to deal with that? Also did we switch MCP plates between calibration and the run? I think possibly we did! I'll have to ask the eLog.

Does this thing even have a TOF cut?

Figure 3.4: Photoion Hit Positions in 2D. This is the entirety of the good photoion data taken at 535 V/cm. The central bright spot is an image of the atom cloud arising from photoionization events of unpolarized atoms; the rest is background. Vertical stripes of indeterminate cause can be seen across the face of the image – it has not been possible to eliminate them in analysis.

3.4 Measurements of the Atom Cloud

With the rMCP detector calibrated (Section 3.3), several types of data may be extracted. It is possible to extract the hit positions and times-of-flight for the incident nuclear recoils, and an analysis of such data could be used to perform a test of right-handed currents within the nuclear weak force, as discussed in Chapter 6.2. However, we will focus here on what may be learned about the *atom cloud* from rMCP events in coincidence with the photoionization laser.

This class of data (events with both an rMCP hit and a photoionization laser hit in coincidence) can be used to measure cloud polarization, and the methodology and results of that process as it applies to this particular experiment are discussed in a recent publication [44]. We are also interested in the cloud’s position and size during the periods of time where decay data is collected, since this represents a potential systematic effect that must be accounted for within our models. The latter will be the primary focus of this section.

Also... does the camera data go in this section??

The first step in such a measurement is to try to eliminate as much background as possible. We have already required that every event considered here must include both an rMCP hit and a photoionization laser pulse. As we are interested in measurements of trap position, it makes sense to also require a *complete* set of position data recorded on the rMCP’s delay lines. This is further trimmed by a ‘10% cut’ on the timing sums, as described in Sec. 3.2. Any event including a scintillator hit is rejected, as these events have an increased likelihood for a recoiling ion to be detected on the rMCP instead of- or in addition to the photoion we expect (It is at this stage of the process that Fig. 3.4 is created.). Finally, some fairly loose cuts are applied about the central x- and z-positions, as well as the ion’s time of flight (measured with respect to the arrival of a photoionization laser pulse).

With these basic cuts performed, the cloud position and size must be measured. We are particularly interested in measurements of the cloud during the time when it is considered to be *polarized* — however the great majority of photoionization events occur when the cloud is *not polarized* (see Fig. 3.5). This is because the photoionization laser acts only on excited atomic states, which are readily available during the operation of the MOT. When the MOT is shut off, the atoms quickly de-excite. At the start of optical pumping 300 μs later (in the case of the 535 V/cm data), there is a short burst of photoions due to the atoms being temporarily placed

into an excited state as part of the optical pumping process. The photoion burst falls away rapidly as atoms are optically pumped into the stretched state and can no longer be excited by the optical pumping laser.

A projection of the cloud's position on the x- and z-axes, and its TOF (indicative of position along the y-axis) is plotted over the course of the repeating AC-MOT/OP cycle in Fig. 3.5. The mysterious vertical stripes seen Fig. 3.4 are clearly evident in the top plot of Fig. 3.5, and their positions do not change over the AC-MOT cycle, even though cloud motion is clearly visible.

To extract the size and position of the atom cloud as projected onto all three axes, time slices of several hundred μs are taken from the beginning of the AC-MOT cycle, and from the part of the AC-MOT cycle immediately before the MOT is turned off. A gaussian is fitted to the cloud projection, with its parameters describing the trap's size and position during these parts of the cycle. A linear interpolation applied to describe the cloud's 3D size and position during polarized times, as functions of time since the AC-MOT cycle started. Results are shown in Table 3.3.

Runsets		Initial Position	Final Position	Initial Size	Final Size
EB \leftarrow RB	x	1.77 \pm 0.03	2.06 \pm 0.08	0.601 \pm 0.013	1.504 \pm 0.047
	y	-3.51 \pm 0.04	-3.33 \pm 0.05	1.009 \pm 0.013	1.551 \pm 0.018
	z	-0.661 \pm 0.005	-0.551 \pm 0.021	0.891 \pm 0.004	1.707 \pm 0.015
EC \leftarrow RD	x	2.22 \pm 0.05	2.33 \pm 0.11	1.18 \pm 0.04	1.538 \pm 0.087
	y	-3.68 \pm 0.04	-3.31 \pm 0.06	0.965 \pm 0.012	1.460 \pm 0.030
	z	-0.437 \pm 0.09	-0.346 \pm 0.037	0.927 \pm 0.007	1.797 \pm 0.026
ED \leftarrow RE	x	2.274 \pm 0.012	2.46 \pm 0.06	0.386 \pm 0.016	1.382 \pm 0.046
	y	-4.54 \pm 0.04	-4.28 \pm 0.04	0.986 \pm 0.08	1.502 \pm 0.013
	z	-0.587 \pm 0.04	-0.481 \pm 0.018	0.969 \pm 0.003	1.861 \pm 0.013

Sig figs here need work.

Parameters measured with the recoil runs, and applied on the appropriate electron runs.

Table 3.3: Cloud Positions and Sizes – Measured immediately before and immediately following the optical pumping phase of the trapping cycle. Measurements are evaluated using rMCP runs, and are taken to describe the cloud during associated eMCP runs as well. All entries are expressed in units of millimetres, and the size parameters describe the gaussian width.

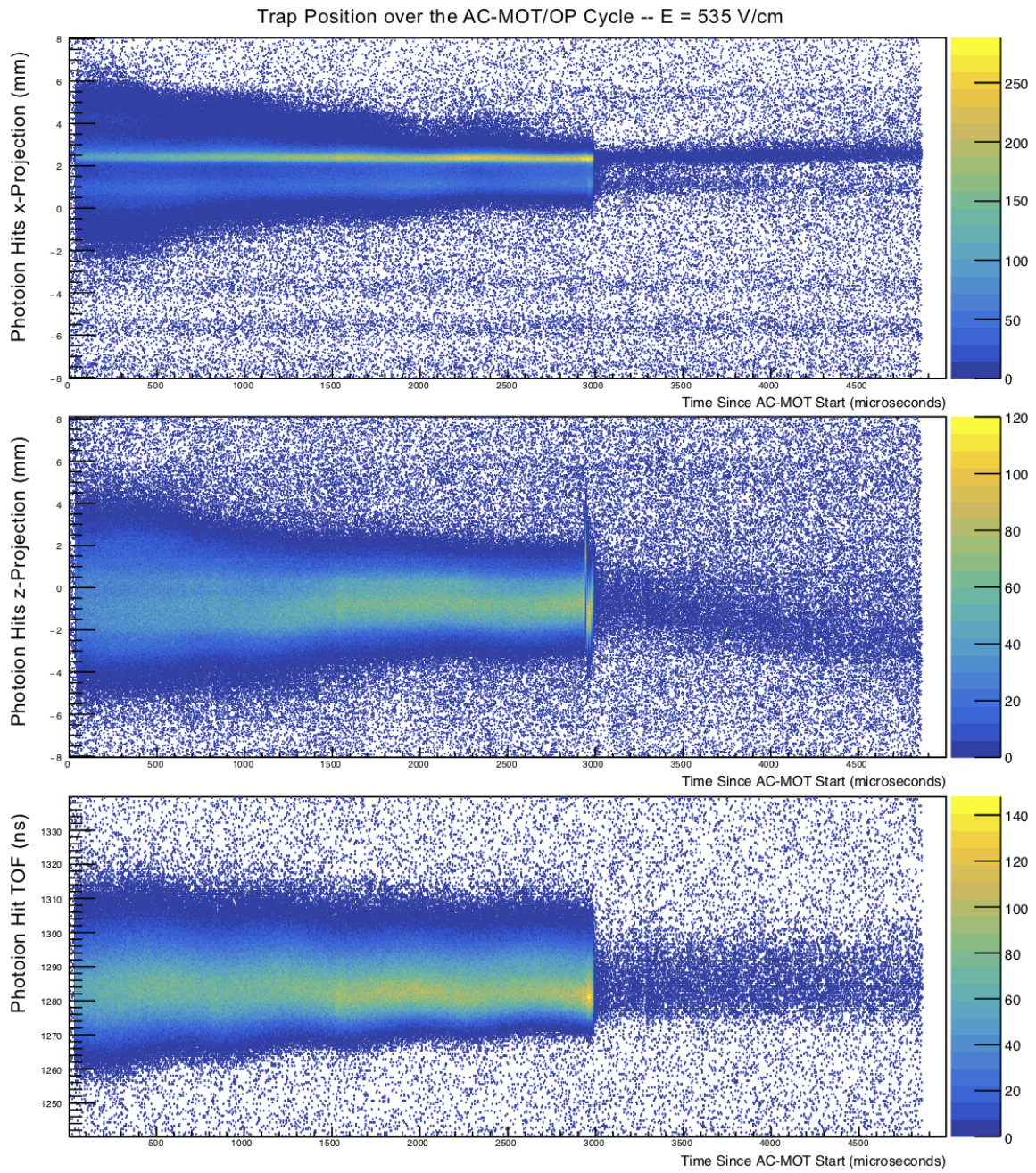


Figure 3.5: Projections of photoion hit positions and TOF at 535 V/cm, as a function of time since the start of the last AC-MOT cycle. The trap's periodic motion can be seen in sync with the AC-MOT's cycles, and it is clear that the cloud is also being compressed during this time, before being allowed to expand ballistically when the MOT is shut off. The photoion burst at the start of optical pumping 300 μ s after the AC-MOT is shut off can be seen on the lower two plots.

Also, we noticed the trap drifting after one of the runs, because one of the batteries on one of the thingies adjusting the laser frequency (I think) was failing.

JB: "If we rejected the data with the MOT moving (indeed a battery determining the voltage controlled oscillator frequency offset between absorption in stable ^{41}K cell and the ^{37}K resonance) then that's all you need to say."

describe how you'd turn this into a physical description of the cloud, with like a temperature and a sail velocity and shit. with equations.

3.5 Electron Run Data Selection and Preliminary Cuts

Before proceeding further, several basic cuts are performed on the data. For the Electron Runs which are to be processed directly into a physical measurement, we consider only events in which there was a recorded hit *both* on the eMCP *and* on exactly one of the scintillators. The required scintillator hit, of course, is potentially a beta, and so it is obvious why this must be present. Events in which both scintillators record a hit are discarded, as they fall into two categories: an accidental coincidence, where we are seeing two different decays that, by chance, both occurred within the time window allocated to a single event (a few μs before and after the first recorded scintillator hit), a backscatter event in which a beta was incident on one scintillator before being scattered out into the opposite scintillator. Although it would be possible to process the former event type into usable information if we could be certain that it was truly an accidental coincidence, contamination from the latter event type would serve to increase the systematic uncertainty arising from beta scattering—already a dominant source of error.

The eMCP is used primarily to record incident shake-off electrons. As described in Section 1.8, every beta decay event will produce one or more SOEs. Most (but not all) SOEs originating from the atom cloud will be incident on the eMCP, however not all incident SOEs on the eMCP will produce a recorded hit. The electric field is such that SOEs originating elsewhere within the chamber may or may not be incident on the eMCP. Therefore, while imposing an eMCP hit requirement will eliminate some 'good' events originating from the cloud, it also eliminates a much larger fraction of background events originating from other surfaces within the chamber. This ability

Point at that other conclusion-ier section.

to ‘tag’ good events originating in the cloud is absolutely essential to any analysis involving angular correlations within this geometry.

In later sections, we will consider how to evaluate a further cut to be imposed on the time difference between scintillator and eMCP hits (Section 3.8), and some subtleties within analysis relating to this choice (Sections 4.4 and 4.5).

It is also necessary to remove from direct consideration any event which is coincident with a pulse from the photoionization laser. When photoionization occurs within the atom cloud, an orbital electron is removed from the atom and will be accelerated by the electric field into the eMCP, just as a shake-off electron from a decay would be. If, by chance, this photoelectron arrives in coincidence with a scintillator hit, it would be interpreted as a decay event from the trap – unless we preemptively discard it.

Over the course of the runtime, there were several instances where we noted an apparent electrical discharge within the experimental chamber, producing enormous backgrounds for a short time. The detectors typically recovered quickly afterward, so it was neither necessary nor useful to stop an entire run to wait for the system to recover. Instead, the time when the discharge occurred was recorded, and events within approximately one minute of the spark time were discarded.

We use only the “fully polarized” events for which we have a detailed understanding of the nuclear polarization (described in more detail in [44]). This means we must use *only* events from the “optical pumping” portion of the duty cycle (see Fig. 2.3), and discard events when the DC- or AC-MOT is active. After the AC-MOT is shut off, there is a short delay before optical pumping begins (see Tables 3.1 and 3.2) to allow the magnetic field to decay, and it is only after $100\ \mu s$ of optical pumping that we consider the atoms to be fully polarized. Furthermore, because the magnetic field from the DC-MOT is slow to decay (relative to the field from the AC-MOT), all events from the first five AC/OP cycles after every atom transfer are discarded. A further benefit of our insistence on considering only polarized data is that the scintillators’ gains are more stable in the presence of only the (small, stable) magnetic field used for optical pumping than they are in the presence of a larger oscillating magnetic field used for trapping [50].

change by 0.2% of its value vs change by 0.5% of its value, according to Ben’s thesis pg 143.

Ben didn't do the 5 cycle discarding thing in his Abeta analysis, but he *did* do it in his OP analysis.

Finally, because this analysis depends heavily on energy measurements from the two scintillators as a proxy for beta energy, it is necessary to remove events in which the pulser LED fired. Although the pulser LED is useful for evaluating the stability of the scintillators, in the case where an LED pulse occurs together with a true beta hit in the scintillator, it may change the measured energy. Therefore, we discard all events that include an LED pulse.

3.6 Further Cuts Using the DSSD

Which cuts did I use by default on the DSSD? Also, which did Ben use?

Add 2D DSSD plots?

Missing figure

Show individual beta energy spectra. ...with a variety of different cuts, perhaps?

The DSSDs are critical to our ability to veto background events in which the particle incident on the detector is a gamma ray rather than a beta — e.g., from annihilation radiation — however, they must be properly calibrated in order to be useful. The calibration was performed by other members of the collaboration, and the methodology is described in detail in [50]. It is summarized here for clarity.

Although it was not possible to use the DSSD in real-time analysis or event triggering, the DSSDs may be used, after the data has been collected, to distinguish between different types of particles incident on the detector, as more energy will be deposited by heavier particles. When a scintillator hit is triggered by a particle originating within the experimental chamber, that particle will typically have passed through the DSSD before arriving at the scintillator.

In the present experiment, the two primary particles that will concern us are β^+ particles originating from the decay of ^{37}K , and γ rays, which may be produced through a variety of processes, e.g. directly from the 2% decay branch, through

annihilation of β^+ particles upon their interaction with regular-matter electrons, or bremsstrahlung radiation from emitted β s.

We would like to look specifically at events involving β^+ particles arriving direct from a decay within the atom cloud, and the DSSD may be used to eliminate events in which the scintillator is triggered by a γ . An incident β will typically deposit some portion of its energy in the DSSD as it passes through, however an incident γ will deposit significantly less energy; for this setup the energy deposited by a γ is generally indistinguishable from background on the DSSDs. Therefore, we require that a ‘good’ event must include a ‘good’ hit to the DSSD as well as a hit to the associated scintillator.

In order to proceed at this point, and because the DSSD readout records so much information, it is necessary to develop some criteria to determine whether or not we will accept any given DSSD readout as a β hit.

JB: “If you have some way of documenting the coding you used, that would be great.” ... yeah, it would, wouldn’t it?

We read out the full waveform for every strip at each event with a scintillator hit, but in post-processing take *only* the ‘time’ and ‘energy’ from the waveform’s peak. Each strip will have its own noise spectrum, energy calibration, and energy resolution. To classify an event as a good DSSD hit, we first require a good scintillator hit (as determined by the associated TDC readout) with energy above a nominal 10 keV to eliminate pedestal events, and no pulser LED.

We further require at least one ‘x’ strip and one ‘y’ strip within that same detector record an energy above the ‘noise threshold’, which is determined individually for each strip, and is defined according to the signal-to-noise (SNR) ratio. In other words, for each individual strip, the energy at which a certain fraction of events are ‘real’ events (as opposed to electronic noise) defines a particular ‘noise threshold’. Values are tabulated for each strip at SNRs of 0.25, 0.5, 0.75, 1.0, and 2.0. As a default, the strip-by-strip SNR of 0.25 is used.

We require that the x strip and the y strip agree (to within some number of standard deviations — this is a parameter that can be varied) in amount of energy deposited, and in the time at which that hit occurred. In order to avoid problems resulting from the strips’ non-uniform noise thresholds, we further require that the energy deposited be greater than some lower-end cutoff which is selected so as to be higher than every individual strip’s noise threshold. In this case, the DSSDs’ lower

In Ben’s thesis, he says it’s *actually* an SNR of 0.17 ...

energy uniform threshold was set at 50 keV, a departure from the choice of 60 keV in an earlier analysis [48] [50].

We also elect to use only events where a beta hit the DSSD within a 15.5 mm radius of the center of the detector, as a large fraction of the DSSD hits at larger radii are from betas that have scattered from the collimator walls. Furthermore, events with more than *one* DSSD hit are rejected, as these events are likely either accidental coincidences of two beta decays, or else the result of betas scattering out of a scintillator before their energy can be fully absorbed.

In Ben's thesis, he says he uses $r = 10.0$ for the DSSDs, but in the PRL, $r = 15.5^{+3.5}_{-5.5}$ is the range.

Did I even mention the collimator? Like, in the previous chapter or something..?

3.7 Further Cuts Using the Scintillators

After all other cuts have been performed, a further cut is made on scintillator energy. It is important that this cut must be performed *after* event vetoes from more than one scintillator being hit are applied, and after the DSSD event vetoes have also been applied, in order to avoid unexpected behaviour in which we fail to reject certain classes of events that we had intended to reject.

For both scintillators, only events where the absorbed energy is between 400 and 4800 keV are accepted. The high energy cutoff is selected so far below the beta cutoff energy ($Q = 5.125$ MeV) because the low counting statistics at higher energies result in our observable, the superratio asymmetry, being poorly defined and poorly behaved. In later evaluating the systematic error associated with that cut, spectra with lower cutoffs ranging from 300 to 600 keV are considered, and spectra with upper energy cutoffs between 4600 and 5100 keV are considered separately.

Should I calculate somewhere what the cutoff energy even is? Ugh.

Low cutoff is because it's really hard to model what's going on down there to the required level of precision. The observable depends most heavily on low beta energy events, so it is imperative that the lower energy portion of the spectra be thoroughly understood if they are to be used for analysis.

3.8 Timing Improvements with the Leading Edge and Scintillator Walk Correction

MJA: I can describe the eMCP calibration here, even though it mostly wasn't implemented by me. It is tangentially relevant to data selection and background estimation by providing an experimental energy spectrum for shake-off electrons. It's actually a pretty neat algorithm that I basically wasn't involved with.

...

JB: eMCP. You need to describe the timing information obtained. You also need a statement of whether or not you used the position information in your cuts.

...

MJA: Wait. So have I done that yet in this section?

I described the HEX-75 somewhere in a previous chapter, right??

I dislike how this section is organized.. should discuss the cut we *didn't* make at the end.

The eMCP features a set of three delay lines, intended to be used to record the position of a hit. Though only two delay lines is sufficient to determine the position within the plane of the MCP if they are both hit, the presence of a third delay line allows for some redundancy. In practice, however, a large fraction of otherwise ‘good’ events include a hit on the eMCP, but have insufficient information recorded on the delay line channels to reconstruct a position.

Because a SOE from the trap is most likely to land in the centre of the plate, while *a priori* the background from other sources not expected to have any particular spatial distribution, it might make sense to accept only events where the eMCP hit is within some radius of the central peak. This methodology was seriously considered because the remaining data after this cut is taken has a much lower fraction of background events polluting it – however even for the most generous eMCP radius cuts, this results in a loss of about half of the events. The overall measurement is limited by statistics rather than systematics, so it was decided that no cuts on eMCP hit position would be taken in the final analysis.

A shitty TOF spectrum plot used to be here. It was supposed to compare TOFs with and without position cuts. It's gone, but not forgotten.

Several years after the data was initially collected, a problem was discovered with our low-level analyzer software, which we had been using to convert large and unwieldy MIDAS data sets into somewhat smaller and more manageable ROOT data sets. In particular, for every timestamp recorded, our raw MIDAS data actually included both

a timestamp for the leading edge (LE) of the pulse, and a timestamp for the trailing edge (TE). The analyzer had—for years—been reporting the timestamp associated with the trailing edge of the pulse. Initially it was unclear if there might have been a reason behind this choice, but a closer examination of the data showed that the LE data included less timing jitter and noise, as well as a sharper peak for timing pulses across the board (as in Fig. 3.6), with some channels showing a larger effect than others. This was corrected, and the entirety of this analysis has been performed now using the cleaner LE spectra.

The LE spectra allows for us to use a more precise model of the SOE TOFs, so that's nice.

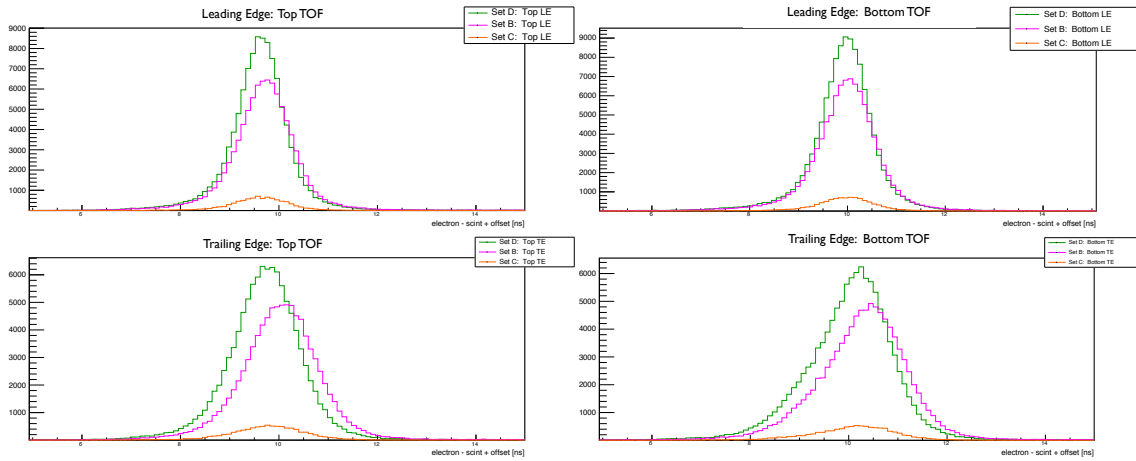


Figure 3.6: SOE TOF peaks (eMPC - Scintillator), using the leading edge (LE) and using the trailing edge (TE). Data is sorted according to runset. For each individual runset, the TE peak is broader than the LE peak. The centroid of each runset is also more variable in the TE plots.

The place where this change between the TE and LE timestamps had the biggest impact on the analysis is in the shake-off electron time-of-flight spectra, on which a cut must eventually be taken. Although this problem was not discovered in time to be used in the previous measurement of A_β using this same data [48], it likely would have had a negligible effect on the final result, because the SOE TOF cut that was used there was comparatively loose, and the evaluation of the background that remained was not a dominant systematic effect.

With the data reprocessed using the leading edge for timestamps, I wanted to eliminate as much background as possible from the SOE TOF spectrum. With this goal in mind, the next step was to correct the scintillator timing for its low energy

This goes in that one appendix, if I haven't already put it there.
...Also, is this even fucking true???

‘walk’ (see Fig. 3.7). A quartic polynomial was fit to each of the 2D timing vs energy spectra (the top and bottom detectors were treated separately), and the result was used to produce a ‘straightened’ SOE TOF spectrum with respect to measured scintillator energy, and as expected, the resulting SOE TOF spectrum was a bit more sharply peaked.

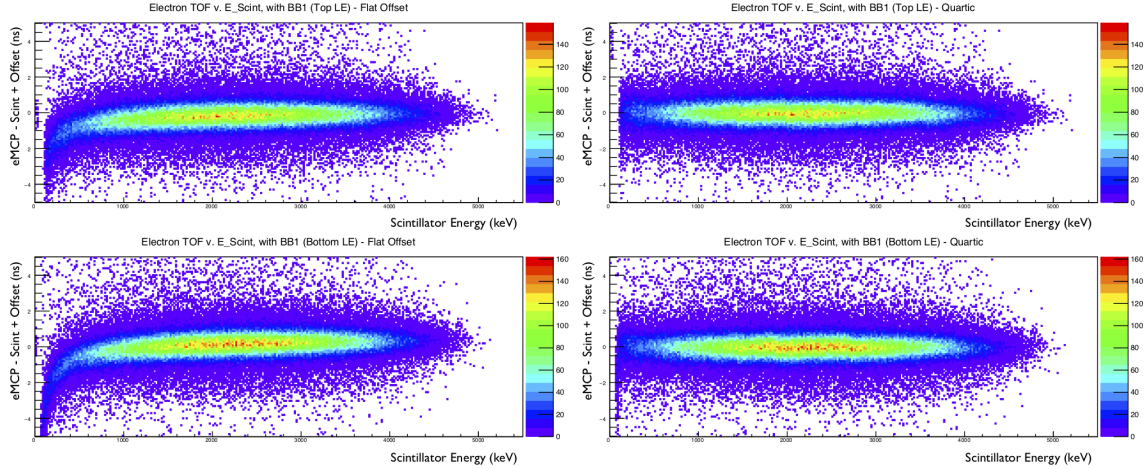


Figure 3.7: SOE TOF walk, before (left) and after (right) applying a quartic adjustment to straighten out the effective TOF.

With the SOE TOF spectra cleaned up, a cut can be taken to reduce the fraction of background events. Informed by the model of background spectra described in Section 4.5, a cut was made to include only a 2.344 ns window around the primary peak in further analysis (see Fig. 4.12). With all cuts included, the four cleaned scintillator spectra corresponding to combinations of detector and polarization direction are plotted in Fig. 3.8.

“...removing X fraction of the remaining events.”

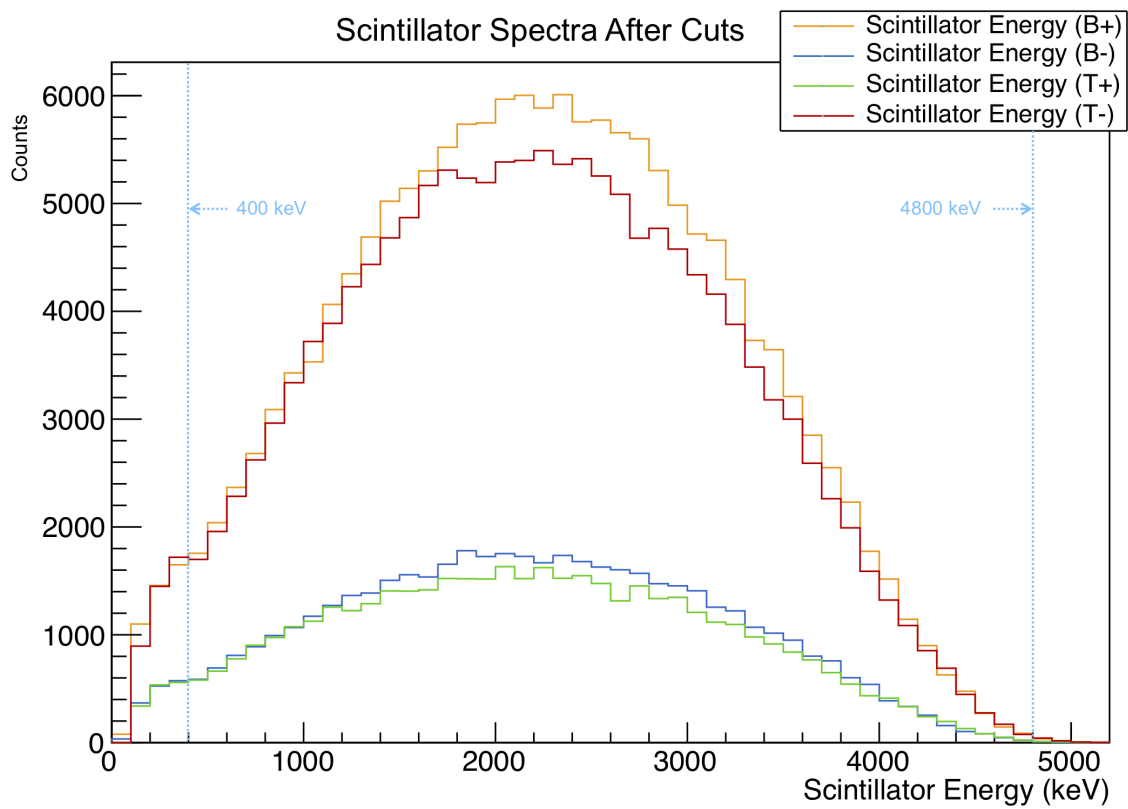
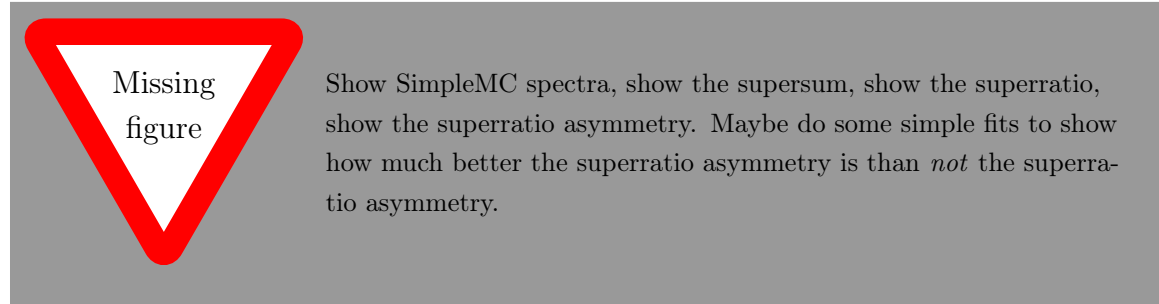


Figure 3.8: Experimental scintillator spectra, for both detectors in both polarization states. These spectra are what remain after all cuts have been taken, and all runsets are included. Binning is selected to match the convention used for the final analysis.

Experimental scint. spectra plot needs to be referenced in text.

Chapter 4

Simulations



The TRINAT collaboration has created a Geant4 (G4) simulation which models the geometry and materials within the experimental chamber, and uses a monte carlo algorithm to describe generalized physical processes such as particle scattering and energy loss, within the geometry specific to the experiment. This software library has been maintained and updated over several generations of graduate students [50] [51].

add comment about how you need G4 to do scattering/backscattering. I think I wrote a blurb like this *somewhere* already....

4.1 Considerations for Software Upgrade Implementation

Prior to the simulations required for this particular experiment, two different sets of changes to the G4 code were needed – the first to enable multithreading, and the second to introduce certain BSM interactions to the decay distribution.

Enabling multithreading allows for a single instance of the Geant4 simulation to run on several processors at once, effectively speeding up the overall simulation by a factor of the number of processors used. In the years since the simulation was originally created, the Geant4 collaboration had created libraries intended specifically to support multithread usage, and since the running G4 simulations had historically been very time consuming for the TRINAT collaboration, the decision was made to implement multithreading within our own monte carlo software, on the hopes that this would enable faster progress in analysis.

Enabling multithreading support turned out to be quite time consuming, and in the end it might have been faster to have spent those months running simulations one processor at a time. Perhaps the improvement will prove valuable for use in future TRINAT experiments.

The TRINAT G4 monte carlo package had never been used to directly model interactions beyond the standard model within the decay physics. It had previously been set up by the collaboration to use a probability density function (PDF) including most of the terms from Holstein's Eq. (51) [39], which describes both electron and neutrino momenta from polarized beta decay. This treatment is quite robust, and includes corrections at recoil-order, as well as certain other corrections of similar size.

Unfortunately, terms arising from interactions beyond the standard model are not included in Holstein's description of the decay process. To understand the kinematic results of the exotic interactions of interest to us here, we turn to the classic JTW treatment of beta decay [1] [2]. In addition to the (expected) vector and axial interactions, JTW also describes the interaction in terms of (exotic) scalar and tensor interactions, should such be present.

Furthermore, although it is currently understood that the weak interaction is predominantly or perhaps entirely ‘left-handed’, the JTW treatment leaves certain phase angles unfixed, and is therefore able to accurately describe a decay which is, for example, partially ‘right-handed’ – however the latter feature is not directly relevant to the project at hand. [It’s several phase angles in JTW, but maybe it’s fundamentally only like one angle on some level? Also I think it’s not actually a “gauge freedom,” per se. No, I’m pretty sure this ‘phase angle’ description is all wrong.] Also, consider time reversal! Anyway, most of this paragraph probably goes better in Section 1.6.

because for A_β even a BSM interaction will *basically* look like a SM interaction, and I think something somewhere isn't precise enough to distinguish it.

which other corrections? coulomb and/or radiative corrections, but somehow when I say that, I'm apparently talking about a different thing than everyone else who uses those terms. also, weak magnetism. also ... ???

Is this true? Does it not include *any* BSM interactions?

Despite JTW’s broad ability to describe beta decay under a variety of physical models, this treatment includes only the leading-order terms, and smaller terms, such as recoil-order corrections, are neglected entirely.

Because the present project is a precision measurement of the Fierz interference, a term which arises from scalar and tensor couplings, it was imperative to create an event generator for our G4 simulations that could account for these exotic interactions while also including in its PDF the higher-order effects which, in some cases, can mimic the effects of a scalar or tensor current.

While it might have been possible to directly combine JTW’s result with Holstein’s Eq. (51), it should be noted that JTW’s expression is not compatible in general with the principle of conservation of momentum; as recoil momentum is neglected entirely, the description is only of two leptons emerging from a nucleus in directions that do not directly oppose one another. Therefore, the prospect of combining these two slightly incompatible expressions directly might be enough to give one pause. On an experimental level, the mathematical description of an emerging neutrino is only of interest to us to the extent we can reconstruct it based on detecting both a beta and the recoiling nucleus from a single decay event, and within the present experiment we do not have simultaneous access to both a beta detector and a recoil detector.

In light of the above considerations, it was decided that an entirely new event generator must be created, based instead on Holstein’s Eq. (52), in which neutrino momentum has been integrated over and is therefore no longer an explicit part of the PDF [39]. As one might guess, Holstein’s Eq. (52) is greatly simplified in comparison to Holstein’s Eq. (51). A similar integration over all possible neutrino momenta can also be performed on the JTW PDF, causing several terms to vanish. The result in both the Holstein and JTW cases is a PDF over only beta energy and direction as measured with respect to nuclear polarization, and the two expressions can be combined in a straightforward manner by comparing similar terms.

It is this combined Holstein+JTW expression that forms the basis of the new G4 event generator. It must be noted that although the largest effect from any present scalar or tensor interactions would likely (depending on certain phase angles) be in a non-zero value of b_{Fierz} , these interactions can also introduce a perturbation to A_β at a higher order. In order for any precision experimental measurement of b_{Fierz} to be generalized to limits on the parameter space of scalar and tensor currents, it is important to incorporate an accurate representation of the results of such exotic interactions on *all* available observables, and the new G4 event generator does this.

Things that the G4 simulation did that I kept include: an accurate representation of the complex details of our experimental geometry. Also, the noise spectra on the DSSDs.

OK, somewhere I really have to say specifically the parameter that I varied and chi-squared-ed... it's some sort of pseudo-Holstein-eque g_S , which combines "left handed" and "right handed" scalar couplings. Also, no tensors. Pretty sure it comes out equivalent to looking for tensors within bFierz, but gives a slightly different value of Abeta. But maybe this goes in the Analysis chapter?

4.2 Simulations for the Ninety-eight Percent Branch and the Two Percent Branch

With the new event generator, our G4 simulations are able to generate ^{37}K decay events mediated by Weak interactions with arbitrarily sized scalar and tensor couplings. For simplicity of analysis, and because scalar and tensor couplings produce similar effects on parameters A_β and b_{Fierz} , the decision was made to vary only the scaling of one particular set of BSM coupling constants within the Geant4 simulations. In particular, high-statistics simulations were performed using scalar coupling values,

$$g_S := \frac{1}{\sqrt{2}}(C_S + C'_S) = \{0, \pm 0.1\}, \quad (4.1)$$

a combination that describes left-handed scalar interactions. These sets of parameters produce values of b_{Fierz} , and perturbations to values of A_β , given by:

$$b_{\text{Fierz}} \approx \{0, \mp 0.148661\} \quad (4.2)$$

$$\Delta A_\beta \approx \{0, -0.004259\}, \quad (4.3)$$

where we note that the change to the value of A_β is small relative to b_{Fierz} , and always has the same (negative) sign no matter the sign of b_{Fierz} , because while b_{Fierz} scales linearly with g_T , the perturbation to A_β arises from a quadratic term.

though, I think the sign change to A_β values could, in principle, help us tell the difference between scalar and tensor couplings in the decay. In practice, it would never work though.

In addition to simulations of the dominant decay branch, it is also necessary to create simulations with sufficient statistics of the subleading ("two percent") branch. Because it is responsible only for a small fraction of the overall spectrum, we do not include corrections from BSM parameters in these simulations. These simulations

are performed separately from the main branch simulations, and are evaluated using the older Geant4 event generator based on Holstein's Eq.(51) [39]. Simulated events from both branches are combined together in the appropriate ratio before further processing is performed.

4.3 The Simple Monte Carlo and Response Function

Scattering (both forward scattering and backscattering) is an important effect to consider within this experiment, and it must be evaluated through extensive and time consuming monte carlo simulations – in this case, using Geant4. However, there are a number of other systematic uncertainties that must also be evaluated, and it is computationally prohibitive (even after multithreading support was implemented) to evaluate all of them via the same sort of high statistics, scattering included, full monte carlo that we use for scattering effects. Luckily, the systematic effects arising from scattering are largely decoupled from other effects, and this section describes the framework that has been implemented in order to evaluate certain other systematic effects separately.

To this end, a fast-running Simple Monte Carlo (SMC) was developed together with an empirical “response function” similar to the one described by Clifford et al [52] to describe probabilistic beta energy loss before its detection in a scintillator. In the end, the lineshape description became quite involved, and it is unclear whether, in the end, any time was saved this way.

The purpose of the SMC was to *quickly* generate initial particle kinematics probabilistically for beta decay events, and it uses the very same event generator based on Holstein's Eq. (52) [39] that was developed for use with the more sophisticated Geant4 simulations. However, unlike in a G4 simulation, the SMC makes no attempt to track particles through the chamber, and instead simply calculates detector hits based on initial particle momentum. This procedure obviously neglects scattering effects, which can (in differing regimes) both *increase* and *decrease* the number of beta particles incident on a detector. Furthermore, this procedure also neglects any energy absorption in materials through which the beta passes before hitting a scintillator – and the beta *must* pass through several such materials (see Fig. 2.5).

Reference previous
section where I discuss
this, maybe?

To make the best use of the SMC for evaluating systematic errors, the energy

lost before a beta hits a scintillator must be accounted for somehow in order to ensure all relevant physical effects are propagated through. In particular, before hitting a scintillator, a beta must pass through a $275\ \mu m$ thick silicon carbide mirror, a $229\ \mu m$ thick beryllium foil, and finally a set of $300\ \mu m$ thick double-sided silicon strip detectors (DSSDs), before finally having its remaining energy absorbed within a scintillator. Although the DSSDs are themselves detectors with the ability to record the amount of energy deposited by an incident particle, there are some known problems in achieving a uniform level of precision across the full surface of the DSSDs, so adding the DSSD energy back to the scintillator energy to produce a better estimate of the original beta energy has the potential to create some problems for the analysis. Furthermore, given the presence of the mirror, an object with a similar thickness and scattering properties to the DSSDs, re-adding the energy lost in the DSSDs would not eliminate the need to estimate probabilistic energy loss in similar materials.

See: Some other section? Maybe?

In order to create a quantitative description of the effective response function, which varies with initial beta energy, an analytic function of 14 parameters has been created to model scintillator output for decays from the central cloud for each of the two polarization states in use. In other words, although the form of the model is always the same, the 14 individual parameters will take different values for each of the four detector and polarization combinations. The full response function model is given by the expression,

Is it definitely 14 of them?

$$R(E_0, \text{Detector}, \text{Polarization}) = p_{\text{norm}} (f_{\text{moyal}} + f_1 + f_2 + f_3 + f_4 + f_5) + f_{511}, \quad (4.4)$$

where p_{norm} is one parameter, and the other terms within the expression are themselves functions of multiple parameters and are given by,

$$f_{\text{moyal}} = (1 - p_{\text{gfrac}}) \left(1 + \frac{-p_\alpha - p_\beta}{|E_0|} - \frac{p_\Delta}{p_\gamma p_W} - p_\gamma p_W \right) \\ \times \left(\frac{e^{\left(\frac{x - (E_0 - \frac{1}{2}p_{dE0})}{2p_{lres}|E_0 - \frac{1}{2}p_{dE0}|} \right)} e^{\left(-\frac{1}{2}e^{\left(\frac{x - (E_0 - \frac{1}{2}p_{dE0})}{p_{lres}|E_0 - \frac{1}{2}p_{dE0}|} \right)} \right)}}{\sqrt{2\pi p_{lres} |E_0 - \frac{1}{2}p_{dE0}|}} \right), \quad (4.5)$$

Obviously, from a physical standpoint, the initial beta energy E_0 must be positive, but the response function still includes several expressions of the form, $|E_0|$. This is not done by accident, but rather is an intentional adjustment used to encourage the parameters to behave well within a fit.

$$f_1 = p_{\text{gfrac}} \left(1 + \frac{-p_\alpha - p_\beta}{|E_0|} - \frac{p_\Delta}{p_\gamma p_W} - p_\gamma p_W \right) \left(\frac{e^{\left(-\frac{(x - (E_0 + \frac{1}{2}p_{dE0}))^2}{2p_{toeres}|E_0 + \frac{1}{2}p_{dE0}|} \right)}}{\sqrt{2\pi p_{toeres} |E_0 + \frac{1}{2}p_{dE0}|}} \right), \quad (4.6)$$

$$f_2 = \frac{p_\alpha}{|E_0|} \left(\frac{1 - \text{Erf} \left[\frac{(x - |E_0|)}{\sqrt{2p_{toeres}|E_0|}} \right]}{2 |E_0|} \right), \quad (4.7)$$

In these response functions, $x = ?$

$$f_3 = \frac{p_\beta}{|E_0|} \left(\frac{e^{\frac{p_k * (x - E_0)}{|E_0|}} * e^{\frac{p_{toeres} p_k^2}{2|E_0|}}}{2(1 - e^{-p_k})} \right) \left(1 - \text{Erf} \left[\frac{(x - E_0 + p_{toeres} p_k)}{\sqrt{2p_{toeres} |E_0|}} \right] \right), \quad (4.8)$$

$$f_4 = \frac{p_\gamma}{2} \left(\operatorname{Erf} \left[\frac{x - E_0}{\sqrt{(2 p_{\text{toeres}} |E_0|)}} \right] - \operatorname{Erf} \left[\frac{x - E_0 - p_W}{\sqrt{2 p_{\text{toeres}} |E_0 + p_W|}} \right] \right), \quad (4.9)$$

To evaluate Erf [] for parameter fits, root's built-in function was used. Root also includes a built-in Landau function, but it makes everything very slow if we use it.

$$\begin{aligned} f_5 = & \frac{p_\Delta}{2 p_\gamma p_W^3} \left[(x - E_0) \left(\operatorname{Erf} \left[\frac{(x - E_0)}{\sqrt{2 p_{\text{toeres}} |E_0|}} \right] - 2 \operatorname{Erf} \left[\frac{(x - E_0 - p_W)}{\sqrt{2 p_{\text{toeres}} |E_0 + p_W|}} \right] \right. \right. \\ & + \operatorname{Erf} \left[\frac{(x - E_0 - 2p_W)}{\sqrt{2 p_{\text{toeres}} |E_0 + 2p_W|}} \right] \left. \right) + (2 p_W) \left(\operatorname{Erf} \left[\frac{(x - E_0 - p_W)}{\sqrt{2 p_{\text{toeres}} |E_0 + p_W|}} \right] \right. \\ & \left. \left. - \operatorname{Erf} \left[\frac{(x - E_0 - 2p_W)}{\sqrt{2 p_{\text{toeres}} |E_0 + 2p_W|}} \right] \right) + (2 p_{\text{toeres}} |E_0|) \left(\left(\frac{e^{\left(\frac{-(x-E_0)^2}{(4 p_{\text{toeres}} |E_0|)} \right)}}{\sqrt{2\pi p_{\text{toeres}} |E_0|}} \right) \right. \right. \\ & \left. \left. + \left(\frac{-2e^{\left(\frac{-(x-E_0-p_W)^2}{(4 p_{\text{toeres}} |E_0+p_W|)} \right)}}{(\sqrt{2\pi p_{\text{toeres}} |E_0+p_W|})} \right) + \left(\frac{e^{\left(\frac{-(x-E_0-2p_W)^2}{(4 p_{\text{toeres}} |E_0+2p_W|)} \right)}}{\sqrt{2\pi p_{\text{toeres}} |E_0+2p_W|}} \right) \right) \right], \quad (4.10) \end{aligned}$$

and

$$\begin{aligned} f_{511} = & |p_{\text{scale}}| \left[\left(\frac{195}{17} \sqrt{\frac{2}{\pi}} e^{\left(\frac{-(x-308)^2}{578} \right)} \right) + \left(40 + \frac{(x-210)^2}{900} \right) \left(1 - \operatorname{Erf} \left[\frac{x-334}{30} \right] \right) \right. \\ & \left. + \left(\frac{(x-505)^2}{1440} \right) \left(1 - \operatorname{Erf} \left[\frac{x-505}{30} \right] \right) \left(1 + \operatorname{Erf} \left[\frac{x-334}{30} \right] \right) \right], \quad (4.11) \end{aligned}$$

where a p with any subscript is taken to be a variable parameter that must be evaluated. The expressions f_1 , f_2 , f_3 , f_4 , and f_5 are motivated by or taken directly from expressions of the same name within Clifford's description, and the individual parameters p_α , p_β , p_γ , p_Δ , p_W , and p_k are closely related to their counterparts of similar name [52]. The expressions f_{moyal} and f_{511} represent a departure from the published treatment, however, and arise from physical behaviours within this experiment which are not described within Clifford's treatment.

In particular, f_{511} is a rather inelegant representation of the annihilation radiation compton edge within our geometry. Although the DSSD provides an effective veto for

the overwhelming majority of these events—and indeed within Clifford’s treatment this veto is treated as being perfect in its discernment—it is clear both from experimental spectra and the Geant4 simulations intended to represent them that there exist a small number of such events within our scintillator spectra that cannot be vetoed in this manner. These events must be understood and adequately accounted for.

It should be noted that no attempt is made to derive the expression for f_{511} from first principles; the expression was chosen only because of its visual similarity to the spectrum’s fit residuals before its inclusion. This expression’s contribution to the overall function is negligible at all but the lowest initial beta energies (Eq. 4.11’s p_{scale} parameter, showing the absolute normalization of f_{511} , is plotted in the top right of Fig. 4.7.), and is always negligible at scintillator energies above $\sim 500 \text{ keV}$, as can be seen in Fig. 4.5. We note that within the final analysis, all scintillator spectra will be given a low energy cutoff at 400 keV , so the only the higher energy tail of f_{511} will make any contribution.

The expression f_{moyal} arises from the beta particles’ energy loss within materials (i.e. the mirror, the beryllium foil, and the DSSD itself, as in Fig. 2.6) before its eventual absorption within the scintillator. Although Clifford’s treatment does include a ΔE detector (our DSSD would be the equivalent), the energy absorbed in this detector is added back in to the total before Clifford’s final spectra are modeled. Although it would be possible to do something similar with our DSSD spectra, we would still be left with the problem of accounting for the similarly-shaped energy loss within the mirror and foil.

The distribution for energy deposition within a thin material by an energetic charged particle, first described by Lev Landau in 1944 [53], is now known as a Landau distribution. This distribution has a variety of properties that make it challenging to work with – notably its mean, variance, and all higher moments are undefined, and the distribution itself cannot be written in closed form. Its primary redeeming mathematical feature, however, is the fact that the convolution of a Landau distribution with another Landau distribution is, itself, a Landau distribution, and this means that we can represent the sum total of energy absorption within three successive thin materials as a single Landau distribution.

Within the present context, an expression for energy absorption that can be evaluated and re-evaluated quickly by computer with adjusted parameters is needed, as this must be used within a fit function. To this end, we employ a so-called ‘Moyal

Also, I think for this particular part of analysis, the cutoff was like 600 keV.

Some of this content needs to go somewhere else.

We never attempt to do this, because reasons. Don’t I talk about this somewhere?

function', which was developed in 1955 to be used as a closed form approximation to the Landau distribution [54]. Indeed, Eq. 4.5 is little more than a Moyal function.

...as previously mentioned, re-introducing the energy from the BB1s invites problems with maintaining a uniform energy threshold over the entire detector.

somewhere I have to talk about the empirical noise spectrum etc. on the BB1s. Or maybe I've already mentioned it somewhere.

The values of these parameters are allowed to vary with initial beta energy, and must be determined empirically by a series of fits to simulated spectra. To effect this result, the TRINAT Geant4 simulation is used to generate a series of 'mono-energetic' spectra. That is, for each energy value under consideration (with discrete values selected to span the energy range of betas in our decay), events are generated in which every outgoing beta initially has the same amount of kinetic energy, and the angular distribution of these betas is physically appropriate for the polarization and beta energy under consideration. These mono-energetic betas are propagated through the experimental geometry via Geant4, and the resulting scintillator spectra are recorded. Each polarization state must be considered separately, but spectra for both detectors are generated simultaneously, as it is necessary to generate events into a full 4π steradians in order to fully account for betas scattered into- or away from the detectors. Cuts identical to those imposed on the experimental data are applied (see Chapter 3). Several such spectra are shown for the Bottom Detector in the '-' polarization state, with their best fit response functions, components thereof, and residuals of the fit, in Figs. 4.1, 4.2, 4.3, 4.4, and 4.5.

The values of the individual parameters contributing to the fit functions in, eg, Figs. 4.1, 4.2, 4.3, 4.4, and 4.5 are allowed to vary with initial beta energy, and the energy dependence of each parameter must be modeled in order to extrapolate the shape of the response function to intermediate initial beta kinetic energy values that are not explicitly modeled. For each parameter, the energy dependence is modeled by an analytic function selected to have similar characteristics. Each of these analytic functions is itself a function of several parameters which can be adjusted to optimize its fit to the true best-fit energy dependence of the parameter it models. Because some parameters are only weakly independent, it is necessary to perform these fits iteratively on only a single parameter at a time, revisiting earlier parameter fits after fixing other parameters to updated models. The results of this process are shown in Figs. 4.6, 4.7, 4.8, and 4.9.

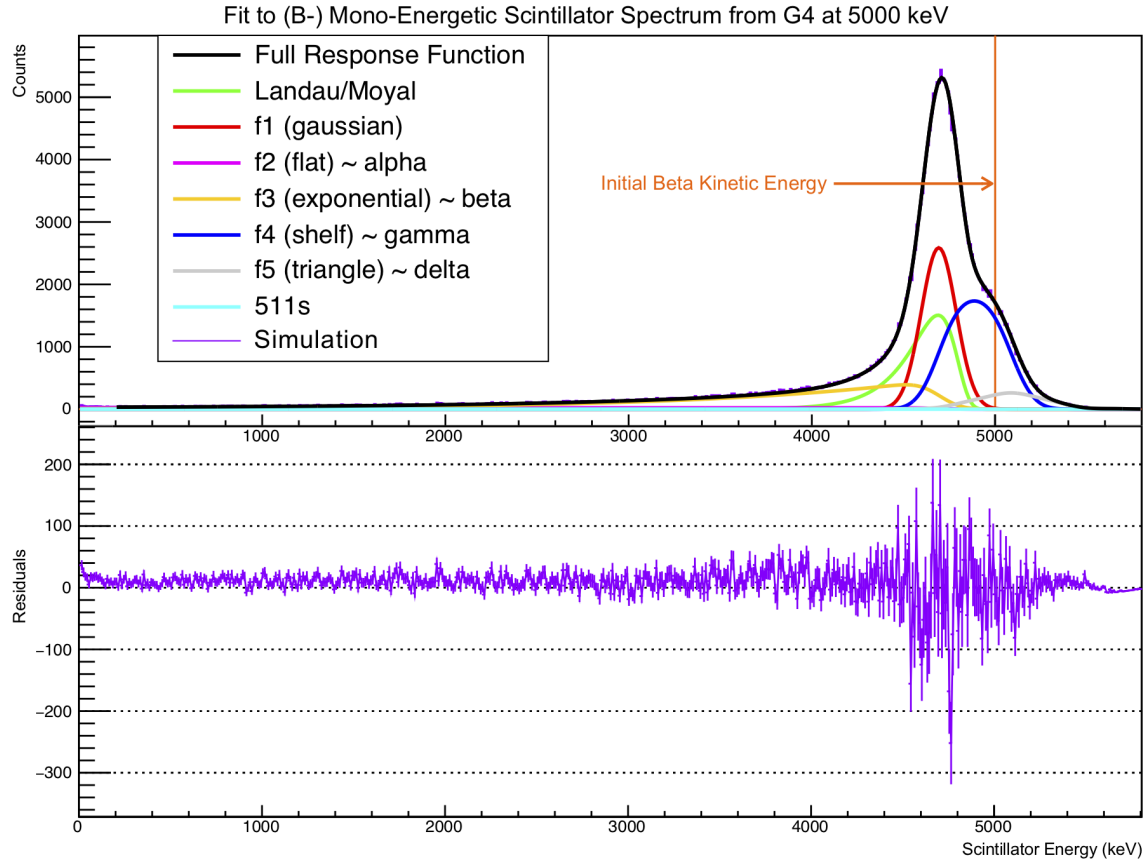


Figure 4.1: Fit to Mono-Energetic Spectrum, 5000 keV (B-)

It is useful to consider how well this empirical response function works to model the spectra. One can see clearly from Figs. 4.1, 4.2, 4.3, 4.4, and 4.5 that the fit residuals appear noticeably *worse* at lower initial beta energies. Fig. 4.10 shows the reduced χ^2 values arising from comparing mono-energetic G4 spectra to the empirical response functions described above, for all four detector and polarization combinations.

With the energy dependence for each of the response function's parameters carefully modeled, it becomes possible to make proper use of the full response function. Given a decay event with a known beta energy from a nucleus with its initial polarization known, we can now predict a probabilistic response from *both* scintillator detectors. Obviously, for a single decay event, the full spectrum cannot be realized – however in aggregate the modeled response function agrees well with results from the full Geant4 simulation, particularly at higher beta energies.

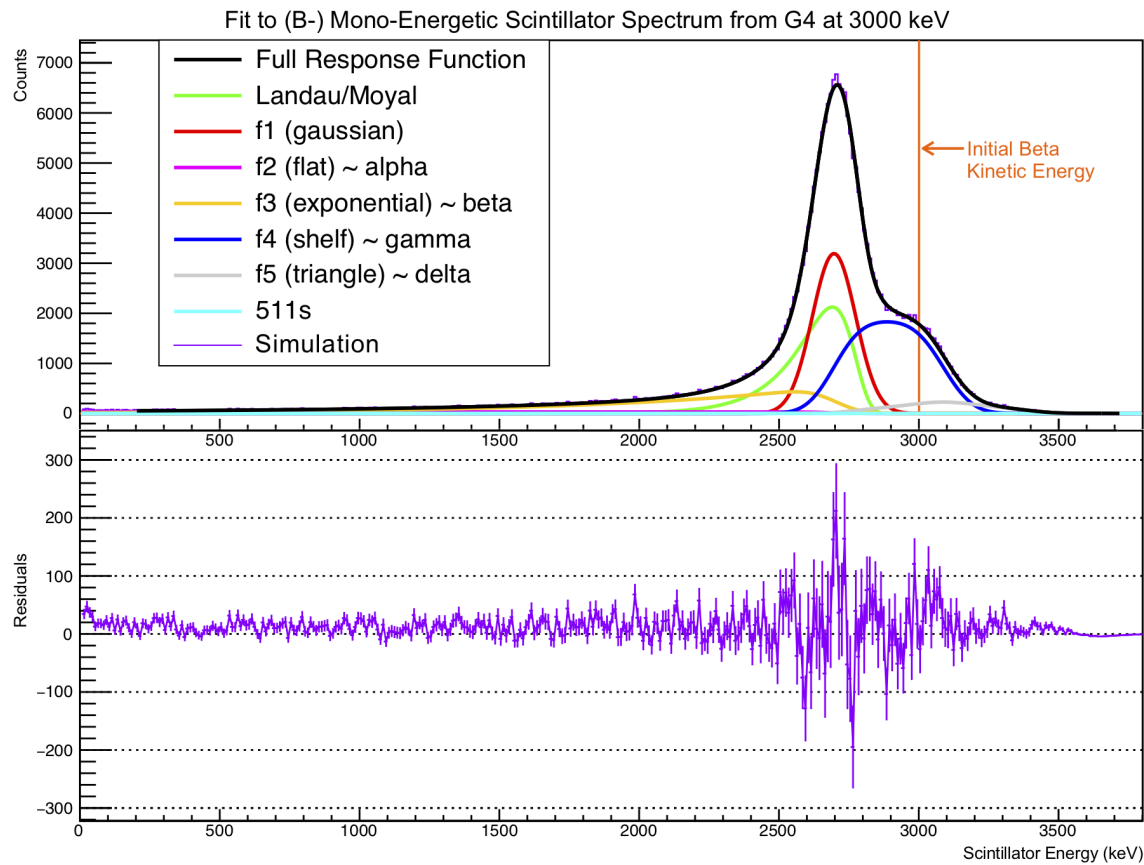


Figure 4.2: Fit to Mono-Energetic Spectrum, 3000 keV (B-)

Missing figure

Show SimpleMC spectra, and show SimpleMC+Lineshape spectra with RealData.

Needs a picture of the *full* beta energy distributions that come out of the lineshape thing. To compare with (a) data and (b) G4. Probably a superratio in there somewhere too.

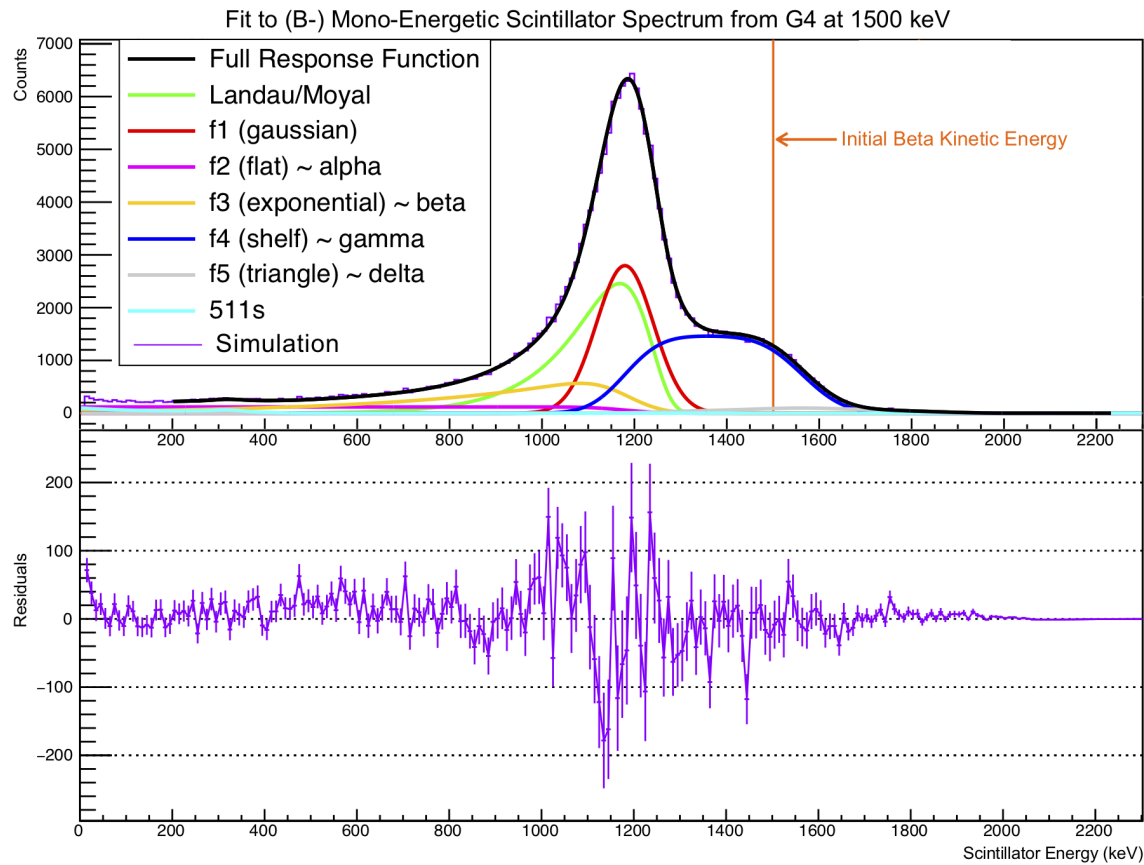


Figure 4.3: Fit to Mono-Energetic Spectrum, 1500 keV (B-)

Um. Which of the scattering things did I actually put in at the end? And when did I do it?
 Like, how did I account for (back-)scattering? I tried with/without scattering, I think? and eventually decided not to do it. for some reason. I think it breaks normalization in some way that's more subtle than you would think.

...

Do I need the angular distribution in the end? I think maybe I put in scattering later, and just used a cone for the first round. I re-did this to do the opposite thing at some point.

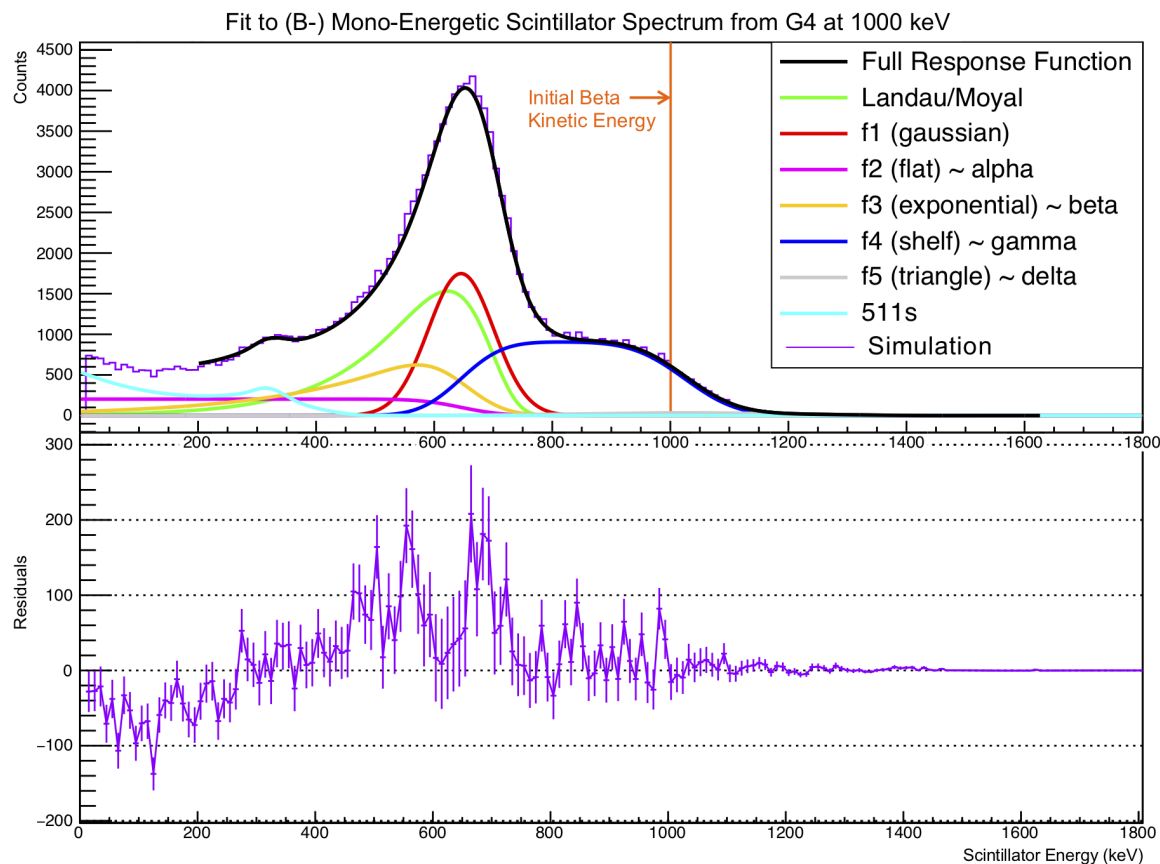


Figure 4.4: Fit to Mono-Energetic Spectrum, 1000 keV (B-)

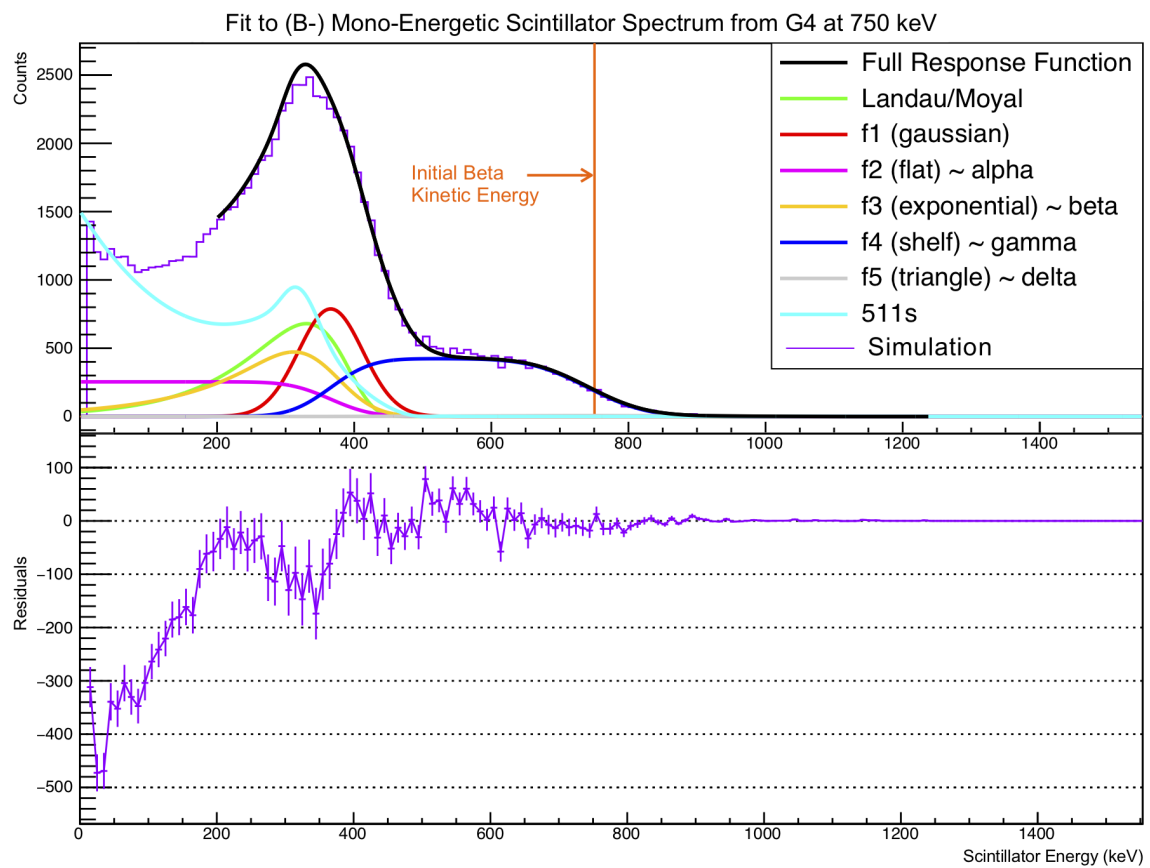
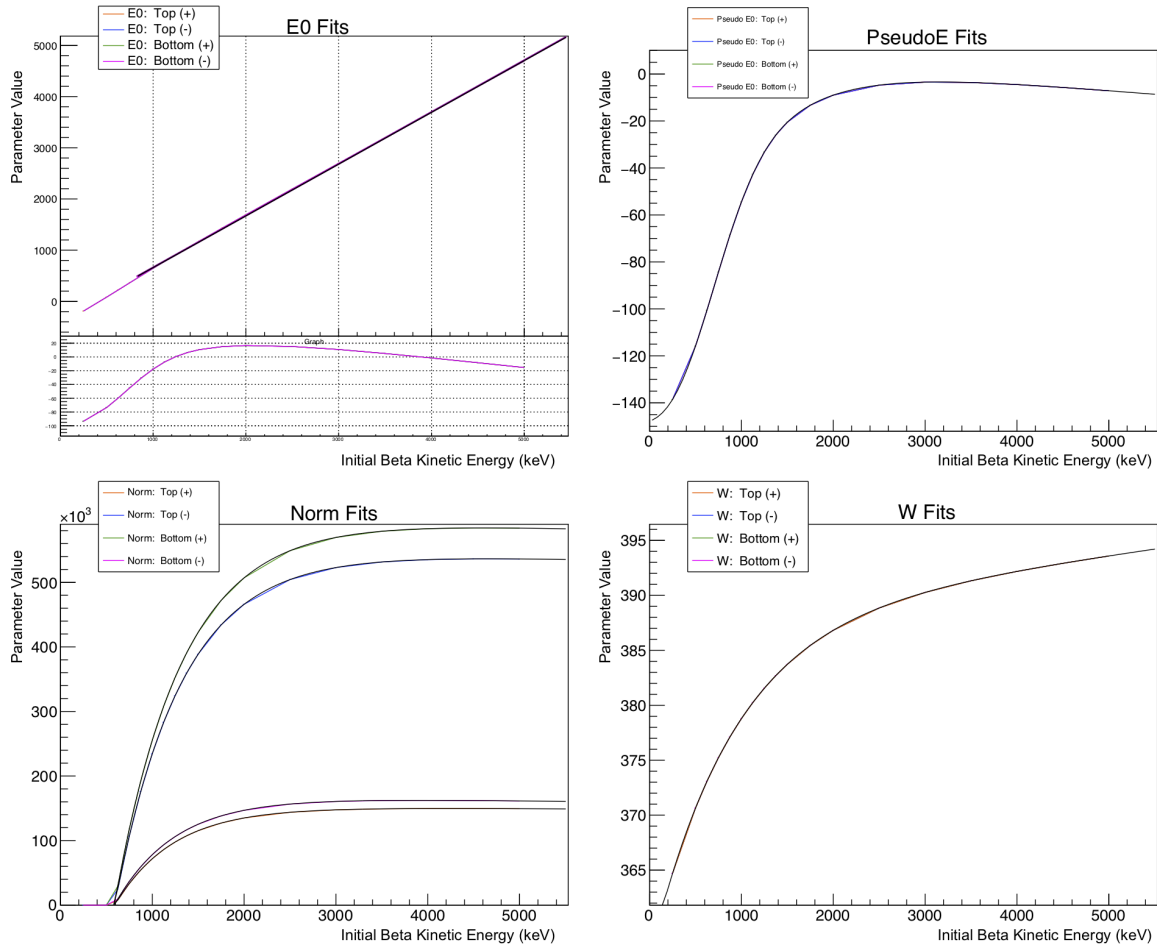


Figure 4.5: Fit to Mono-Energetic Spectrum, 750 keV (B-)



What even *is* the thing plotted below E0 in the ‘residuals’ spot, you ask? It’s ‘PseudoE’, which is describes the difference between the original input energy, E_0 , and the energy where the output spectrum is maximal. Or something. To ‘pretty good’ order, it’s a straight line. the ‘PseudoE’ plot shows what’s left after you fit it to a straight line. It’s fucking weird that it’s negative everywhere. Like, what?

Figure 4.6: Lineshape Parameter Fits (Part 1)

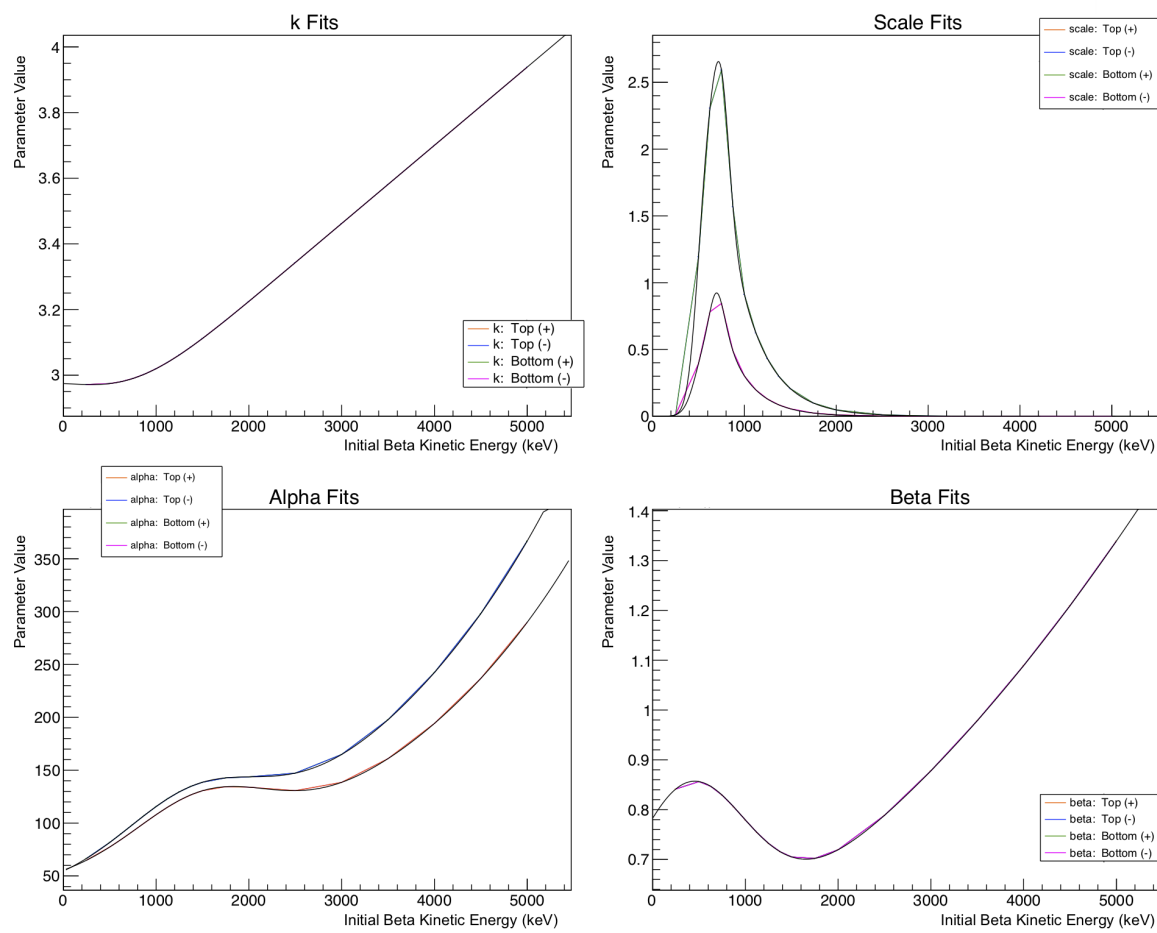


Figure 4.7: Lineshape Parameter Fits (Part 2)

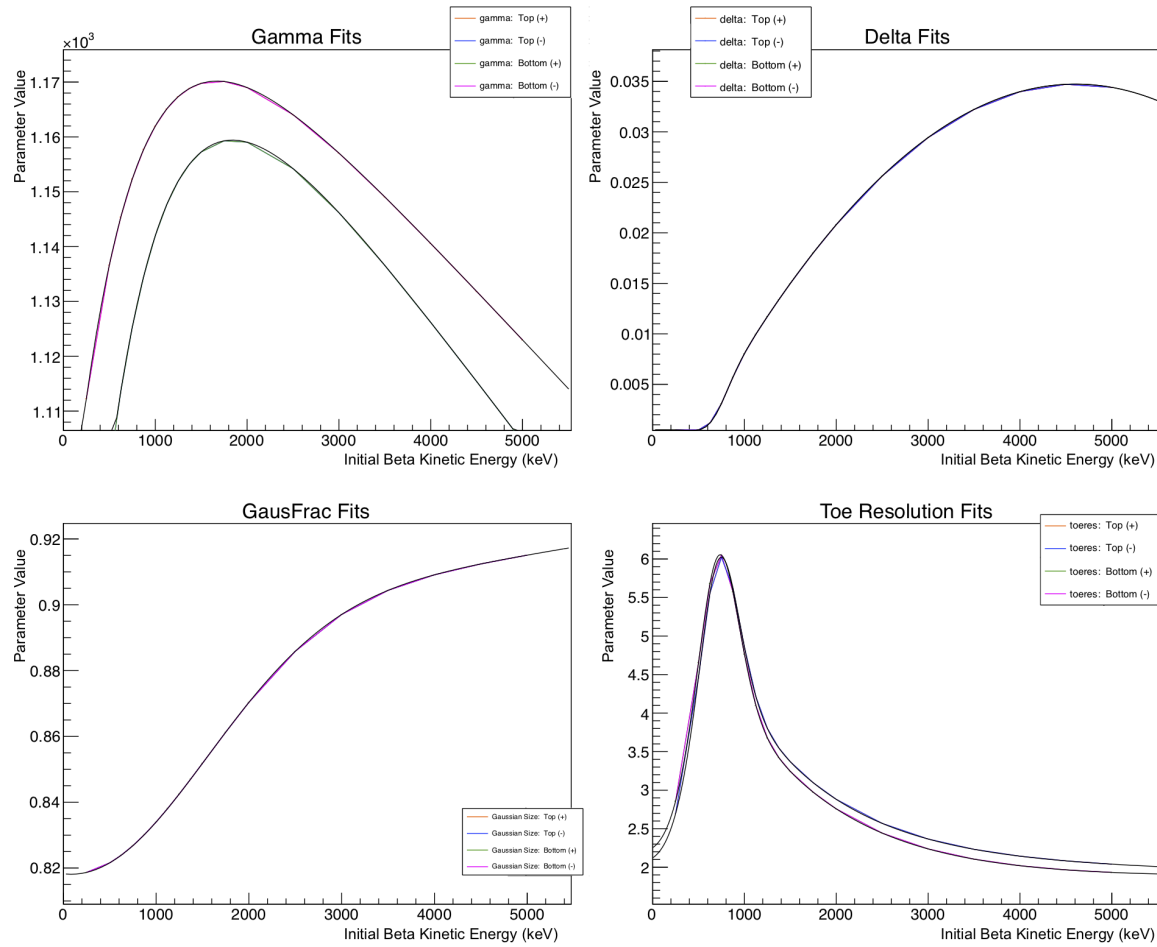


Figure 4.8: Lineshape Parameter Fits (Part 3)

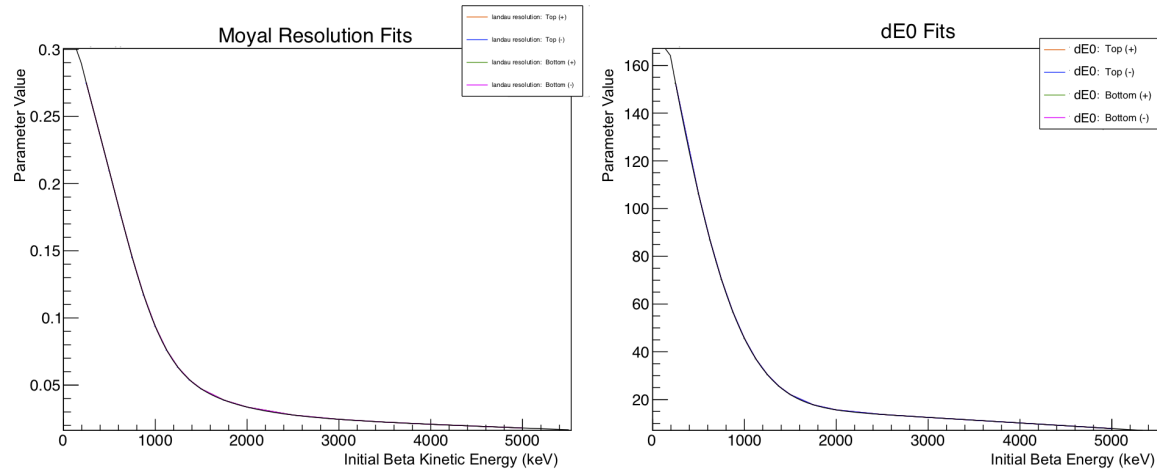
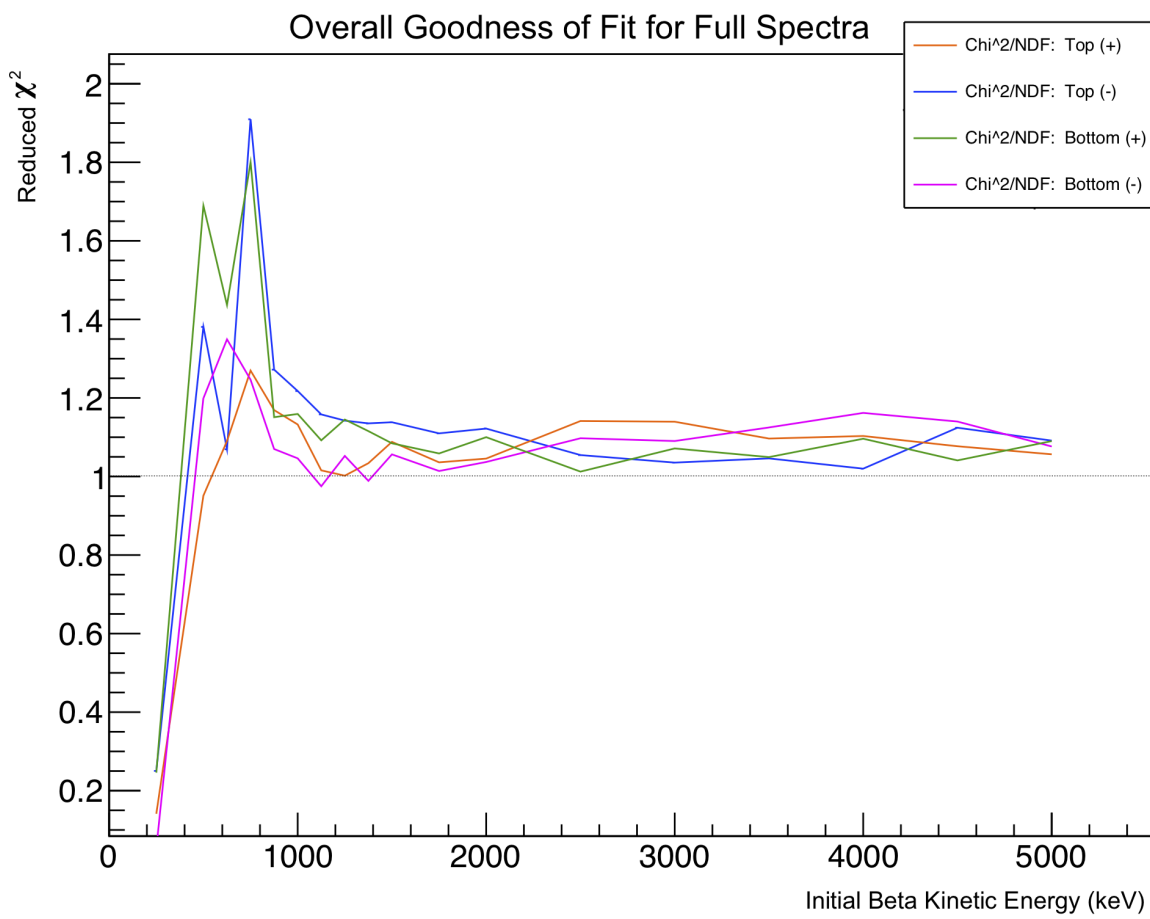


Figure 4.9: Lineshape Parameter Fits (Part 4)



How many DOF for these things? I should put it on the picture.

Figure 4.10: Goodness of fit for modeled response functions, for all four detector+polarization combinations. The models are clearly much better behaved at initial energies above ~ 1200 keV.

4.4 Modeling the Scattering Effects from the Cloud

Beta scattering — in which a beta originating within the atom cloud is incident on a surface within the chamber and changes its trajectory, losing some of its energy in the process — is a significant systematic within this experiment, and it must be evaluated, quantified, and corrected for. While only a small fraction of events are affected, the process results in a change to the beta energy spectrum that can easily be misinterpreted as the exact signal we are searching for. It is therefore imperative that this be well understood.

The scattering process can result both in scenarios where a beta that was initially directed away from the detectors is scattered *into* a detector, and scenarios where a beta that was initially traveling towards a detector is scattered *away* from it. Since this is a polarized decay and the beta asymmetry is not zero, the relative likelihoods of each of these two scenarios depends on whether the nuclear polarization vector is directed toward- or away from the detector in question. In either case, it is clear that some events will be removed, and other events will be added in. As a further complication, betas that have been scattered into a detector will necessarily have a very different energy spectrum than unscattered betas, and neither are the betas that are scattered away from a detector removed uniformly from the original energy spectrum. With the four beta energy spectra comprising the essence of our observable, we must have a clear understanding of the results of this process within our data.

Despite these complications, it is clear that for events in which the beta is scattered from a surface prior to its incidence on a detector, the beta particle will take longer to travel from the position of its initial creation to the detector. Although it is not possible to fully separate scattered and non-scattered events from one another, a judicious choice of cut within the SOE-Beta TOF spectrum can still be used to lower the fraction of scattered events, improve our signal-to-noise ratio, and decrease the overall size of any systematic uncertainties associated with scattering.

It is useful to remember in the discussion that follows that a beta particle emerging from a nuclear decay is, in general, fairly energetic, with perhaps a few MeV of kinetic energy. In comparison, a shake-off-electron (“SOE” – see Chapter 1.8) typically has only a few eV of kinetic energy. As a result, within our experimental time-of-flight spectra, because it is not possible to observe the *true* time of decay, we have commonly used as a proxy the time at which a beta hit is detected. The betas are relativistic

long high-energy tail.
it's actually critical to
the analysis.

and can be treated (for these purposes) as travelling at the speed of light – therefore if we suppose that all detected betas proceed from the position at which they were created directly into a detector, then the beta hit timestamp provides an excellent proxy for the true decay time, with only a small and easily calculable timing offset. Fig. ??, for example, is a spectrum of this sort for the shake-off-electrons’ “times of flight”.

Fix link to Fig. ?? !

Within this section, however, where the experimental SOE TOF spectra are examined in detail, the above assumption is insufficient, as it is necessary to consider effects from beta scattering – both to the observed beta energy spectra, and also to the observed beta time-of-flight spectra (which, of course, are only experimentally meaningful in comparison with another timed observation).

Using Geant4, a set of beta time-of-flight spectra is generated for decays originating from within the atom cloud for all four detector+polarization combinations, and it is clear that there is a small but non-negligible fraction of such events that arise from beta scattering events. Even within Geant4, where it is possible to measure the beta time of flight with respect to the initial time of decay, the scattered and unscattered spectra cannot be fully separated from one another. The strong correlation between emission angle and time-of-flight does, however, suggest that the signal-to-noise ratio could be improved by a judicious cut on the TOF spectra. In order to produce something which can be directly compared with experimental data, a TOF spectrum for SOEs must also be produced and merged with the beta TOF spectrum. Experimentally, this is done as an event-by-event subtraction, so that is also what must be done for the simulations. Unfortunately, these two time-of-flight spectra cannot easily be produced within a single type of simulation. Because scattering is an important effect within the beta time of flight spectra (and resulting beta energy spectra), Geant4 is the tool of choice for this type of particle. For shake-off electrons, which are emitted with little energy and accelerated through the electric field within the chamber, it is much more important to have an accurate model of the electric field and its effects on charged particles. The shake-off electrons’ time of flight is therefore evaluated by the TRINAT collaboration using COMSOL to track individual electrons through a model of the electric field within the experimental geometry.

The COMSOL SOEs were generated with starting positions taken from a 3D gaussian distribution near the chamber centre, with the precise position and size parameters taken from measurements using the rMCP, as in Table 3.3. They are

emitted with initial trajectories distributed isotropically. Three sets of SOE events are created: two with initial energies taken from the Levinger $4S$ and $3P$ spectra in the range of 0–100 eV, and the third with no initial kinetic energy. The origin of these SOE energy distributions is discussed in Section 1.8. A final simulated SOE TOF spectrum (relative to the time of decay) was produced as a linear combination of these spectra, comprised of 9% 0 eV events, 77% $4S$ events, and 14% $3P$ events. The relative contributions of each of these components arose from a comparison with experimental data, and the collaboration found that the distribution of hit positions on the eMCP was well modeled by Levinger’s formulae. There was only a very weak dependence on the relative number of SOEs removed from the $4S$ and $3P$ shells, though it turned out to be very important that the distributions not be truncated at too low an energy—a surprising result given the fact that both distributions are strongly peaked at much lower energies, and many of the higher energy SOEs are able to escape the central electric field region and therefore escape detection. The addition of the 0 eV events from $^{37}\text{Ar}^-$ ions to the spectrum also greatly improved the fit.

With both a SOE TOF spectrum generated by COMSOL and a beta TOF spectrum generated by Geant4, the two spectra were combined event-by-event to produce a simulated “SOE – Beta” TOF spectrum to match the form of the data collected from the experiment. Note that although the simulated SOEs were generated from a model of the atom cloud, the betas generated by Geant4 were simply treated as originating from a pointlike distribution at the chamber centre. Since the betas are relativistic and the cloud is small, any changes to the beta spectrum as a result of this model would be too small to be seen given the timing resolution of our detectors (~ 0.1 ns).

This “SOE – Beta” spectrum is convoluted with a gaussian of width $\sigma = 0.443$ ns to model the timing jitter within our detectors. The width of this gaussian is taken from a measurement of the “prompt” peak (betas incident on the eMCP before scattering into a scintillator) within the equivalent experimental spectrum. Results for Levinger SOEs and 0 eV SOEs are shown in Fig. 4.11.

Is this even what these events are?

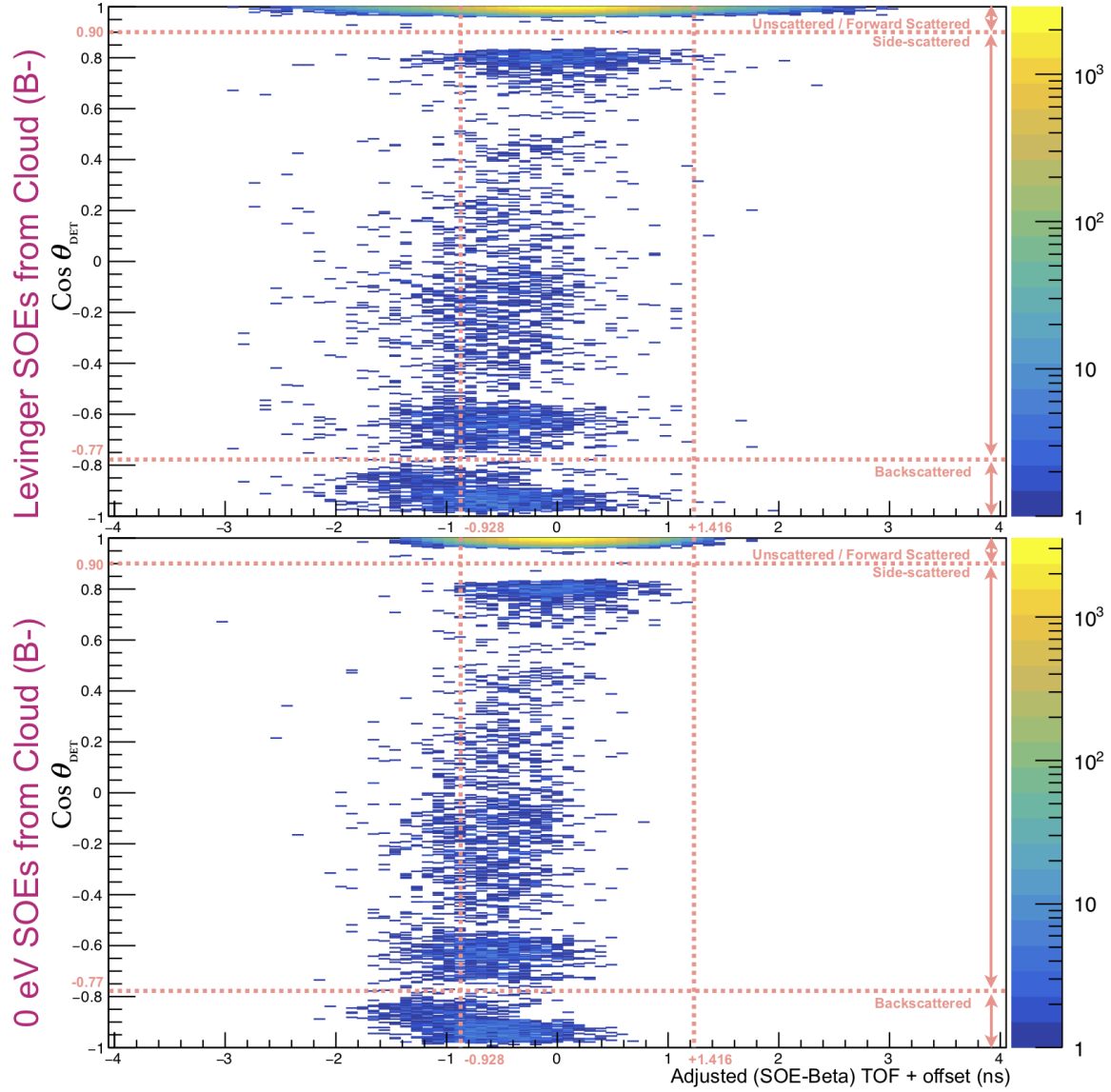


Figure 4.11: Simulated Beta emission angle with respect to the detector in which the event is eventually observed(G4), plotted versus an adjusted SOE – Beta TOF (COMSOL, G4). SOEs are simulated with initial energy distributions adapted from Levinger (top), and with no kinetic energy at all (bottom). The TOF cut that will eventually be taken is shown, and events are classified into scattering categories for later evaluation as a systematic (see Ch. 5.2.1).

4.5 Simulating the Background and Time of Flight

One of the largest sources of background events in this experiment is from decaying ^{37}K atoms that have escaped from the trap and become stuck on the other surfaces

within the chamber. The majority of these events can be eliminated simply by taking a time-of-flight cut on the eMCP relative to a scintillator hit time (as described in Section 3.8). Unfortunately, this procedure cannot remove the entirety of the background, so what remains—both background events from chamber surfaces, and events from the atom cloud itself—must be modeled and understood.

The model used for events originating from the atom cloud is described in Section 4.4, and this section will discuss events originating from other surfaces within the chamber. The methodology used is very similar.

Spectra for both the beta time of flight and shake-off electron time of flight (calculated with respect to the time of decay) were generated, using Geant4 and COMSOL, respectively. For these background events, the SOE and beta were both generated to originate on certain surfaces within the experimental chamber. Because the surfaces from which generated SOEs had a viable path through the electric field onto the eMCP is relatively large, the SOE and beta spectrum must be generated, event-by-event, to originate at the same position. This procedure not only allows us to account for differing beta times of flight resulting from different distances to either detector, it also captures the differing energy loss from scattering for observed betas originating at different positions.

To model the distribution of atoms stuck to surfaces within the chamber, we suppose that all escaped atoms were lost from the central cloud in an isotropic manner, so that the number of atoms on an object’s (infinitesimal) surface element is given by the (infinitesimal) solid angle spanned by it. This principle is used both to normalize the relative number of decay events between different surfaces, and also to produce the distribution of events on a given surface. Then, for each surface of interest to us, a set of Geant4 beta decay events are generated from starting points on that surface, with those starting points distributed as described above. The beta particles are tracked through the geometry, and only events in which a beta is incident on a scintillator are saved.

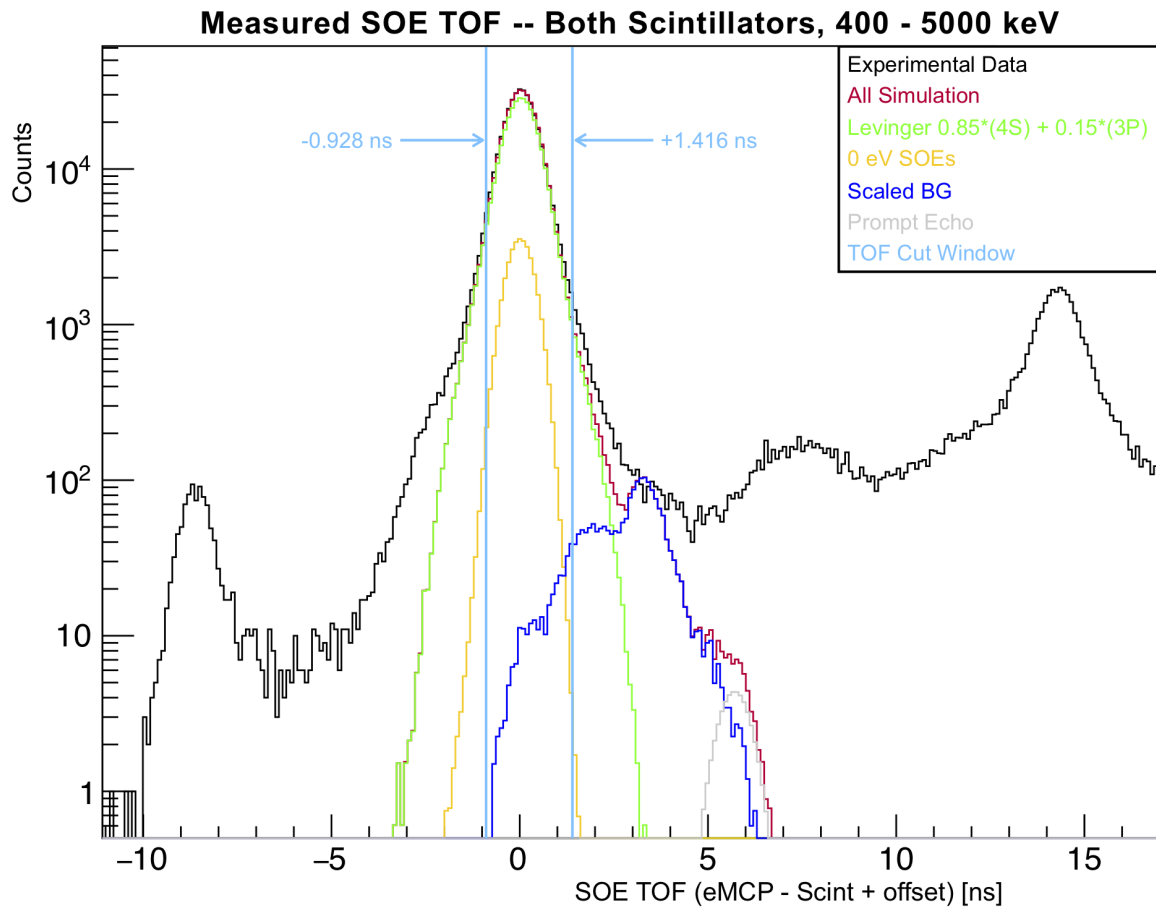
For Geant4 events in which a scintillator hit is recorded, these events’ start positions are then fed into COMSOL and used as start positions for SOE events, generated by the collaboration with the same energy spectrum that was used for events from within the cloud, as described in Sec. 4.4. For these events, only the ones in which an SOE was incident on the eMCP were preserved. An event-by-event subtraction is then performed on the timing results of the Geant4 and COMSOL Monte Carlo

spectra, such that for every event that is preserved, the SOE in COMSOL and the beta in Geant4 will have originated from the same starting position. The results are then convoluted with a $\sigma = 0.443\text{ ns}$ width gaussian to model timing jitter, as in the case of events originating from the cloud (Sec. 4.4).

With a simulated “SOE – Beta” TOF spectrum to compare with experimental data, it is possible to estimate how many such events remain (and what their energy distribution looks like) after a cut on the experimental spectrum is performed. The results are shown in Fig. 4.12. An upper limit for the fraction of events generated this way can be estimated by assuming that all losses from the cloud not attributable to radioactive decay must emerge isotropically and then stick to whatever object is in its path. This method overestimates the amount of background by around a factor of 2.

In order to check this model’s performance, the energy-averaged superratio asymmetry is assembled for each time-of-flight bin within both our simulated and experimental spectra, as in Fig. 4.13. The modeled background is treated as being unpolarized. Although the two plots diverge rapidly outside this TOF range, an evaluation of the χ^2 statistic within this range produces a suspiciously good result.

“.... To check the agreement of the model with reality, we compare the averaged superratio asymmetries from both, as in Fig. 4.13.”



Reference Section 3.8, probably.

Figure 4.12: (SOE-Beta) TOF, with both model and experimental data shown. Spectra from simulations are separated according to their source, and the final TOF cut is drawn on. The background spectra have been scaled down by about a factor of 2 from their estimated maximum in order to match experimental data. Similar quality results are achieved no matter how the Levinger SOEs are distributed between 4S and 3P orbital shells, however adding the 0 eV electrons to the spectrum produces a large improvement to the agreement between the model and experiment.

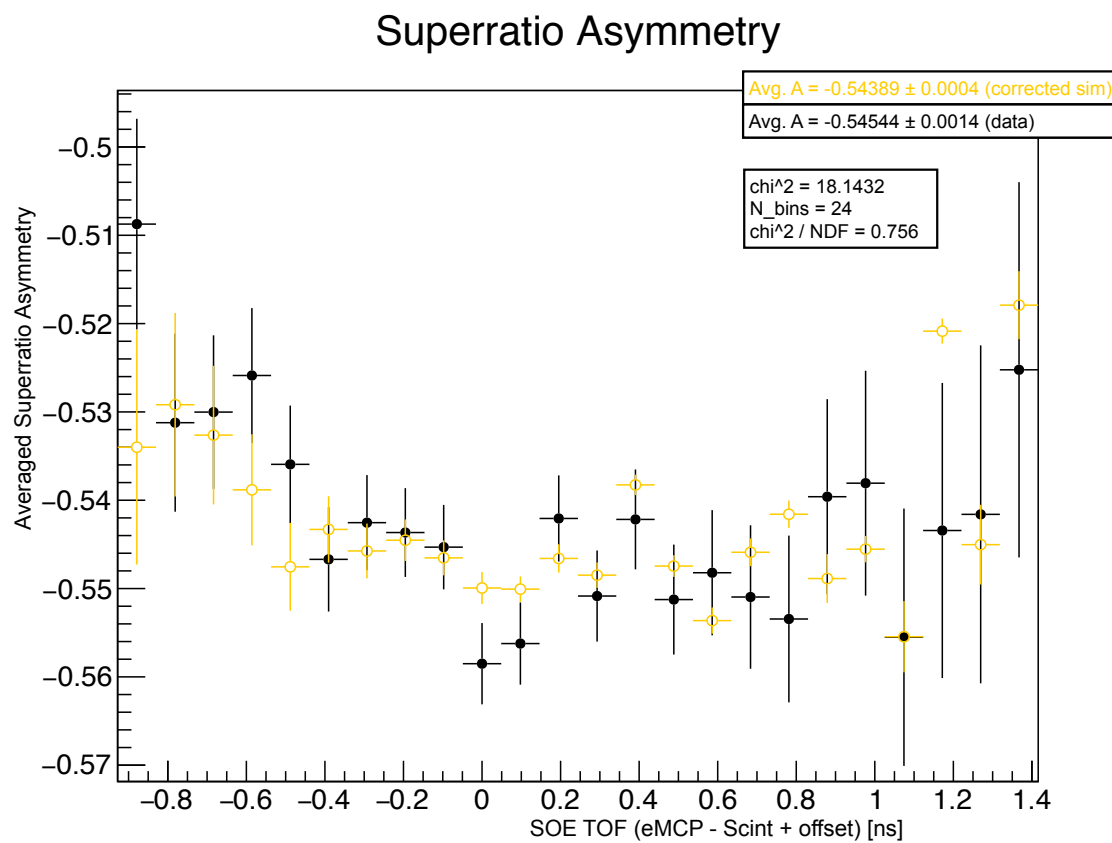


Figure 4.13: The superratio asymmetry, averaged over all scintillator energies between 400-4800 keV, is used to compare the experimental data and simulated TOF model as a proxy for the quality of the model to estimate the background. Background events are treated as being entirely unpolarized. All other cuts have been applied.

Chapter 5

Analysis and Estimates of Systematic Effects

Go through and change all instances of "Beta - SOE"/"Beta—SOE"/etc to "SOE - Beta"/etc., *within the whole thesis*.

John proposes the following intro statement for this Ch. 5. The following two(one) paragraphs are (almost) a direct quote from him:

The collaboration has performed an independent analysis using (mostly) the same set of data to measure A_β , fixing b_{Fierz} to zero. Differences with that analysis are interleaved in this section and summarized in Appendix B. Critical physics improvements concern an eMCP-beta timing walk correction which enabled an improved cut against background, also incorporating a more complete modelling of decay backgrounds from untrapped atoms. Technical corrections include a correct treatment of the polarization cycle. An arbitrary change in the DSSD radius cut is kept self-consistent.

Are they even though??

JB:

I've tried to email you the paragraphs on "collaboration determination of uncertainties" for (((Ch. 5)))

My intent of all that other advice was to keep your time spent on Chs 1-4 ((Now Ch. 1-2)) concise, so you could concentrate on these real jobs. (n.b.: the advice he's already sent was almost all about chapters 1-4, which are the various intros/background info and experimental setup stuff)

...

I can only say that if you have an equal choice between including a detail or not, pick "not." "

5.1 Comparing Simulations to Experimental Data: The General Methodology

The primary parameter measurement strategy in this project involved comparing the experimental data to a 2D parameter space of simulations, and this is true both for evaluation of the best parameter values, and also for evaluations of the uncertainties.

As described in Section 1.9, and in more detail in Appendix E, the primary experimental observable is the superratio asymmetry, which is constructed from four experimental *rates* of beta detection:

$$A_{\text{super}}(E_\beta) = \frac{\sqrt{r_{T-} r_{B+}} - \sqrt{r_{T+} r_{B-}}}{\sqrt{r_{T-} r_{B+}} + \sqrt{r_{T+} r_{B-}}}. \quad (5.1)$$

This quantity is closely related to the two fundamental parameters we hope to extract, and in the absence of certain systematic effects, we can cleanly describe a relationship between the observable and the two physical parameters (A_β and b_{Fierz}) that we might use to describe the shape of an experimentally measured $A_{\text{super}}(E_\beta)$ curve:

$$A_{\text{super}}(E_\beta) = \frac{A_\beta \frac{v}{c} |\vec{P}| \langle |\cos \theta| \rangle}{1 + b_{\text{Fierz}} \frac{mc^2}{E_\beta}}. \quad (5.2)$$

Of course, when all systematics are properly accounted for, Eq. 5.2 is no longer an adequate description of the full relationship between the observable and physical parameters and a comparison to monte carlo must be used. A series of Geant4 simulations are performed and the results are (re-)processed with slightly different cuts and calibrations so as to match with the experimental conditions in each of the three electron datasets, and the superratio asymmetries are constructed. The degree to which the simulations and experiment match is evaluated by using a χ^2 comparison of the superratio asymmetries as the figure of merit (see Figs. 5.1,5.2,5.3). This is repeated for a range of A_β and b_{Fierz} values, and a χ^2 mapping of the 2D parameter space is produced.

For each superratio asymmetry constructed from simulated spectra, the scintillator spectra from which the superratio asymmetry is comprised are created as a linear combination of Geant4 beta decay events originating from the atom cloud and from surfaces within the chamber. Both components of the spectra are combined event-by-

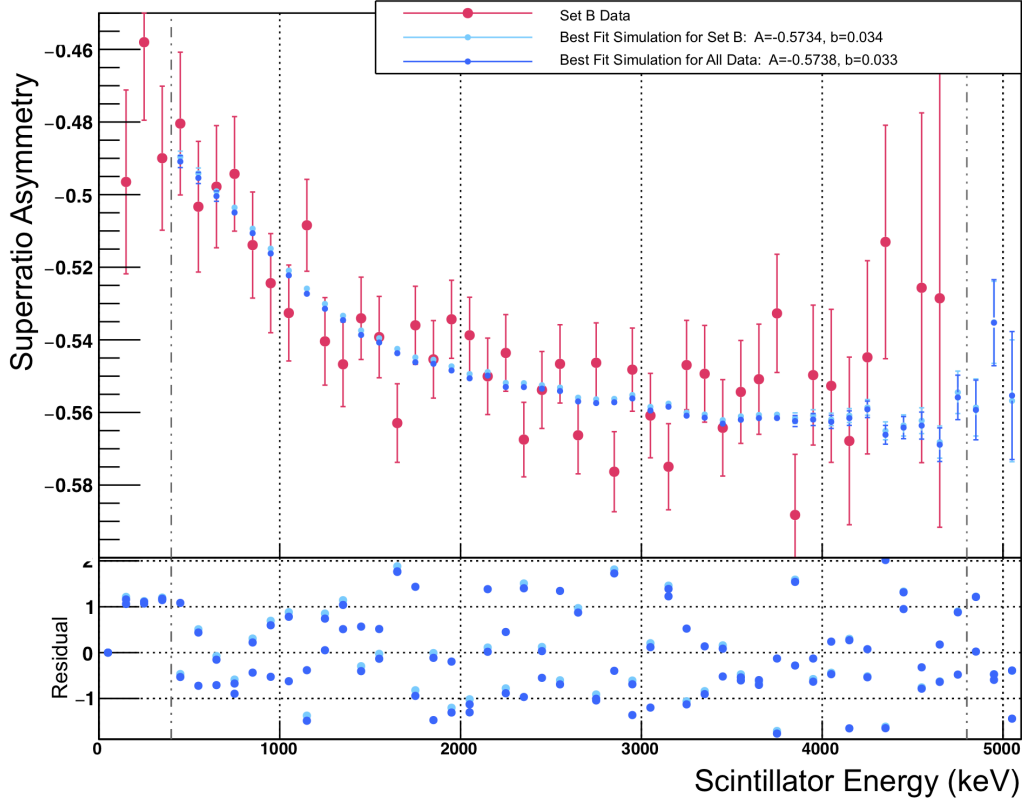


Figure 5.1: A superratio asymmetry from Dataset B, and the best fits from simulations.

event with SOE events generated in COMSOL, as described in Sections 4.4 and 4.5, as this is necessary for the critical time-of-flight cut on the “SOE – Beta” spectra. For decays originating within the atom cloud, both the primary decay branch and the subdominant ‘two percent’ branch are allowed to contribute events, and only the dominant branch is varied as a function of BSM couplings. For background events, only the Standard Model primary branch is simulated.

A major caveat to the above description is that running a high statistics G4 simulation of our experiment is a computationally expensive process, so it was not possible to perform a separate simulation at every ‘pixel’ within the parameter space. Instead, to evaluate how well the experimental data matched to the expectation for varying values of A_β and b_{Fierz} , only three simulations were performed for different values of b_{Fierz} , all using the same nominal value for A_β . The $A_{\text{super}}(E_\beta)$ spectra representing

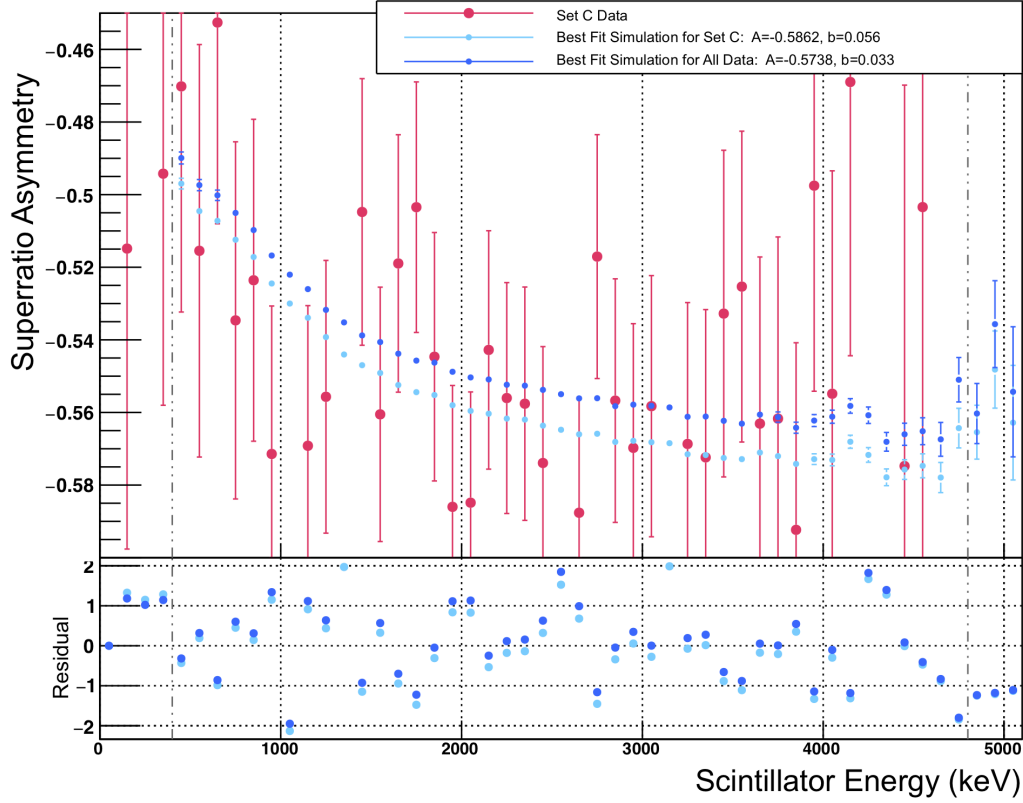


Figure 5.2: A superratio asymmetry from Dataset C, and the best fits from simulations.

intermediate b_{Fierz} values were created from a linear combination of spectra generated at the two closest values of b_{Fierz} .

To vary the effective A_β value, the generated $A_{\text{super}}(E_\beta)$ spectrum was simply scaled. From Eq. 5.2 it is clear that this works well so long as b_{Fierz} is small and any systematics are evaluated separately. This method allows for an arbitrarily finely pixellated 2D χ^2 map to be created. It is done separately for each of the three experimental data sets so as to facilitate evaluation of systematic effects that changed between runsets. See Figs. 5.4, 5.5, 5.6.

We can do this whole chi2 map thing again for real- and simulated data sets with different values of parameters that we vary as *systematics.* Note how the best values of A_β and b_{Fierz} change when each of the systematics are varied.

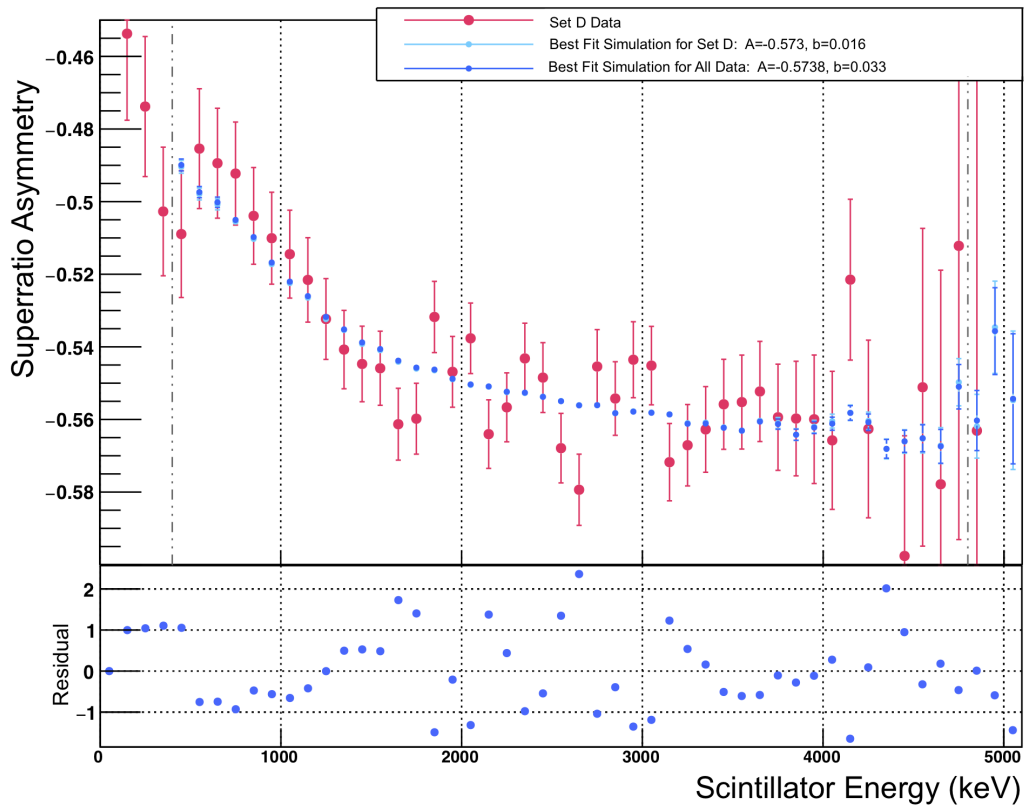
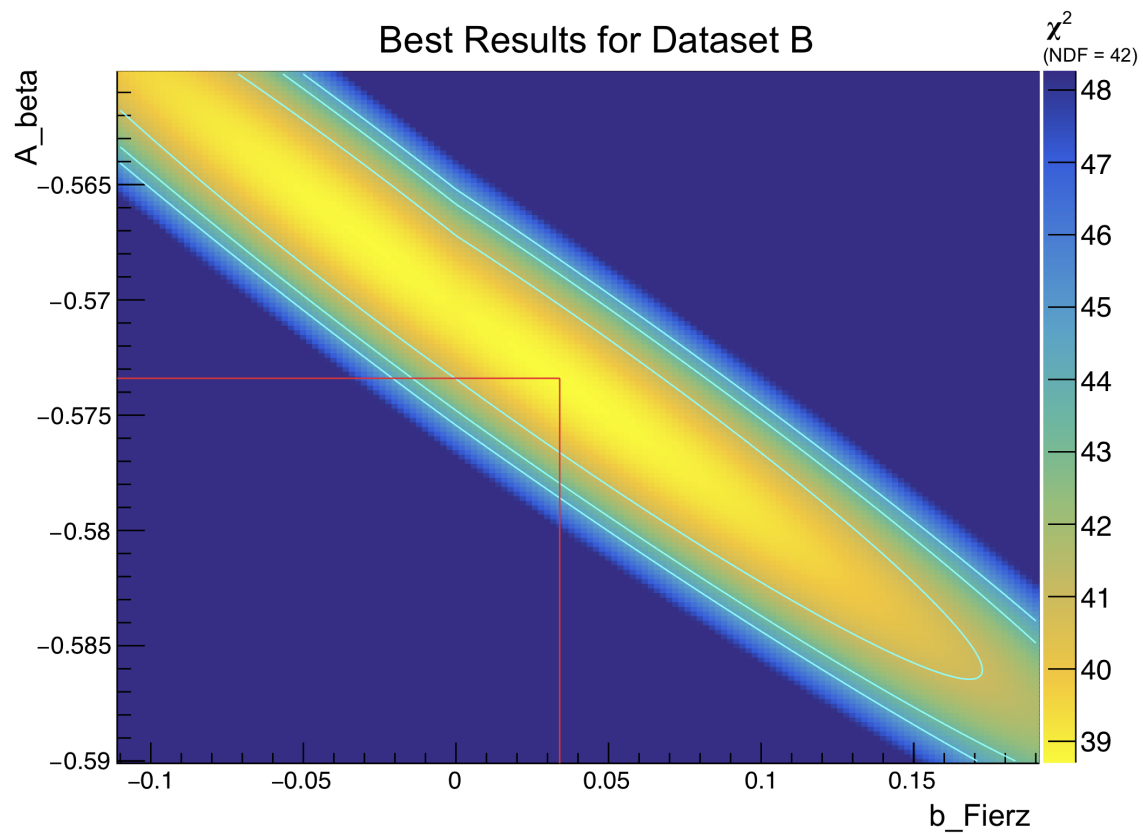


Figure 5.3: A superratio asymmetry from Dataset D, and the best fits from simulations.



Systematic uncertainties are evaluated by adjusting parameters and creating a new (set of) chi2 maps very much like this one.

Figure 5.4: A χ^2 map to compare data from Runset B to a parameter space of A_β and b_{Fierz} values. The contours show 1σ , 90%, and 95% statistical confidence intervals.

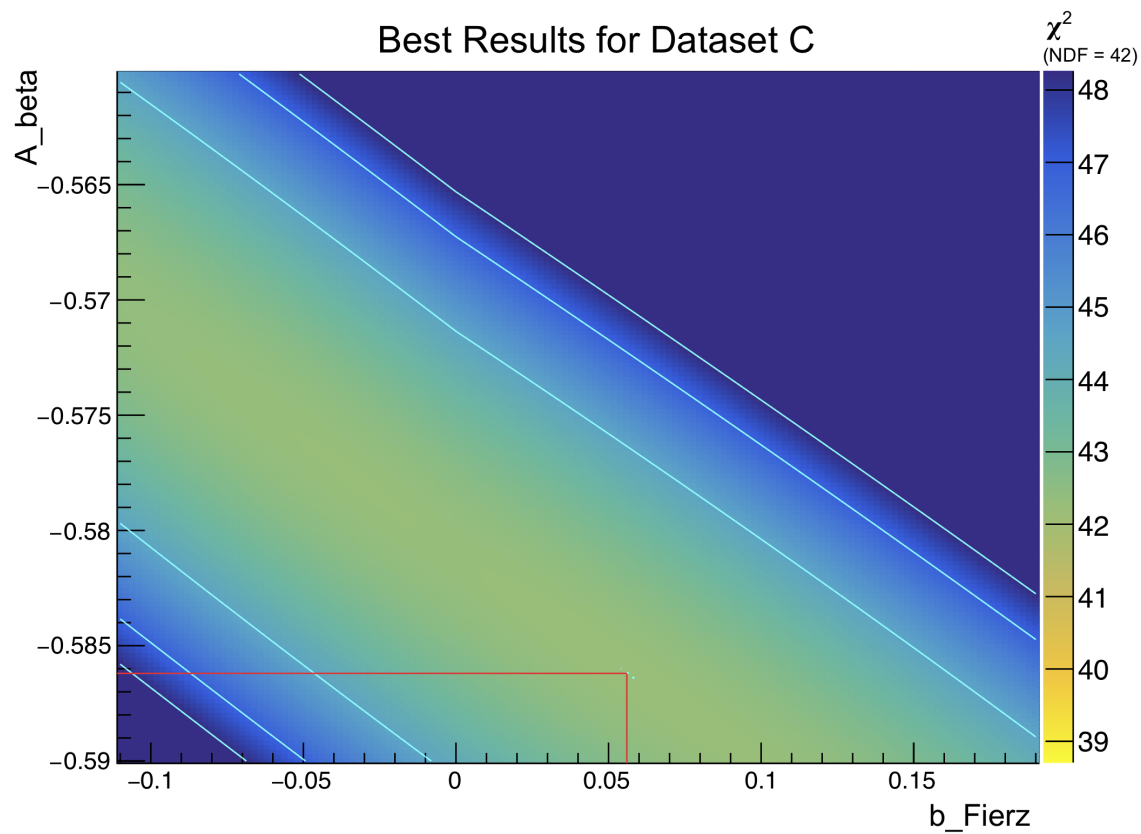


Figure 5.5: A χ^2 map to compare data from Runset C to a parameter space of A_β and b_{Fierz} values. The contours show 1σ , 90%, and 95% statistical confidence intervals.

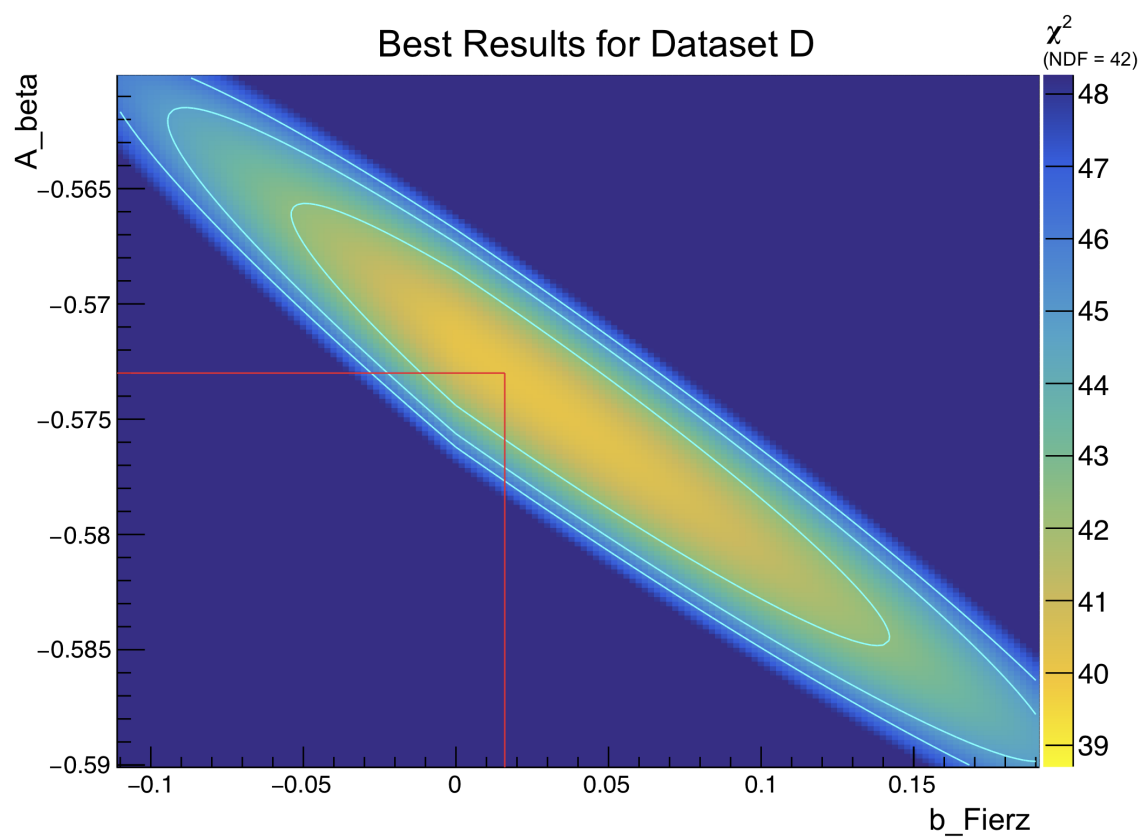


Figure 5.6: A χ^2 map to compare data from Runset D to a parameter space of A_β and b_{Fierz} values. The contours show 1σ , 90%, and 95% statistical confidence intervals.

5.2 Evaluation of Systematic Effects

5.2.1 Beta Scattering

The methodology used to simulate and model scattered events is described in Section 4.4. To evaluate the systematic effect on the final measurements arising from incomplete knowledge of how much beta scattering is present (i.e., how well we can trust the simulation to correctly model the amount of scattering), two sets of χ^2 maps very much like those in Section 5.1 are created, with the amount of scattering varied by one standard deviation. This does not require a new simulation; instead, for the three high statistics G4 simulations varying the BSM scalar coupling, all events passing the cuts are categorized into ‘unscattered and forward-scattered’ events, ‘sidescattered’ events, and ‘backscattered’ events, depending on a comparison of the beta’s emission angle to the detector in which it was eventually observed, as shown in Fig. 4.11.

The contribution from unscattered and forward scattered events is not allowed to vary, but the weights attributed to sidescattered and backscattered events was varied by $\pm 10\%$ and $\pm 5.1\%$ (respectively) relative to their ‘best’ values. Fig. 5.7 clearly shows the change in superratio asymmetry produced by this variation in the amount of scattering. The method by which it was determined how much the scattering weights should be allowed to vary is described in the supplementary material of a recent publication by the collaboration [48]. Since errors in evaluating both side-scatter and backscatter arise from limitations on how well Geant4 is expected to perform, it is not clear how correlated these errors are, but it seems foolish to suppose they should not be correlated at all. Therefore, the conservative assumption that the two are *fully* correlated is taken, and the errors from side-scatter and backscatter are added *linearly* to one another before being combined in quadrature with the other uncertainties.

As this is the dominant systematic error, the TRINAT collaboration is working to improve the experimental design to use lower-Z materials to reduce the size of this effect.

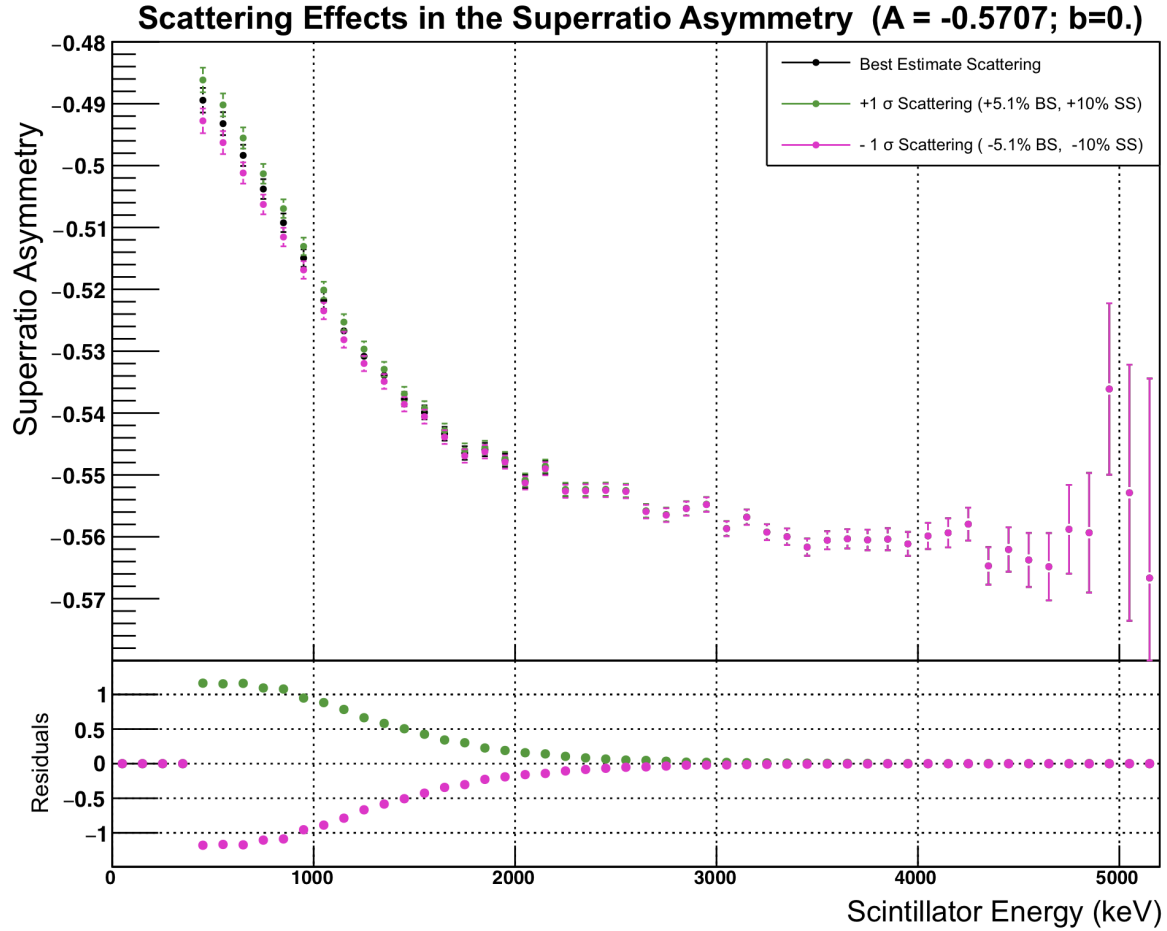


Figure 5.7: The amount of scattering is adjusted by one standard deviation in both directions, and the results to the superratio asymmetry are plotted. The bulk of the effect occurs at lower energies, where sensitivity to b_{Fierz} is at its highest.

5.2.2 Detector Calibrations and Thresholds

Scintillators

I could and probably *should* add a description of the scintillator threshold uncertainty evaluation. But I'm going to skip that for Round 1 and see if anybody notices.

The two plastic scintillators were calibrated by the collaboration using online data, with reference points from the beta spectrum endpoint and the compton edge arising from annihilation radiation. Calibration was performed using only *polarized* data, because the final measurements use only polarized data, and the scintillator gain is more stable in the absence of the stronger oscillating magnetic fields from the

AC-MOT.

A linear calibration is used, with

$$E_{\text{scint}} = \frac{1}{m}(Q_{\text{QDC}} - b), \quad (5.3)$$

and the detector resolution arising from photon counting statistics is given by

$$\sigma = \sqrt{\lambda E_{\text{scint}}}. \quad (5.4)$$

During online data collection, one QDC module failed abruptly and had to be replaced. As a result, the collected data is calibrated separately before and after the module failure, and the calibrations change slightly at this time. The methodology used is described in detail within [50], so the results will simply be stated here in Table 5.1.

Runsets			b	m	λ
EA, EB	RA, RB	Top	110.0 ± 0.3	0.3985 ± 0.0004	1.55 ± 0.09
		Bottom	142.0 ± 0.3	0.4234 ± 0.0004	1.28 ± 0.08
EC, ED	RC, RD, RE	Top	110.7 ± 0.2	0.3883 ± 0.0004	1.42 ± 0.08
		Bottom	143.0 ± 0.3	0.4132 ± 0.0004	1.32 ± 0.08

Maybe this thing needs units?

Table 5.1: Scintillator Calibrations

To evaluate the systematic effects associated with the scintillators' calibrations, the calibration for each scintillator is adjusted independently to produce energy measurements that are higher by one standard deviation, and lower by one standard deviation, and the resulting changes to the χ^2 map's A_β and b_{Fierz} centroids is measured. For this, the datasets corresponding to both sets of calibration numbers have their calibrations adjusted simultaneously, but each individual scintillator is treated separately. There is no reason to think the two scintillators' calibration accuracies should be correlated, so errors resulting from a changed scintillator calibration are added to one another in quadrature.

DSSD Radius, Energy Threshold, Agreement

Several parameters relating to our choice of cuts relating to DSSD calibrations are varied within both the experimental data and the simulated data to which it is compared. The detection radius, the overall energy threshold, the strip-by-strip SNR, and the energy and timing agreement (See Ch. 3.6) are each adjusted separately at the start of data processing, and the changes are propagated through to a final χ^2 map.

The changes to measured values of b_{Fierz} and A_β from these adjustments are comparatively small, and the errors are believed to be uncorrelated, so they are added in quadrature to the total systematic uncertainty.

JB: I hope the discussion is clear in your head. Any effect that relies on scattering computation in G4 should have an uncertainty on order 10% of the correction – hopefully you are keeping a distinction here between the finite geometry acceptance (which I guess is exact) scattering off the collimator.

As per JB's comment in section ??: "statistical agreement between BB1 X and Y detectors' energies only makes a small effect on results" does not need the technical details beyond that statement."

Missing figure

Surely this requires at *least* one image of the pixelated BB1 data. Maybe some of a few waveforms and energy distributions too.Feels like cheating to include some of that stuff, since Ben was the one who actually used it mostly.

JB on missing figure: "if you used such an image as part of your uncertainty estimate, yes [include it]"

Remember: There's noise applied to simulated BB1s, matching some spectrum.

This probably should go somewhere else: "In the end, we get our results from the scintillator energy only, without summing the BB1 energy back in. Energy absorbed in DSSDs is only used as (a) a tag for events, and (b) contributing to the total beta energy loss before the beta arrives at the scintillator."

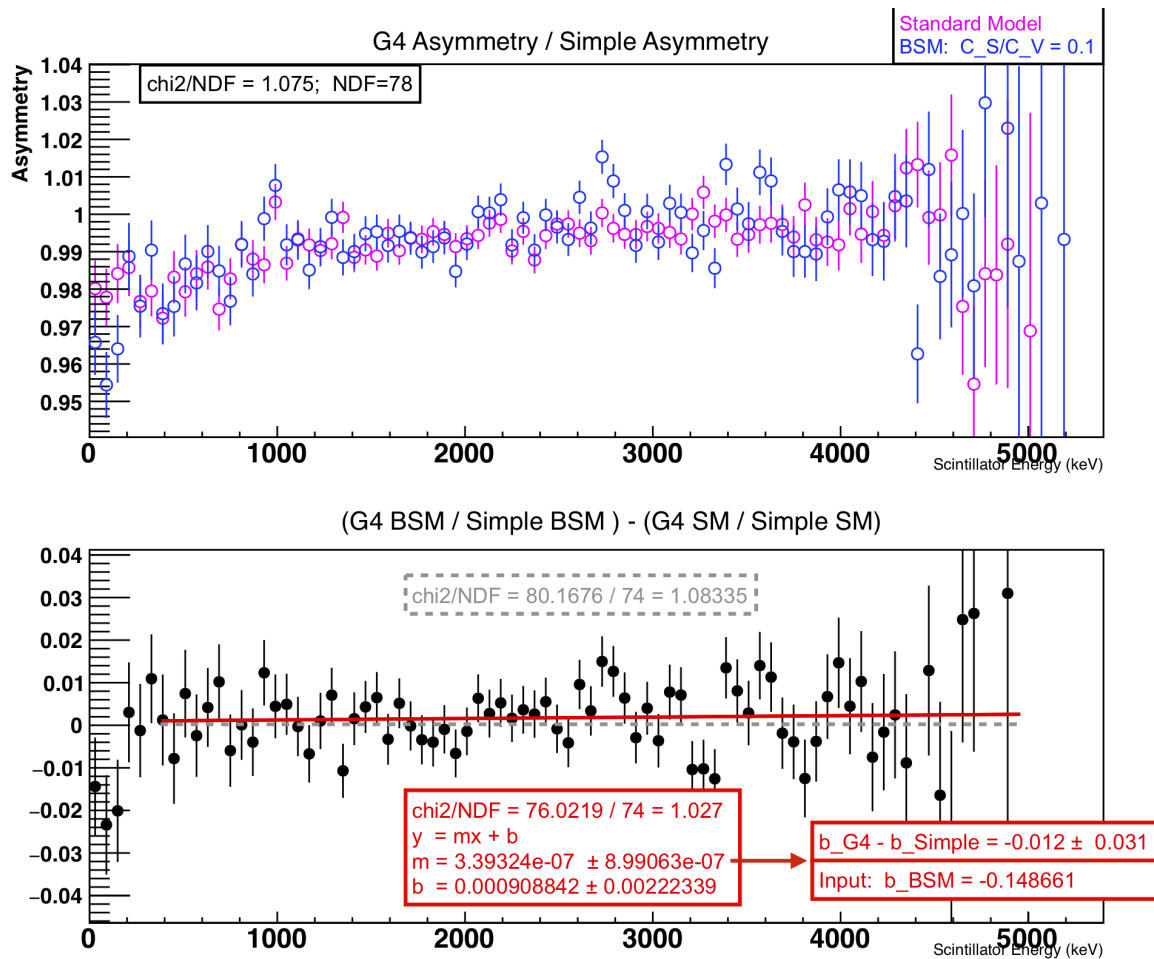
JB: The simulations of course include it event-by-event, not just a minimally ionizing average loss.

5.2.3 The Atomic Cloud

A lot of this content has gone into (Section 4.3) instead. I really need to just mention it here (Sec. 5.2.3) and give an indication of how good the result is. Then evaluate stuff.

Uncertainties relating to the position, size, motion, and expansion of the atomic cloud are evaluated using the response function, which is implemented as described in Ch. 4.3. To evaluate how well the simple monte carlo + response function (SMC+RF) performs in evaluating uncertainties, the relationship between how the SMC+RF and the full G4 simulation changes when a BSM parameter is adjusted is considered in Fig. 5.8.

To evaluate the propagated systematic effects arising from our knowledge of the cloud position, the simple monte carlo is used to generate events originating at points chosen randomly from the distributions produced by linear interpolation of the parameters in Table 3.3, with each parameter describing the distribution allowed to vary in accordance with its stated uncertainty, assuming gaussian-distributed errors. The results for each of the three datasets are shown in Fig. 5.9 for A_β and Fig. 5.10 for b_{Fierz} .



This is a horrible and ugly picture, and it should be replaced.

Figure 5.8: Superratio asymmetries generated by G4 and SMC+RF are compared against one another for a change in BSM parameters. The results show a consistent behaviour when the value of b_{Fierz} is adjusted, suggesting that the SMC+RF can safely be used to evaluate systematic effects such as those arising from a change in cloud position.

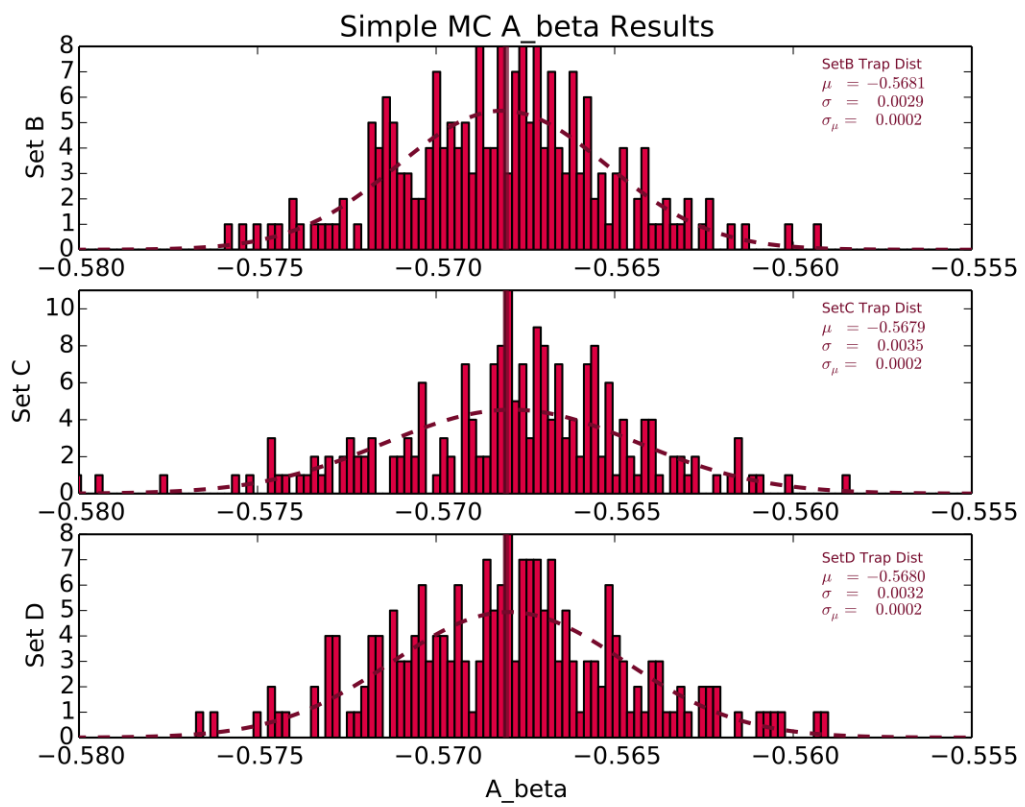


Figure 5.9: Estimated offset and uncertainty in A_β resulting from an imperfectly centred cloud of finite size, and the uncertainty and variation within these parameters. Evaluated by using the SMC+RF method.

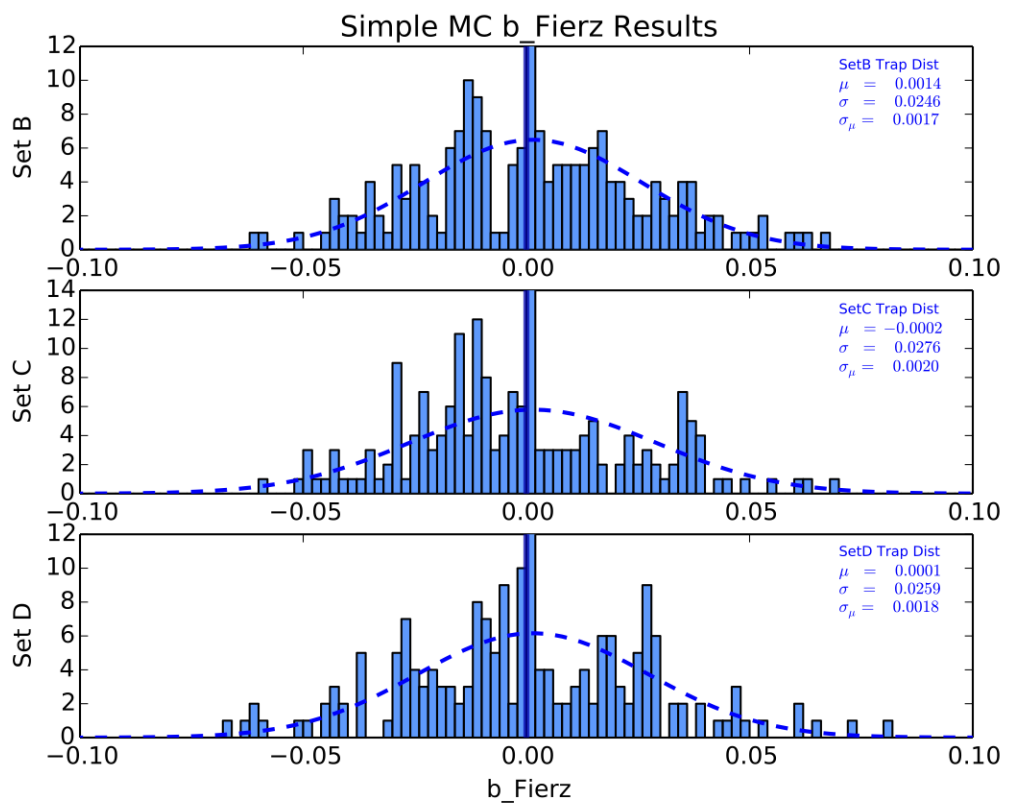


Figure 5.10: Estimated offset and uncertainty in b_{Fierz} resulting from an imperfectly centred cloud of finite size, and the uncertainty and variation within these parameters. Evaluated by using the SMC+RF method.

5.2.4 The Response Function's Low Energy Tail

Bremsstrahlung. It does Bremsstrahlung.

Here is Subsection 9.5.5 “The low-energy tail uncertainty, and what it does” complete. There should be no figure.

Direct quote from John follows in the next two paragraphs. Maybe I should paraphrase, but it’s so nicely written!

This subsection has the collaboration’s evaluation of the uncertainty from the scintillator detector’s lineshape tail. The energy from a monoenergetic beta is not always fully absorbed in a plastic scintillator. Although most backscattered betas are vetoed by the DSSD, some produce bremsstrahlung photons, and these frequently escape low-Z plastic scintillator— all cross-sections are known to high accuracy, but there is always uncertainty entailed in the MC implementation. This lineshape tail will then effectively move events from higher to lower measured energy, artificially altering the lower-energy asymmetries and mimicking the effects of a Fierz term.

Since this detector effect is difficult to disentangle from the other scattering effects off volumes, the collaboration adds a linear function down to zero for the tail to a Gaussian for the peak, with linewidth varying by photon statistics [52]. The convolution of this simple detector response function with v/c then scales the centroid MC, with the lineshape tail varied by $\pm 10\%$ of its value, a generic uncertainty accepted by the community for MC electromagnetic simulations. The fit b_{Fierz} centroid changes by ± 0.0076 , summarized as the 0.008 “Low Energy Tail” in the systematics table at the start of this chapter. When compared with other uncertainties of the present data set, this is small enough that the accuracy of this estimate is adequate.

5.2.5 Background Events

Modeling of background events is covered comprehensively in Ch. 4.5. Because the background model doesn’t fully fit the experimental TOF spectrum, a relatively large variation in the number of background events is considered. The background spectrum is scaled from its nominal size up by a factor of 2 and down by a factor of 2.

Since the background has been reduced greatly by the improved time-of-flight analysis, this even this large variation in the number of background events makes a relatively small contribution to the final result.

This content got moved to Ch. 4.5.

John on Section 5.4 Background Modeling – Decay from Surfaces within the Chamber:

...

Either add here, or omit this section and add to preamble of chapter 5:

"The background modelling is covered comprehensively in Section 4.4 "Simulating the Background and Time of Flight" Since the background was reduced greatly by the improved time-of-flight analysis, this uncertainty makes a relatively small contribution to the final result.

5.2.6 Material Thicknesses

There are three distinct objects a beta emitted from the central atom cloud must pass through before arriving at a scintillator: a $(275 \pm 6)\mu\text{m}$ silicon carbide mirror, a $(229 \pm 23)\mu\text{m}$ beryllium foil, and a $(295 \pm 5)\mu\text{m}$ double-sided silicon strip detector, as shown in Fig. 2.5.

The propagated uncertainties are treated as uncorrelated (added in quadrature), and evaluated by running high-statistics Geant4 simulations with a parameter adjusted, then propagating the result through the analysis pipeline to compare against superratio asymmetries constructed to span the 2D BSM parameter space. Because of the processor time required for this, certain simplifying assumptions were used to reduce the necessary number of simulations. In particular, the top and bottom for each type of object were treated as producing the same size propagated uncertainty, though the top and bottom errors were not treated as being correlated. Simulations were run to ensure there would not be any large nonlinear effects when combining a change in thickness for one type of object.

Furthermore, since the DSSD and the mirror have a similar density of silicon, which is the dominant material in causing scattering from the mirrors, and because the two have similar thicknesses and thickness uncertainties, the propagated uncertainties from the DSSDs and mirrors were assumed to produce similar size effects on the result. Thus, the uncertainties arising from uncertainties in the beryllium foil and mirror thicknesses were the only ones evaluated directly within Geant4. The propagated uncertainty arising from DSSD thickness was assumed to be the same size as the uncertainty arising from mirror thicknesses.

All uncertainties from material thicknesses are believed to be uncorrelated, and are added in quadrature to the final systematic uncertainty.

These numbers are really *not* what's shown in that picture. The ones *here* are what I got from notes in my G4 scripts. I don't know where the uncertainties came from before that.

Chapter 6

Results and Conclusions

JB: Dan and I independently discussed (((Ch. 6))) yesterday, and he has suggestions to help. So I will also schedule a meeting with Dan and you to discuss (((Ch. 6))) Results and whether the S,T part must be deleted and left to a paper. You don't have enough time, and although this should be quite straightforward, it is not your critical result and it's the only thing that can go.

JB on simple things still missing:

I would have expected a separate uncertainty for b and Abeta for each data set, either on each 2D figure in ch. 6, are collected in a table in Ch. 6.

Remember to cite these dudes for (I think) the low-energy tail in the spectrum: [55] [56].

6.1 Measured Limits on b_{Fierz} and A_β

JB on Ch. 6.1:

...

you just have to summarize the figures. Point out the natural dilution of Abeta result if energy-dependent new physics is allowed to float.

John says to just skip doing the C_S and C_T stuff, for now. No time. ... Really, C_S is already basically done, but then that'll lead to awkward questions about C_T .

After corrections have been applied and uncertainties evaluated, statistical confidence intervals for the 2D A_β vs b_{Fierz} parameter space are shown in Fig. 6.1 for all datasets combined. The final estimates of A_β and b_{Fierz} with uncertainties at the 1σ

level are given by:

$$b_{\text{Fierz}} = 0.033 \pm 0.084(\text{stat}) \pm 0.039(\text{sys}) \quad (6.1)$$

$$A_\beta = -0.5738 \pm 0.0082(\text{stat}) \pm 0.0041(\text{sys}), \quad (6.2)$$

and a list of uncertainties is provided in Table 6.1.

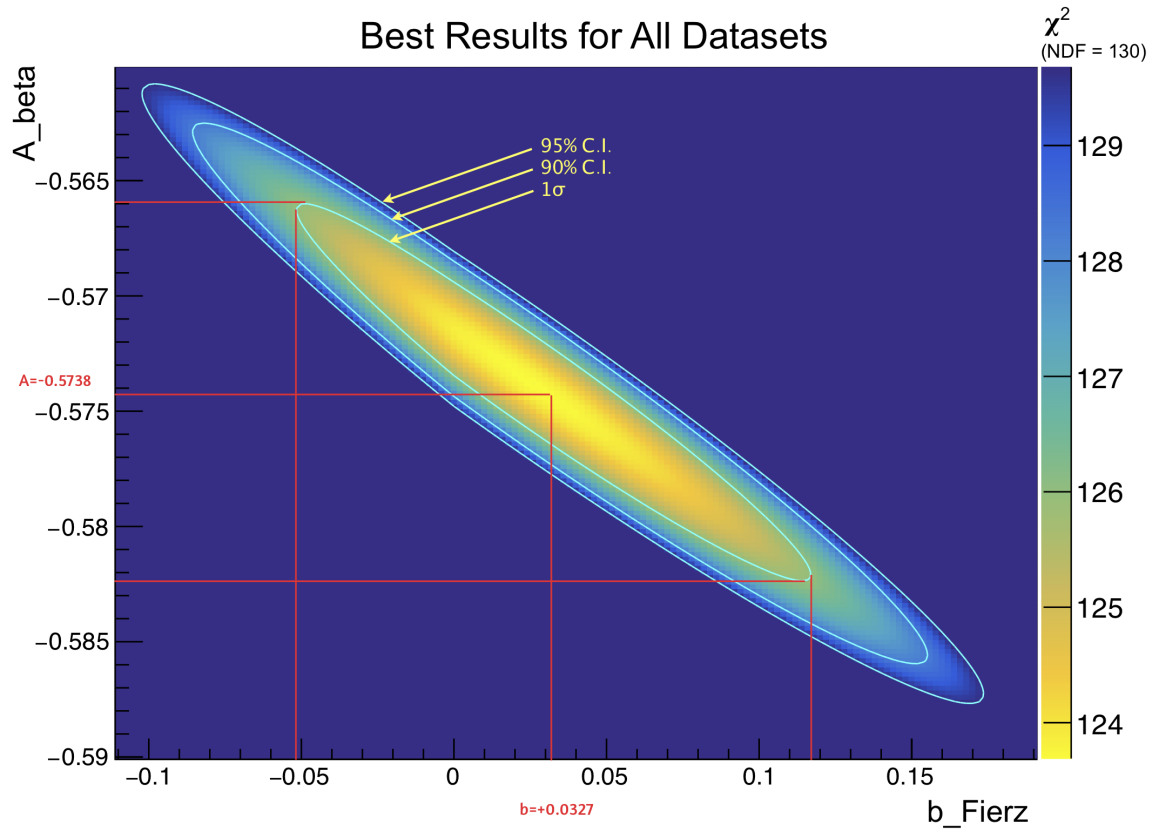


Figure 6.1: A χ^2 map to compare all data to a parameter space of A_β and b_{Fierz} values. All corrections have been included, however only statistical confidence intervals are shown.

The uncertainty associated with this measurement of A_β is significantly larger than the collaboration's previous measurement of using the same data, in which the final result was $A_\beta = -0.5707 \pm 0.0013(\text{stat}) \pm 0.0013(\text{sys}) \pm 0.0005(\text{pol})$. However, it must be noted that the present measurement is a two-parameter measurement rather than a one-parameter measurement, so it is expected that the uncertainty associated with a single parameter should be larger.

Source	Uncertainty	
	b_{Fierz}	A_β
Scintillator Calibration	0.003	0.0003
Scintillator Threshold	0.004	0.0004
DSSD Individual Strip SNR	0.006	0.0007
DSSD Energy Agreement	0.005	0.0006
DSSD Detection Radius	0.006	0.0017
DSSD Energy Threshold	0.005	0.0005
Atomic Cloud	0.002	0.0002
Background	0.004	0.0003
Beta Scattering	0.031	0.0025
Low Energy Tail	0.008	0.0007
Mirror Thickness	0.013	0.0017
DSSD Thickness	0.013	0.0017
Beryllium Foil Thickness	0.004	< 0.0001
Total Systematics	0.039	0.0041
Statistics	0.084	0.0082

Table 6.1: Error budget for the two-parameter analysis, with all data included. Uncertainties are believed to be uncorrelated, and are added in quadrature. Final results: $b_{\text{Fierz}} = 0.033 \pm 0.084(\text{stat}) \pm 0.039(\text{syst})$ and $A_\beta = -0.5738 \pm 0.0082(\text{stat}) \pm 0.0041(\text{syst})$

To evaluate whether the two measurements are consistent, a thin vertical slice of Fig. 6.1 can be extracted at $b_{\text{Fierz}} = 0$, and its projection will provide the centroid (including systematic offsets) and statistical error associated with a one-parameter analysis for A_β – though this method cannot produce an estimate of the extent to which systematic uncertainties might be reduced. This ‘check’ gives a one-parameter measurement of $A_\beta = -0.5714 \pm 0.0020(\text{stat})$.

The above one-parameter result for A_β is consistent with the collaboration’s prior result, even after one accounts for the fact that the previous result suffered from an oversight in which some partially polarized data was not removed from the final analysis for A_β , despite the fact that this cut *was* implemented in the associated polarization measurement. This accounts for 5% of the data used in that analysis, and is estimated to decrease the average polarization by approximately 0.3%.

An estimate of the size of the effect on the previous measurement of A_β suggests that the true value of A_β is likely to be ~ 0.0016 more negative than reported.

Accounting for this, a more accurate one-parameter measurement might produce the result, $A_\beta \approx -0.5723 \pm 0.0014(\text{stat}) \pm 0.0013(\text{sys}) \pm 0.0005(\text{pol})$.

Kludgily removed an entire section: “Discussion of Corrections and Uncertainties”. But comments from John on that section still remain.

Just write a blurb to qualitatively summarize a bunch of the stuff in Ch. 5. Do I want to put my error budget table here? If not, here it is! (6.1).

Other things to discuss here: which things are dominant error sources, and how viable it would be to improve those for future experiments.

6.2 Other Possible Future Work for the Collaboration: R_{slow}

Probably shouldn't get a clearpage in the end. It's for my sanity during writing.

John says the whole R_{slow} thing should go in here somewhere.

Appendix I keep, it's excellent. It should be moved as is to Conclusions under "Future Experiment for the collaboration"! so people know you worked so hard on it!!

The nuclear weak force is known to be a predominantly left-handed vector and axial-vector (V-A) interaction. An experiment is proposed to further test that observation, constraining the strength of right-handed (V+A) currents by exploiting the principle of conservation of angular momentum within a spin-polarized beta decay process. Here, we focus on the decay ${}^{37}\text{K} \rightarrow {}^{37}\text{Ar} + \beta^+ + \nu_e$. The angular correlations between the emerging daughter particles provide a rich source of information about the type of interaction that produced the decay.

6.2.1 Motivation

The nuclear weak force has long been known to be a predominantly left-handed chiral interaction, meaning that immediately following an interaction (such as a beta decay) with a weak force carrying boson (W^+ , W^- , Z), normal-matter leptons (such as the electron and electron neutrino) emerge with left-handed chirality while the anti-leptons (e.g. the positron and electron anti-neutrino) emerge with right-handed chirality. In the limit of massless particles, the particle's chirality is the same as its helicity. Thus, in a left-handed model, the direction of an (ultrarelativistic) normal lepton's spin is antiparallel direction of its motion, and the direction of spin for an anti-lepton is parallel to its direction of motion. For a non-relativistic particle the property of chirality is fairly abstract, and describes the appropriate group representation and projection operators to be used in calculations. It should be noted that a fully chiral model is also one which is maximally parity violating.

This odd quirk of the nuclear weak force is not only *predominantly* true, but it is, to the best of our current scientific knowledge, *always* true – that is, attempts to measure any right-handed chiral components of the weak force have produced results consistent with zero [36][57]. This project proposes a further measurement to constrain the strength of the right-handed component of the weak interaction.

6.2.2 The Decay Process

The kinematics of nuclear β^+ decay are described by the following probability density function:

$$\begin{aligned}
W(\langle I \rangle | E_\beta \hat{\Omega}_\beta \hat{\Omega}_\nu) = & \left(\frac{1}{2\pi} \right)^5 F(-Z, E_\beta) p_\beta E_\beta (E_0 - E_\beta)^2 dE_\beta d\hat{\Omega}_\beta d\hat{\Omega}_\nu \xi \\
& \times \left[1 + a_{\beta\nu} \frac{\vec{p}_\beta \cdot \vec{p}_\nu}{E_\beta E_\nu} + b_{\text{Fierz}} \frac{m_e}{E_\beta} \right. \\
& + c_{\text{align}} \left(\frac{\frac{1}{3} \vec{p}_\beta \cdot \vec{p}_\nu - (\vec{p}_\beta \cdot \hat{j})(\vec{p}_\nu \cdot \hat{j})}{E_\beta E_\nu} \right) \left(\frac{I(I+1) - 3\langle (\vec{I} \cdot \hat{i})^2 \rangle}{I(2I-1)} \right) \\
& \left. + \frac{\langle \vec{I} \rangle}{I} \left(A_\beta \frac{\vec{p}_\beta}{E_\beta} + B_\nu \frac{\vec{p}_\nu}{E_\nu} + D_{\text{TR}} \frac{\vec{p}_\beta \times \vec{p}_\nu}{E_\beta E_\nu} \right) \right], \quad (6.3)
\end{aligned}$$

where \vec{I} is the nuclear spin-polarization, $F(-Z, E_\beta)$ is the Fermi function, and parameters ξ , $a_{\beta\nu}$, b_{Fierz} , c_{align} , A_β , B_ν , and D_{TR} are functions that vary with the strengths of the vector, axial, scalar, and tensor couplings (constant throughout nature), as well as the Fermi and Gamow-Teller nuclear matrix elements (specific to the individual decay) [1][2].

The decay may be treated as a three-body problem in which the available kinetic energy is divided up between the beta, the neutrino, and the recoiling ^{37}Ar nucleus, and (of course) the total linear and angular momentum are conserved. While the neutrino cannot be detected directly, its kinematics may be reconstructed from observations of the beta and the recoiling daughter nucleus. By placing detectors above and below the decaying atom along the axis of its polarization, we are able to obtain information about the outgoing beta's energy and momentum, in the cases of interest to us, where it is emitted along (or close to) the axis of polarization.

The recoiling ^{37}Ar nucleus is a bit trickier to work with, but the task is not impossible. One useful feature of the $^{37}\text{K} \rightarrow {}^{37}\text{Ar}$ transition is that, in addition to the β^+ emitted in the decay itself, one or more *orbital* electrons from the parent atom are typically lost. In the majority of decay events only one orbital electron is ‘shaken off’ and so the daughter ^{37}Ar atom is electrically neutral [45][58]. In the remaining cases, two or more orbital electrons are lost this way, and the daughter atom is positively charged. If we apply an electric field perpendicular to the direction of polarization,

these positively charged $^{37}\text{Ar}^{(+n)}$ ions may be collected into a detector, from which hit position and time of flight information may be extracted. These shake-off electrons are emitted with an average energy of only $\sim 2\text{ eV}$ so to a very good approximation the other decay products are not perturbed by the presence of shake-off electrons.

It should be noted that for the class of decays of greatest interest, where the beta and the neutrino emerge back-to-back along the polarization axis, the recoiling daughter nucleus will have zero momentum along the directions perpendicular to this axis, and on average less total energy than if the beta and neutrino were emitted in a parallel direction. Henceforth, daughter nuclei from a back-to-back decay as shown in Figure ?? will be described as ‘slow’ recoils. In terms of observables, this means that if the electric field is configured to point along one of the axes perpendicular to the polarization direction, then when the recoiling ion is swept away into a detector, the slow recoil’s hit position should be exactly along the projection of the polarization axis. Furthermore, the slow recoil’s time of flight should be in the middle of the time of flight spectrum, since other recoils will be emitted with momentum towards or away from the detector.

10. P. 93 contains a reference to “Figure ??” (that’s actually the thing above, Figure ??, no matter what page it’s on now.)

6.2.3 Status of the R_{slow} Measurement

In June 2014, after several years of preparatory work beforehand (the author has been continuously involved with this project since 2010), approximately 7 days of beam time at TRIUMF was dedicated to the TRINAT ^{37}K beta decay experiment. Approximately half of this data is suitable for use in this project. During this period, approximately 10,000 atoms were held within the trap at any given time. The cleaned spectra show around 50,000 polarized beta-recoil coincidence events in total, divided among measurements at three different electric field strengths (535 V/cm, 415 V/cm, 395 V/cm).

A fit to simulation has shown that the data that has already been collected has sufficient statistical power to measure the *fractional* contribution of any polarized ‘new physics’ beta decay parameter (ie right-handed, scalar, and tensor currents within the weak interaction) to a sensitivity of $\sim 2\%$ of its true value. Systematic limitations are still being assessed.

6.3 Conclusions

This two-parameter analysis to measure A_β and b_{Fierz} has produced the results:

$$b_{\text{Fierz}} = 0.033 \pm 0.084(\text{stat}) \pm 0.039(\text{sys}) \quad (6.4)$$

$$A_\beta = -0.5738 \pm 0.0082(\text{stat}) \pm 0.0041(\text{sys}), \quad (6.5)$$

where uncertainties are evaluated at 1σ . This measurement of b_{Fierz} is consistent with the Standard Model value of $b_{\text{Fierz}} = 0$, and A_β is consistent both with the collaboration's prior measurement of A_β , as well as with the value predicted by the Standard Model at $A_\beta = -0.5706 \pm 0.0007$.

The result for b_{Fierz} is dominated by statistical uncertainty, suggesting that the measurement could be improved simply by counting longer. There is also room for improvement in the systematic uncertainty, which is dominated by scattering and the related measurements of material thicknesses.

JB on Ch. 6.1 – ‘discussion of corrections and uncertainties’:

...

could be as simple as "The bFierz result in Table 5.1 is dominated by statistical uncertainty. Largely because of this result, the collaboration is working to reduce the largest systematics, using lower-Z materials to reduce backscattering, and changing the silicon delta-E to a multi-wire proportional chamber with very thin windows. The collaboration has already implemented very thin pellicle mirrors. The projected systematic uncertainty could approach 0.01 in a future experiment, which would then likely continue to be limited by statistics."

...

or all of that could go at the end of Chapter 5.

put in that thing John said.

Bibliography

- [1] Jackson, J. D., Treiman, S. B. and Wyld, H. W., *Possible Tests of Time Reversal Invariance in Beta Decay*, Phys. Rev., Vol. 106, pp. 517–521, May 1957.
- [2] Jackson, J. D., Treiman, S. B. and Wyld, H. W., *Coulomb Corrections in Allowed Beta Transitions*, Nuclear Physics, Vol. 4, pp. 206–212, Nov. 1957.
- [3] Anholm, M., Characterizing the AC-MOT, Master's thesis, University of British Columbia, 2014.
- [4] Hong, R., Sternberg, M. G. and Garcia, A., *Helicity and nuclear β decay correlations*, American Journal of Physics, Vol. 85, No. 1, pp. 45–53, 2017.
- [5] Saul, H., Roick, C., Abele, H., Mest, H., Klopff, M., Petukhov, A. K., Soldner, T., Wang, X., Werder, D. and Märkisch, B., *Limit on the Fierz Interference Term b from a Measurement of the Beta Asymmetry in Neutron Decay*, Phys. Rev. Lett., Vol. 125, pp. 112501, Sep 2020.
- [6] de Shalit, A. and Talmi, I., Nuclear Shell Theory, Nuclear Shell Theory, Academic Press, 1963.
- [7] Falkowski, A., González-Alonso, M. and Naviliat-Cuncic, O., *Comprehensive analysis of beta decays within and beyond the Standard Model*, Journal of High Energy Physics, Vol. 2021, No. 4, pp. 1–36, 2021.
- [8] Becquerel, H., *Sur les radiations émises par phosphorescence*, Comptes rendus de l'Academie des Sciences, Paris, Vol. 122, pp. 420–421, 1896.
- [9] Rutherford, E., *VIII. Uranium radiation and the electrical conduction produced by it*, The London, Edinburgh, and Dublin Philosophical Magazine and Journal of Science, Vol. 47, No. 284, pp. 109–163, 1899.

- [10] Villard, P., *Sur la réflexion et la réfraction des rayons cathodiques et des rayons déviables du radium*, CR Acad. Sci. Paris, Vol. 130, pp. 1010, 1900.
- [11] Rutherford, E., *XV. The magnetic and electric deviation of the easily absorbed rays from radium*, The London, Edinburgh, and Dublin Philosophical Magazine and Journal of Science, Vol. 5, No. 26, pp. 177–187, 1903.
- [12] Becquerel, H., *Influence d'un champ magnétique sur le rayonnement des corps radio-actifs*, Journal de Physique Théorique et Appliquée, Vol. 9, No. 1, pp. 71–78, 1900.
- [13] Glashow, S. L., *The renormalizability of vector meson interactions*, Nuclear Physics, Vol. 10, pp. 107–117, 1959.
- [14] Salam, A. and Ward, J., *Electromagnetic and weak interactions*, Physics Letters, Vol. 13, No. 2, pp. 168–171, 1964.
- [15] Weinberg, S., *A Model of Leptons*, Phys. Rev. Lett., Vol. 19, pp. 1264–1266, Nov 1967.
- [16] 't Hooft, G., *Renormalization of massless Yang-Mills fields*, Nuclear Physics B, Vol. 33, No. 1, pp. 173–199, 1971.
- [17] Yang, C. N. and Mills, R. L., *Conservation of Isotopic Spin and Isotopic Gauge Invariance*, Phys. Rev., Vol. 96, pp. 191–195, Oct 1954.
- [18] Severijns, N., Tandecki, M., Phalet, T. and Towner, I. S., *Ft values of the T = 1/2 mirror β transitions*, Phys. Rev. C, Vol. 78, pp. 055501, Nov 2008.
- [19] Shidling, P. D., Melconian, D., Behling, S., Fenker, B., Hardy, J. C., Iacob, V. E., McCleskey, E., McCleskey, M., Mehlman, M., Park, H. I. and Roeder, B. T., *Precision half-life measurement of the β⁺ decay of ³⁷K*, Phys. Rev. C, Vol. 90, pp. 032501, Sep 2014.
- [20] Hardy, J. and Towner, I., *Superallowed 0+ → 0+ nuclear β decays: 2014 critical survey, with precise results for V u d and CKM unitarity*, Physical Review C, Vol. 91, No. 2, pp. 025501, 2015.

- [21] Naviliat-Cuncic, O. and Severijns, N., *Test of the Conserved Vector Current Hypothesis in $T = 1/2$ Mirror Transitions and New Determination of $|V_{ud}|$* , Physical Review Letters, Vol. 102, pp. 142302, April 2009.
- [22] Naviliat-Cuncic, O. and Severijns, N., *$|V_{ud}|$ from $T = 1/2$ mirror transitions and the role of atom and ion traps*, The European Physical Journal A, Vol. 42, No. 3, pp. 327–331, June 2009.
- [23] von Platen, C., Bonn, J., Köpf, U., Neugart, R. and Otten, E. W., *Spin exchange polarization and hfs anomaly measurement of β -active ^{37}K* , Zeitschrift für Physik, Vol. 244, No. 1, pp. 44–69, 1971.
- [24] Pitt, M. L., Test of the Linearity of Quantum Mechanics Using ARGON-37 Polarized by Spin-Exchange Optical Pumping., Princeton University, January 1992.
- [25] Minamisono, K., Mantica, P., Crawford, H., Pinter, J., Stoker, J., Utsuno, Y. and Weerasiri, R., *Quadrupole moment of ^{37}K* , Physics Letters B, Vol. 662, No. 5, pp. 389–395, 2008.
- [26] Klein, A., Brown, B., Georg, U., Keim, M., Lievens, P., Neugart, R., Neuroth, M., Silverans, R., Vermeeren, L. and ISOLDE Collaboration, *Moments and mean square charge radii of short-lived argon isotopes*, Nuclear Physics A, Vol. 607, No. 1, pp. 1–22, 1996.
- [27] Towner, I., Private Communication, August 2011.
- [28] Fermi, E., *Versuch einer Theorie der β -Strahlen. I*, Zeitschrift für Physik, Vol. 88, No. 3, pp. 161–177, 1934.
- [29] Tanabashi, M. i. P. D. G., *Review of Particle Physics*, Phys. Rev. D, Vol. 98, pp. 030001, Aug 2018.
- [30] Lee, T.-D. and Yang, C.-N., *Question of parity conservation in weak interactions*, Physical Review, Vol. 104, No. 1, pp. 254–258, 1956.
- [31] Wu, C. S., Ambler, E., Hayward, R. W., Hopps, D. D. and Hudson, R. P., *Experimental Test of Parity Conservation in Beta Decay*, Phys. Rev., Vol. 105, pp. 1413–1415, Feb 1957.

- [32] Rustad, B. M. and Ruby, S. L., *Gamow-Teller Interaction in the Decay of He⁶*, Phys. Rev., Vol. 97, pp. 991–1002, Feb 1955.
- [33] Burgoyne, M. T., Epstein, R. J., Krohn, V. E., Novey, T. B., Raboy, S., Ringo, G. R. and Telegdi, V. L., *Measurement of Beta Asymmetry in the Decay of Polarized Neutrons*, Phys. Rev., Vol. 107, pp. 1731–1733, Sep 1957.
- [34] Shidling, P., Behling, R., Fenker, B., Hardy, J., Iacob, V., Mehlman, M., Park, H., Roeder, B. and Melconian, D., *High-precision half-life measurement of the β+ decay of Na 21*, Physical Review C, Vol. 98, No. 1, pp. 015502, 2018.
- [35] Ozmetin, A., Melconian, D. G., Iacob, V. E., Shidling, P., Kolhinin, V. S., McClain, D. J., Nasser, M., Schroeder, B., Roeder, B., Park, H.-I., Anholm, M., Saastamoinen, A. J. and Trinat Collaboration, *Improving the ft value of 37K via a precision measurement of the branching ratio*, APS Division of Nuclear Physics Meeting Abstracts, Vol. 2020 of APS Meeting Abstracts, p. KF.005, Jan. 2020.
- [36] Severijns, N., Beck, M. and Naviliat-Cuncic, O., *Tests of the standard electroweak model in nuclear beta decay*, Rev. Mod. Phys., Vol. 78, pp. 991–1040, September 2006.
- [37] Krane, K. S., Introductory Nuclear Physics, Wiley, New York, 1988.
- [38] Wong, S., Introductory Nuclear Physics, Prentice Hall Advanced Reference Series Prentice Hall Labora, Prentice Hall, 1990.
- [39] Holstein, B. R., *Recoil effects in allowed beta decay: The elementary particle approach*, Reviews of Modern Physics, Vol. 46, No. 4, pp. 789–814, Oct. 1974.
- [40] Levinger, J. S., *Effects of Radioactive Disintegrations on Inner Electrons of the Atom*, Phys. Rev., Vol. 90, pp. 11–25, Apr 1953.
- [41] Sun, X., Adamek, E., Allgeier, B., Bagdasarova, Y., Berguno, D. B., Blatnik, M., Bowles, T. J., Broussard, L. J., Brown, M. A.-P., Carr, R., Clayton, S., Cude-Woods, C., Currie, S., Dees, E. B., Ding, X., Filippone, B. W., García, A., Geltenbort, P., Hasan, S., Hickerson, K. P., Hoagland, J., Hong, R., Holley, A. T., Ito, T. M., Knecht, A., Liu, C.-Y., Liu, J., Makela, M., Mammei, R., Martin, J. W., Melconian, D., Mendenhall, M. P., Moore, S. D., Morris, C. L., Nepal,

- S., Nouri, N., Pattie, R. W., Pérez Gálvan, A., Phillips, D. G., Picker, R., Pitt, M. L., Plaster, B., Salvat, D. J., Saunders, A., Sharapov, E. I., Sjue, S., Slutsky, S., Sondheim, W., Swank, C., Tatar, E., Vogelaar, R. B., VornDick, B., Wang, Z., Wei, W., Wexler, J. W., Womack, T., Wrede, C., Young, A. R. and Zeck, B. A., *Improved limits on Fierz interference using asymmetry measurements from the Ultracold Neutron Asymmetry (UCNA) experiment*, Phys. Rev. C, Vol. 101, pp. 035503, Mar 2020.
- [42] Raab, E. L., Prentiss, M., Cable, A., Chu, S. and Pritchard, D. E., *Trapping of Neutral Sodium Atoms with Radiation Pressure*, Phys. Rev. Lett., Vol. 59, pp. 2631–2634, Dec 1987.
- [43] Corney, A., Atomic and Laser Spectroscopy, Oxford University Press, New York, 1977.
- [44] Fenker, B., Behr, J. A., Melconian, D., Anderson, R. M. A., Anholm, M., Ashery, D., Behling, R. S., Cohen, I., Craiciu, I., Donohue, J. M., Farfan, C., Friesen, D., Gorelov, A., McNeil, J., Mehlman, M., Norton, H., Olchanski, K., Smale, S., Thériault, O., Vantyghem, A. N. and Warner, C. L., *Precision measurement of the nuclear polarization in laser-cooled, optically pumped ^{37}K* , New Journal of Physics, Vol. 18, No. 7, pp. 073028, 2016.
- [45] Gorelov, A., Behr, J., Melconian, D., Trinczek, M., Dubé, P., Häusser, O., Giesen, U., Jackson, K., Swanson, T., D'Auria, J., Dombsky, M., Ball, G., Buchmann, L., Jennings, B., Dilling, J., Schmid, J., Ashery, D., Deutsch, J., Alford, W., Asgeirsson, D., Wong, W. and Lee, B., *Beta-neutrino correlation experiments on laser trapped ^{38m}K , ^{37}K* , Hyperfine Interactions, Vol. 127, No. 1, pp. 373–380, 2000.
- [46] Swanson, T. B., Asgeirsson, D., Behr, J. A., Gorelov, A. and Melconian, D., *Efficient transfer in a double magneto-optical trap system*, J. Opt. Soc. Am. B, Vol. 15, No. 11, pp. 2641–2645, Nov 1998.
- [47] Harvey, M. and Murray, A. J., *Cold Atom Trap with Zero Residual Magnetic Field: The AC Magneto-Optical Trap*, Phys. Rev. Lett., Vol. 101, pp. 173201, Oct 2008.

- [48] Fenker, B., Gorelov, A., Melconian, D., Behr, J. A., Anholm, M., Ashery, D., Behling, R. S., Cohen, I., Craiciu, I., Gwinner, G., McNeil, J., Mehlman, M., Olchanski, K., Shidling, P. D., Smale, S. and Warner, C. L., *Precision Measurement of the β Asymmetry in Spin-Polarized ^{37}K Decay*, Phys. Rev. Lett., Vol. 120, pp. 062502, Feb 2018.
- [49] Audi, G., Wapstra, A. and Thibault, C., *The AME2003 Atomic Mass Evaluation*, Nuclear Physics A, Vol. 729, No. 1, pp. 337 – 676, 2003.
- [50] Fenker, B. B., Precise measurement of the β -asymmetry in the decay of magneto-optically trapped, spin-polarized ^{37}K , Ph.D. thesis, Texas A&M University, 2016.
- [51] Behling, R. S., Measurement of the Standard Model Beta Asymmetry Parameter, β , in ^{37}K , Ph.D. thesis, Texas A&M University, 2015.
- [52] Clifford, E., Hagberg, E., Koslowsy, V., Hardy, J., Schmeing, H. and Azuma, R., *Measurements of the response of a hybrid detector telescope to mono-energetic beams of positrons and electrons in the energy range 0.8–3.8 MeV*, Nuclear Instruments and Methods in Physics Research, Vol. 224, No. 3, pp. 440–447, 1984.
- [53] Landau, L. D., *On the energy loss of fast particles by ionization*, J. Phys., Vol. 8, pp. 201–205, 1944.
- [54] Moyal, J., *XXX. Theory of ionization fluctuations*, The London, Edinburgh, and Dublin Philosophical Magazine and Journal of Science, Vol. 46, No. 374, pp. 263–280, 1955.
- [55] Lonergan, J., Jupiter, C. and Merkel, G., *Electron energy straggling measurements for thick targets of beryllium, aluminum, and gold at 4.0 and 8.0 MeV*, Journal of Applied Physics, Vol. 41, No. 2, pp. 678–688, 1970.
- [56] Rester, D. H. and Derrickson, J. H., *Electron Transmission Measurements for Al, Sn, and Au Targets at Electron Bombarding Energies of 1.0 and 2.5 MeV*, Journal of Applied Physics, Vol. 42, No. 2, pp. 714–721, 1971.
- [57] Severijns, N. and Naviliat-Cuncic, O., *Symmetry tests in nuclear beta decay*, Annual Review of Nuclear and Particle Science, Vol. 61, pp. 23–46, 2011.

- [58] Melconian, D. G., Measurement of the Neutrino Asymmetry in the Beta Decay of Laser-Cooled, Polarized ^{37}K , Ph.D. thesis, Simon Fraser University, 2005.
- [59] Holstein, B. R., *Erratum: Recoil effects in allowed beta decay: The elementary particle approach*, Rev. Mod. Phys., Vol. 48, pp. 673–673, Oct 1976.
- [60] Ebel, M. and Feldman, G., *Further remarks on Coulomb corrections in allowed beta transitions*, Nuclear Physics, Vol. 4, pp. 213–214, 1957.
- [61] Falkowski, A., González-Alonso, M., Palavrić, A. and Rodríguez-Sánchez, A., *Constraints on subleading interactions in beta decay Lagrangian*, 2022.

The citation format I'm using is really stupid. You **must** force yourself to ignore this right now,
Melissa!

Georg says:

6. At first glance, I find a bibliography that contains only 28 entries to be problematic for a Ph.D. thesis. This goes, to some degree, back to my earlier points about embedding the work in the “bigger picture” – doing so would necessarily lead to several additional references – but it might be more than that.

Appendix A

Statement of Contributions

from Georg:

3. As an outsider, it is my understanding that the author worked as part of a larger collaboration. It would be beneficial to clearly lay out what her unique contributions are. This could be done, for instance, in the Introduction, and/or the Conclusions.

Preface goes here. Really, it's going to be a list of contributions that I made. Maybe I should break it down by chapter? Also, should this thing go in an appendix?

Make the phrasing less stupid.

A.1 Chapter 1

A.2 Chapter 2

Much of the experimental apparatus described here was designed and built before the author joined the TRINAT research group, with the notable exception of the AC-MOT, which I played a key part in designing and implementing as part of a previous MSc degree. This includes magnetic field trimming and optimization during all parts of the AC-MOT/OP duty cycle, and logic triggers, both to control relevant instruments over the course of the duty cycle, and to record within data acquisition where within the duty cycle an event must lie.

A.3 Chapter 3

Calibration of the rMCP and subsequent measurements of the atom cloud position was performed by me. Calibration of the eMCP, the two scintillators, and the DSSDs for the relevant experimental data were performed by Ben Fenker. The switch to using the leading rather than trailing edge for all timing data was performed by me. The scintillator walk correction was also done by me.

A.4 Chapter 4

Upgrades to the TRINAT Geant4 package to enable multithreading and allow for scalar and tensor couplings within the decay probability distributions was performed by me. The simulation's representation of the materials and geometry used for our experimental chamber had already been set up by Spencer Behling and Ben Fenker. Ben Fenker also set up the simulated DSSD calibration such that each simulated strip had the same resolution and noise as the real strip that it represented.

The simple monte carlo and associated response functions were created and optimized by me.

Although I was responsible for running the G4 simulations, the SOE simulations in COMSOL were performed by Alexandre Gorelov. The event-by-event combination of G4 and COMSOL spectra and their normalizations was performed by me, and I was also responsible for checking that the TOF background model performed as expected.

A.5 Chapter 5

Yeah, there's stuff here.

Finish writing chapter 5 contributions. And also chapter 6 contributions.

A.6 Chapter 6

There's stuff here too.

Appendix B

Notable Differences in Data Selection between this and the Previous Result

JB says Appendix A should all go in the analysis section, and not in an appendix at all.

JB says: Appendix A (ie, *this appendix*) is very important, and should at least be a subsection in the Analysis chapter.

...

You could condense the Appendix into a set of bullet points at the end of the intro to the Analysis section (which you still need, badly!), and then its content could be interleaved in the Analysis chapter. E.g. you already have redundancy in the LE and TE discussion vs. the Appendix, and the discussion is more complete in the Analysis chapter, which is good.

I really want this appendix to stay here. I'll make sure to mention everything in the body of the thesis though, since it *is* important. But at some point, somebody is going to really want to have this info written into a short summary.

B.1 Polarization Cycle Selection

Data used for our recent PRL article was slightly less polarized than we thought it was, due to an oversight in the data selection procedure. See Ch. ?? for a discussion of the effects.

from Georg:

11. Likewise, p. 98, a reference to “Ch. ??”, as well as a reference to “our recent PRL article” – the latter needs to be referenced properly!

B.2 Leading Edge / Trailing Edge and Walk Correction

Using the leading edge rather than the trailing edge to mark the timing of TDC pulses cleans up jitter, eliminates background, and changes the relative delays between different inputs. It is immediately relevant to the shape of the ‘walk correction’ on scintillator timing pulses, which give a different prediction for beta arrival time as a function of scintillator energy.

B.3 TOF Cut + Background Modelling

A SOE-beta time-of-flight cut is necessary to reduce background. The above mentioned walk correction directly results in an change in which specific events are selected in a given TOF cut. It further results in an adjustment to the expected fraction of background events in any such cut.

Somebody will surely ask for a justification for why I did this differently, and I don’t have one beyond “this seemed more reasonable to me”, which is of course nobody will ever accept as a reason.

B.4 BB1 Energy Threshold

I use an overall 50 keV threshold, (taking +/- 10 keV from that as a systematic to be propagated/checked), but the collaboration’s previous analysis used 60 keV as the default threshold.

Appendix C

Derivation of the Probability Density Function

In order to obtain a probability density function (PDF) to describe the beta decay process, and which includes both a representation of the exotic physics that is the subject of this search, as well as small higher-order corrections which are known to be present, it is necessary to combine features from two disparate formalisms.

Blurb continuation: JTW is for the BSM shit, because they created it before they really knew which form the operators take. [1][2] Holstein is for the small contributions to physics that we actually know to exist. [39][59]

C.1 JTW Formalism

Probably start with the Hamiltonian. That thing ties in to the "what's the form of the operators?" thing from the intro, I guess.

We begin with the five-dimensional PDF taken directly from Jackson–Treiman–Wyld (JTW) [1][2] for beta decay kinematics:

$$\begin{aligned} d^5\Gamma_{\text{JTW}} \equiv & \frac{1}{(2\pi)^5} F_\pm(Z, E_\beta) p_\beta E_\beta (E_0 - E_\beta)^2 dE_\beta d^2\hat{\Omega}_\beta d^2\hat{\Omega}_\nu \\ & \times \xi \left[1 + a_{\beta\nu} \frac{\vec{p}_\beta \cdot \vec{p}_\nu}{E_\beta E_\nu} + b_{\text{Fierz}} \frac{m_e c^2}{E_\beta} + c_{\text{align}} T_{\text{align}}(\vec{J}) \left(\frac{\vec{p}_\beta \cdot \vec{p}_\nu}{3E_\beta E_\nu} - \frac{(\vec{p}_\beta \cdot \hat{\mathbf{j}})(\vec{p}_\nu \cdot \hat{\mathbf{j}})}{E_\beta E_\nu} \right) \right. \\ & \left. + \frac{\vec{J}}{J} \cdot \left(A_\beta \frac{\vec{p}_\beta}{E_\beta} + B_\nu \frac{\vec{p}_\nu}{E_\nu} + D_{\text{TR}} \frac{\vec{p}_\beta \times \vec{p}_\nu}{E_\beta E_\nu} \right) \right], \end{aligned} \quad (\text{C.1})$$

Missing factors of c ??

where, for convenience, we have defined a nuclear alignment term,

$$T_{\text{align}}(\vec{J}) \equiv \frac{J(J+1) - 3\langle(\vec{J} \cdot \hat{j})^2\rangle}{J(2J-1)}. \quad (\text{C.2})$$

In Eq. C.1, E_β , \vec{p}_β , and p_β are the outgoing β particle's (total) energy, momentum 3-vector, and momentum scalar, while E_ν , \vec{p}_ν , and p_ν are the equivalent quantities for the outgoing (anti-)neutrino, and E_0 is the maximum possible β energy associated with the transition. \vec{J} is the nuclear angular momentum vector of the parent, and J is its projection onto the axis of quantization. \hat{j} is a unit vector in the direction of \vec{J} (note that in general, $\hat{j} \neq \frac{\vec{J}}{J}$). As usual, m_e is the mass of the electron, and c is the speed of light. The infinitesimal surface element $d^2\hat{\Omega}_\beta$ ($d^2\hat{\Omega}_\nu$) represents the direction of β (neutrino) emission. The function $F_\pm(Z, E_\beta)$ is known as a Fermi function for outgoing electrons (top) and positrons (bottom), with Z the proton number of the parent nucleus. The Fermi function accounts for the electric force between the nucleus and the charged outgoing beta particle, and its integral over E_β has no closed form expression.

Holstein gives a formula for it. Maybe I should write it out...

For the reader's convenience, the kinematic factors unique to a particular transition are written out here in terms of their couplings.

$$\begin{aligned} \xi &= |M_F|^2(|C_S|^2 + |C_V|^2 + |C'_S|^2 + |C'_V|^2) \\ &\quad + |M_{GT}|^2(|C_T|^2 + |C_A|^2 + |C'_T|^2 + |C'_A|^2) \end{aligned} \quad (\text{C.3})$$

$$\begin{aligned} a_{\beta\nu}\xi &= |M_F|^2 \left[(|C_V|^2 + |C'_V|^2 - |C_S|^2 - |C'_S|^2) \mp 2\frac{\alpha Z m_e c^2}{p_\beta c} \text{Im}[C_S C_V^* + C'_S C'^*_V] \right] \\ &\quad + \frac{1}{3} |M_{GT}|^2 \left[(|C_T|^2 - |C_A|^2 + |C'_T|^2 - |C'_A|^2) \right. \\ &\quad \left. \pm 2\frac{\alpha Z m_e c^2}{p_\beta c} \text{Im}[C_T C_A^* + C'_T C'^*_A] \right] \end{aligned} \quad (\text{C.4})$$

$$b_{\text{Fierz}}\xi = \pm 2\gamma \text{Re}[|M_F|^2(C_S C_V^* + C'_S C'^*_V) + |M_{GT}|^2(C_T C_A^* + C'_T C'^*_A)] \quad (\text{C.5})$$

$$c_{\text{align}}\xi = |M_{GT}|^2 \Lambda_{JJ} \left[(|C_T|^2 - |C_A|^2 + |C'_T|^2 - |C'_A|^2) \pm 2\frac{\alpha Z m_e c^2}{p_\beta c} \text{Im}[C_T C_A^* + C'_T C'^*_A] \right] \quad (\text{C.6})$$

$$\begin{aligned}
A_\beta \xi &= 2 \lambda_{J'J} |M_{GT}|^2 \left[\pm \text{Re}[C_T C'_T - C_A C'_A] + \frac{\alpha Z m_e c^2}{p_\beta c} \text{Im}[C_T C'_A + C'_T C_A^*] \right] \\
&\quad + 2 \delta_{J'J} M_F M_{GT} \left(\frac{J}{J+1} \right)^{1/2} \left[\text{Re}[C_S C'_T + C'_S C_T^* - C_V C'_A - C'_V C_A^*] \right. \\
&\quad \left. \pm 2 \frac{\alpha Z m_e c^2}{p_\beta c} \text{Im}[C_S C'_A + C'_S C_A^* - C_V C'_T - C'_V C_T^*] \right] \tag{C.7}
\end{aligned}$$

$$\begin{aligned}
B_\nu \xi &= 2 |M_{GT}|^2 \lambda_{J'J} \text{Re} \left[\frac{\gamma m_e c^2}{E_\beta} (C_T C'_A + C'_T C_A^*) \pm (C_T C'_T + C_A C'_A) \right] \\
&\quad - \delta_{J'J} M_F M_{GT} \left(\frac{J}{J+1} \right)^{1/2} \text{Re} \left[(C_S C'_T + C'_S C_T^* + C_V C'_A + C'_V C_A^*) \right. \\
&\quad \left. \pm \frac{\gamma m_e c^2}{E_\beta} (C_S C'_A + C'_S C_A^* + C_V C'_T + C'_V C_T^*) \right] \tag{C.8}
\end{aligned}$$

$$\begin{aligned}
D_{\text{TR}} \xi &= 2 \delta_{J'J} M_F M_{GT} \left(\frac{J}{J+1} \right)^{1/2} \left[\text{Im}[C_S C_T^* - C_V C_A^* + C'_S C'_T - C'_V C'_A] \right. \\
&\quad \left. \mp \frac{\alpha Z m_e c^2}{p_\beta c} \text{Re}[C_S C_A^* - C_V C_T^* + C'_S C'_A - C'_V C'_T] \right] \tag{C.9}
\end{aligned}$$

In Eqs. C.3 - C.9, we have used $\gamma := (1 - \alpha^2 Z^2)^{1/2}$, and as usual, α is the fine structure constant. Here, M_F and M_{GT} are the Fermi and Gamow-Teller matrix elements, and are unique to the transition under consideration, while the C_X and C'_X (for $X = \{V, A, S, T\}$) are complex coupling constants describing the strength of vector, axial, scalar, and tensor couplings present in *all* charged weak force transitions. We also make use of the following shorthand definitions of $\lambda_{J'J}$, $\Lambda_{J'J}$, and $\delta_{J'J}$ for transitions with parent and daughter nuclear angular momenta given by J and J' respectively:

$$\lambda_{J'J} = \begin{cases} 1 & J' = J - 1 \\ \frac{1}{J+1} & J' = J \\ \frac{-J}{J+1} & J' = J + 1 \end{cases} \tag{C.10}$$

Somewhere I have to talk about what the primes and the imaginary parts mean. But maybe later. Also, we've just straight-up neglected pseudoscalars.

$$\Lambda_{J'J} = \begin{cases} 1 & J' = J - 1 \\ \frac{-(2J-1)}{J+1} & J' = J \\ \frac{J(2J-1)}{(J+1)(2J-3)} & J' = J + 1 \end{cases} \tag{C.11}$$

$$\delta_{J'J} = \begin{cases} 1 & J' = J \\ 0 & J' \neq J \end{cases} \quad (\text{C.12})$$

Note that Eq. C.1 depends on neutrino momentum, which we cannot observe directly. From an experimental standpoint, we also cannot reconstruct the the neutrino momenta with the available data, because we failed to measure the momenta of the daughters in conjunction with the tagged beta decay events with which we are primarily concerned in this thesis, so there is insufficient kinematic information available. From a theoretical standpoint, JTW has intentionally neglected recoil-order terms – meaning that the daughter nucleus is treated, for the purpose of kinetic energy calculations, as being infinitely massive, and as such it must have no change in kinetic energy from the decay–however the approximation still allows for it to undergo a change in momentum. One result of this approximation is that the neutrino energy, E_ν , is not a free variable within Eq. C.1, since the total amount of energy released is fixed for a given transition. The inherent inconsistencies of this approximation make it a tricky starting point for a description of neutrino and recoil kinematics.

It is fortunately possible to simplify Eq. (C.1) by integrating over all possible neutrino directions such that the resulting distribution no longer depends on parameters that are not observed. We take this as an opportunity to specialize the equations for β^+ decay transitions with $j = J' = \frac{3}{2}$. The result is:

$$\begin{aligned} d^3\Gamma = & \frac{2}{(2\pi)^4} F_-(Z, E_\beta) p_\beta E_\beta (E_0 - E_\beta)^2 dE_\beta d^2\hat{\Omega}_\beta \xi \\ & \times \left[1 + b_{\text{Fierz}} \frac{m_e c^2}{E_\beta} + A_\beta \left(\frac{\vec{J}}{J} \cdot \frac{\vec{p}_\beta}{E_\beta} \right) \right], \end{aligned} \quad (\text{C.13})$$

with the remaining parameters,

$$\begin{aligned}\xi &= |M_F|^2 (|C_S|^2 + |C_V|^2 + |C'_S|^2 + |C'_V|^2) \\ &\quad + |M_{GT}|^2 (|C_T|^2 + |C_A|^2 + |C'_T|^2 + |C'_A|^2)\end{aligned}\tag{C.14}$$

$$b_{\text{Fierz}} \xi = -2(1 - \alpha^2 Z^2)^{1/2} \operatorname{Re}[|M_F|^2 (C_S C_V^* + C'_S C_V'^*) + |M_{GT}|^2 (C_T C_A^* + C'_T C_A'^*)]\tag{C.15}$$

$$\begin{aligned}A_\beta \xi &= \frac{4}{5} |M_{GT}|^2 \left[\operatorname{Re}[C_A C_A'^* - C_T C_T'^*] + \frac{\alpha Z m_e c^2}{p_\beta c} \operatorname{Im}[C_T C_A'^* + C'_T C_A^*] \right] \\ &\quad + 2 \left(\frac{3}{5} \right)^{1/2} M_F M_{GT} \left[\operatorname{Re}[C_S C_T'^* + C'_S C_T^* - C_V C_A'^* - C'_V C_A^*] \right. \\ &\quad \left. - \frac{\alpha Z m_e c^2}{p_\beta c} \operatorname{Im}[C_S C_A'^* + C'_S C_A^* - C_V C_T'^* - C'_V C_T^*] \right]\end{aligned}\tag{C.16}$$

which is a great simplification on Eqs. (C.1)-(C.12). Note that JTW presents slightly different expressions for one component of A_β within [1] and [2], and the latter convention is what is adopted here.

I'm missing factors of c in this. Probably put them in.

We further require that both M_F and M_{GT} must be real, which can be done without loss of generality, however we do not require that they be positive, which would make the two conventions equivalent.

I don't think this is true...

There are a number of degrees of freedom left in the expressions that remain, and it is not immediately obvious how certain choices about these parameters might affect the physical results, or which approximations or assumptions ought to be made in order to arrive at a theory that matches the observational reality. This is in part a result of the fact that the theory behind JTW was developed before we had a detailed experimental understanding of much of the behaviour of beta decay, so all mathematically consistent behaviours are treated with roughly the same amount of consideration within the model.

Perhaps the most notable improvement to our understanding of Eqs. (C.13)-(C.16) is that the weak interaction arises predominantly from vector (C_V, C'_V) and axial-vector (C_A, C'_A) couplings, and the scalar and tensor couplings, if present at all, are comparatively small and must be relegated to the realm of precision measurements

to search for exotic physics. In particular,

$$\frac{|C_S|^2 + |C'_S|^2}{|C_V|^2 + |C'_V|^2} \ll 1 \quad (\text{C.17})$$

$$\frac{|C_T|^2 + |C'_T|^2}{|C_A|^2 + |C'_A|^2} \ll 1. \quad (\text{C.18})$$

Imaginary components of C_X and C'_X are associated with breaking of time-reversal symmetry for the transition. Since this effect has never been observed, it must be comparatively small if it is present, and so it follows that

$$\left| \frac{\text{Im}[C_X]}{\text{Re}[C_X]} \right| \ll 1 \quad (\text{C.19})$$

$$\left| \frac{\text{Im}[C'_X]}{\text{Re}[C'_X]} \right| \ll 1, \quad (\text{C.20})$$

which holds at least for the cases of $X = \{V, A\}$. There is comparatively little experimental information on how scalar and tensor interactions might behave with regard to time reversal, for the obvious reason that they have never been observed.

I think I made an even number of sign errors...

In order to obtain the correct, physically observed value for A_β , we require that the $M_F M_{GT}$ term in Eq. (C.7) have an overall positive value. Because we know that the scalar and tensor couplings must be small, and any imaginary contributions to the term must be small, we conclude that

$$M_F M_{GT} (C_V C'^*_A + C'_V C^*_A) < 0. \quad (\text{C.21})$$

More coulomb corrections in JTW notation: [60]. Also, an update to Falkowski's review article[7], which currently still lives on the arxiv, is here: [61].

JTWcoulomb to find sources that thought that S,T.

Also, $\xi = G_v^2 \cos \theta_C f_1(E)$.

C.2 Holstein Formalism

Probably the phrasing here is way too casual. Fix it.

Holstein [39] [59] generously provides explicit equations to match both Eq. (C.1) (i.e. Holstein's Eq. (51), where neutrino direction is a parameter of the probability

distribution) and Eq. (C.13) (Holstein's Eq. (52), where neutrino direction has already been integrated over).

Here's Holstein's Eq. (52):

$$\begin{aligned} d^3\Gamma_{\text{Holstein}} &= 2G_v^2 \cos^2 \theta_c \frac{F_{\mp}(Z, E_\beta)}{(2\pi)^4} p_\beta E_\beta (E_0 - E_\beta)^2 dE_\beta d^2\hat{\Omega}_\beta \\ &\times \left\{ F_0(E_\beta) + \Lambda_1 F_1(E_\beta) \hat{\mathbf{n}} \cdot \frac{\vec{p}_\beta}{E_\beta} + \Lambda_2 F_2(E_\beta) \left[\left(\hat{\mathbf{n}} \cdot \frac{\vec{p}_\beta}{E_\beta} \right)^2 - \frac{1}{3} \frac{p_\beta^2}{E_\beta^2} \right] \right. \\ &\left. + \Lambda_3 F_3(E_\beta) \left[\left(\hat{\mathbf{n}} \cdot \frac{\vec{p}_\beta}{E_\beta} \right)^3 - \frac{3}{5} \frac{p_\beta^2}{E_\beta^2} \hat{\mathbf{n}} \cdot \frac{\vec{p}_\beta}{E_\beta} \right] \right\} \end{aligned} \quad (\text{C.22})$$

A careful reader will eventually note that Holstein's spectral functions $F_i(E_\beta)$ are not the same as the $F_i(E_\beta, u, v, s)$ in any limit, despite the notational similarities. Among other rules, Holstein's spectral functions obey these:

$$F_i(E_\beta) \neq F_i(E_\beta, u, v, s) \quad (\text{C.23})$$

$$F_i(E_\beta) = H_i(E_\beta, u, v, 0) \quad (\text{C.24})$$

$$f_i(E_\beta) = F_i(E_\beta, u, v, 0). \quad (\text{C.25})$$

For the $F_i(E_\beta)$ functions of interest to us here, we find the following relationships:

$$\begin{aligned} F_0(E_\beta) &= H_0(E_\beta, J, J', 0) = F_1(E_\beta, J, J', 0) &= f_1(E_\beta) \\ F_1(E_\beta) &= H_1(E_\beta, J, J', 0) = F_4(E_\beta, J, J', 0) + \frac{1}{3} F_7(E_\beta, J, J', 0) &= f_4(E_\beta) + \frac{1}{3} f_7(E_\beta) \\ F_2(E_\beta) &= H_2(E_\beta, J, J', 0) = F_{10}(E_\beta, J, J', 0) + \frac{1}{2} F_{13}(E_\beta, J, J', 0) &= f_{10}(E_\beta) + \frac{1}{3} f_{13}(E_\beta) \\ F_3(E_\beta) &= H_3(E_\beta, J, J', 0) = F_{18}(E_\beta, J, J', 0) &= f_{18}(E_\beta). \end{aligned} \quad (\text{C.26})$$

Note that the $f_i(E_\beta)$ in Eq. C.26 are the same spectral functions used to describe a polarized decay spectrum when the neutrino (ie, the recoil) is also observed – though of course such a spectrum must have other terms as well. For the spectrum of interest to us here, in which the neutrino direction has already been integrated over, we can simply look up the $H_i(E_\beta, J, J', 0) = H_i(E, u, v, s=0)$ spectral functions, and leave it

at that. We find:

$$\begin{aligned}
F_0(E_\beta) = & |a_1|^2 + 2 \operatorname{Re}[a_1^* a_2] \frac{1}{3M^2} \left[m_e^2 + 4E_\beta E_0 + 2 \frac{m_e^2}{E_\beta} E_0 - 4E_\beta^2 \right] \\
& + |c_1|^2 + 2 \operatorname{Re}[c_1^* c_2] \frac{1}{9M^2} \left[11m_e^2 + 20E_\beta E_0 - 2 \frac{m_e^2}{E_\beta} E_0 - 20E_\beta^2 \right] \\
& - 2 \frac{E_0}{3M} \operatorname{Re}[c_1^*(c_1 + d \pm b)] + \frac{2E_\beta}{3M} (3|a_1|^2 + \operatorname{Re}[c_1^*(5c_1 \pm 2b)]) \\
& - \frac{m_e^2}{3ME_\beta} \operatorname{Re} \left[-3a_1^* e + c_1^* \left(2c_1 + d \pm 2b - h \frac{E_0 - E_\beta}{2M} \right) \right]
\end{aligned} \tag{C.27}$$

$$\begin{aligned}
F_1(E_\beta) = & \delta_{u,v} \left(\frac{u}{u+1} \right)^{1/2} \left\{ 2 \operatorname{Re} \left[a_1^* \left(c_1 - \frac{E_0}{3M}(c_1 + d \pm b) + \frac{E_\beta}{3M}(7c_1 \pm b + d) \right) \right] \right. \\
& + 2 \operatorname{Re}[a_1^* c_2 + c_1^* a_2] \left(\frac{4E_\beta(E_0 - E_\beta) + 3m_e^2}{3M^2} \right) \Big\} \\
& \mp \frac{(-1)^s \gamma_{u,v}}{u+1} \operatorname{Re} \left\{ c_1^* \left(c_1 + 2c_2 \left(\frac{8E_\beta(E_0 - E_\beta) + 3m_e^2}{3M^2} \right) - \frac{2E_0}{3M}(c_1 + d \pm b) \right. \right. \\
& \left. \left. + \frac{E_\beta}{3M}(11c_1 - d \pm 5b) \right) \right\} + \frac{\lambda_{u,v}}{u+1} \operatorname{Re} \left\{ c_1^* \left[-f \left(\frac{5E_\beta}{M} \right) \right. \right. \\
& \left. \left. + g \left(\frac{3}{2} \right)^{1/2} \left(\frac{E_0^2 - 11E_0E_\beta + 6m_e^2 + 4E_\beta^2}{6M^2} \right) \right] \right\} \pm 3j_2 \left(\frac{8E_\beta^2 - 5E_0E_\beta - 3m_e^2}{6M^2} \right)
\end{aligned} \tag{C.28}$$

$$\begin{aligned}
F_2(E_\beta) = & \theta_{u,v} \frac{E_\beta}{2M} \operatorname{Re} \left[c_1^* \left(c_1 + c_2 \frac{8(E_0 - E_\beta)}{3M} - d \pm b \right) \right] \\
& - \delta_{u,v} \frac{E_\beta}{M} \left[\frac{u(u+1)}{(2u-1)(2u+3)} \right]^{1/2} \operatorname{Re} \left\{ a_1^* \left(\left(\frac{3}{2} \right)^{1/2} f + g \frac{E_\beta + 2E_0}{4M} \right. \right. \\
& \left. \left. \pm \left(\frac{3}{2} \right)^{1/2} j_2 \frac{E_0 - E_\beta}{2M} \right) \right\} + (-1)^s \kappa_{u,v} \frac{E_\beta}{2M} \operatorname{Re} \left[c_1^* \left(\pm 3f \pm \left(\frac{3}{2} \right)^{1/2} g \frac{E_0 - E_\beta}{M} \right. \right. \\
& \left. \left. + 3j_2 \frac{E_0 - 2E_\beta}{2M} \right) \right] + \epsilon_{u,v} \operatorname{Re}[c_1^* j_3] \left(\frac{21E_\beta^2}{8M^2} \right)
\end{aligned} \tag{C.29}$$

$$\begin{aligned}
F_3(E_\beta) = & -\delta_{u,v} (3u^2 + 3u - 1) \left[\frac{u}{(u-1)(u+1)(u+2)(2u-1)(2u+3)} \right]^{1/2} \\
& \times \operatorname{Re}[a_1^* j_3] \left(\frac{E_\beta^2 \sqrt{15}}{4M^2} \right) + \frac{\rho_{u,v}}{u+1} \operatorname{Re} \left[c_1^* (g\sqrt{3} + j_2 \sqrt{2}) \left(\frac{5E_\beta^2}{4M^2} \right) \right] \\
& \pm \frac{(-1)^s \sigma_{u,v}}{u+1} \operatorname{Re}[c_1^* j_3] \left(\frac{5E_\beta^2}{2M^2} \right)
\end{aligned} \tag{C.30}$$

and we might really appreciate if these things could be simplified a bit.

The terms $a_1, a_2, b, c_1, c_2, d, e, f, g, h, j_2, j_3$ are “structure functions”. Holstein gives some predictions for their form, assuming the impulse approximation holds, in his Eq. (67). For the most part, the values and form of these structure functions are beyond the scope of this thesis, so I will not re-write them all here. It should be noted that the numerical values used for these parameters came from a private communication from Ian Towner to the collaboration. However, it is important to note the expressions for a_i and c_i , because these will directly come into play when we try to reconcile Holstein’s expression with JTW’s. Therefore,

$$a(q^2) \approx \frac{g_V(q^2)}{(1 + \frac{\Delta}{2M})} \left[M_F + \frac{1}{6}(q^2 - \Delta^2)M_{r^2} + \frac{1}{3}\Delta M_{\mathbf{r} \cdot \mathbf{p}} \right] \tag{C.31}$$

$$\begin{aligned}
c(q^2) \approx & \frac{g_A(q^2)}{(1 + \frac{\Delta}{2M})} \left[M_{GT} + \frac{1}{6}(q^2 - \Delta^2)M_{\sigma r^2} + \frac{1}{6\sqrt{10}}(2\Delta^2 + q^2)M_{1y} \right. \\
& \left. + A \frac{\Delta}{2M} M_{\sigma L} + \frac{1}{2}\Delta M_{\sigma rp} \right]
\end{aligned} \tag{C.32}$$

There was something wrong with this assumption. Something circular. I forgot.
Blah.

Somewhere I have to define q^2 and Δ are.

...where the M_{xxx} ’s are certain nuclear matrix elements. However, Eqs. (C.27–C.30) are not written in terms of $a(q^2)$ and $c(q^2)$, but rather in terms of a_1, a_2, c_1 , and c_2 . In fact, Holstein is implicitly using series expansions to remove the dependence on recoil momentum, so that

$$a(q^2) = a_1 + \left(\frac{q^2}{M^2} \right) a_2 + \dots \tag{C.33}$$

$$c(q^2) = c_1 + \left(\frac{q^2}{M^2} \right) c_2 + \dots \tag{C.34}$$

Should I just list the values of things that I inherited from Ian Towner’s personal communication that one time?

Next, Holstein goes and tweaks those $F_i(E_\beta)$ terms that we've already written out, by adding in an adjustment for Coulomb corrections. Those corrections have this form:

$$F_i(E_\beta) \rightarrow \tilde{F}_i(E_\beta) := F_{\mp}(Z, E_\beta) [F_i(E_\beta) + \Delta F_i(E_\beta)] \quad (\text{C.35})$$

To obtain expressions for the $\Delta F_i(E_\beta)$, Holstein invokes some Feynman diagrams and provides expressions for several integrals, all of which are both complex and complicated. The modified spectral functions are provided in terms of functions of these integrals. Since nobody wants to have to evaluate those integrals, Holstein makes a further approximation by taking only the first term in an expansion of the $\Delta F_i(E_\beta)$ in terms of $Z\alpha$, where $Z\alpha \ll 1$. Then, the resulting expressions for $\Delta F_i(E_\beta)$ can be written in terms of much more straightforward integrals over form factors for electric charge and weak charge.

If we make the further assumption that these form factors are identical, and that both types of charge are spread over a ball of uniform density with radius R , then we find:

$$X = Y = \frac{9\pi R}{140} \quad (\text{C.36})$$

and also, I think something like that the weak charge is the same distribution as the electric charge

in the Eqs. (C.37 - C.39) that follow.

Because Holstein doesn't actually write this stuff out in terms of $F_i(E_\beta)$, but rather in terms of $F_i(E_\beta, u, v, s)$, this correction presents yet another opportunity for the reader to interpret his notation incorrectly. We note that one must remember to make use of the relations in Eq. (C.26). Furthermore, Holstein notes that some of the terms $F_i(E_\beta, u, v, s)$ are suppressed already, and he does not consider those terms further. We will take this approximation to be adequate for our purposes here.

What is less clear, given the context in the paper, is whether or not when Holstein writes out his simplified expressions for $\Delta F_x(E_\beta, u, v, s)$ he actually means $F_{\mp}(Z, E_\beta)\Delta F_i(E_\beta, u, v, s)$. These terms are pretty small, so it probably doesn't *really* matter, but it would still be really nice to *know*, damn it.

So, we'll write out the functions for these corrections.

$$\begin{aligned} \Delta F_1(E_\beta, u, v, s) &= \mp \left(\frac{8\alpha Z}{3\pi} \right) X \left[E_\beta \left(8|a|^2 + \frac{28}{3}|c|^2 \right) + E_0 \left(|a|^2 - \frac{1}{3}|c|^2 \right) \right. \\ &\quad \left. + 3 \left(\frac{m_e c^2}{E_\beta} \right) (|a|^2 + |c|^2) \right] \end{aligned} \quad (\text{C.37})$$

$$\Delta F_4(E_\beta, u, v, s) = \mp \left(\frac{8\alpha Z}{3\pi} \right) 9XE_\beta \left[2\delta_{u,v} \left(\frac{u}{u+1} \right)^{1/2} \text{Re}[a^*c] \mp (-1)^s \left(\frac{\gamma_{u,v}}{u+1} \right) |c|^2 \right] \quad (\text{C.38})$$

$$\begin{aligned} \Delta F_7(E_\beta, u, v, s) = & \mp \left(\frac{8\alpha Z}{3\pi} \right) X (E_0 - E_\beta) \left[2\delta_{u,v} \left(\frac{u}{u+1} \right)^{1/2} \text{Re}[a^*c] \right. \\ & \left. \mp (-1)^s \left(\frac{\gamma_{u,v}}{u+1} \right) |c|^2 \right] \end{aligned} \quad (\text{C.39})$$

We note that the above corrections have been written in terms of $a(q^2)$ and $c(q^2)$, and we must use Eqs. (C.33, C.34) to put the results in terms of a_1 , a_2 , c_1 , and c_2 so that they can be correctly combined with Eqs. (C.27-C.30).

If we evaluate Holstein's Eqs. (B8), which I will absolutely not type out here, for the case $u = v = J = J' = 3/2$, we find the following values:

$$\begin{aligned} \delta_{u,v} &= 1 & \theta_{u,v} &= 1 & \rho_{u,v} &= \frac{-41}{40} \\ \gamma_{u,v} &= 1 & \kappa_{u,v} &= \frac{1}{2\sqrt{2}} & \sigma_{u,v} &= \frac{-41}{4\sqrt{35}} \\ \lambda_{u,v} &= \frac{-\sqrt{2}}{5} & \epsilon_{u,v} &= \frac{-1}{2\sqrt{5}} & \phi_{u,v} &= 0 \end{aligned} \quad (\text{C.40})$$

Furthermore, in our calculations here, we will be considering only the β^+ decay modes, and therefore we take the *lower* sign when the option arises. We also will use $s = 0$, so that $(-1)^s = +1$.

Also, pretty sure one of those never gets used. Which one was it? idk.

We proceed by defining some notational conventions. Firstly,

$$\text{Holstein's } \hat{n} = \text{JTW's } \mathbf{j}, \quad (\text{C.41})$$

and the Λ_i are given by Holstein's Eq. (48):

$$\Lambda_1 := \frac{\langle M \rangle}{J} \quad (C.42)$$

$$\Lambda_2 := 1 - \frac{3\langle M^2 \rangle}{J(J+1)} \quad (C.43)$$

$$\Lambda_3 := \frac{\langle M \rangle}{J} - \frac{5\langle M^3 \rangle}{J(3J^2 + 3J - 1)}. \quad (C.44)$$

It can be immediately seen that Holstein's Λ_1 is closely related to JTW's $\frac{\vec{J}}{J}$, and Holstein's Λ_2 is closely related to JTW's T_{align} . JTW has no equivalent to Λ_3 . We find:

$$\Lambda_1 \hat{\mathbf{j}} = \frac{\langle M \rangle}{J} \hat{\mathbf{j}} = \frac{\vec{\mathbf{J}}}{J} \quad (C.45)$$

$$\Lambda_2 = T_{\text{align}} \frac{(2J-1)}{(J+1)}. \quad (C.46)$$

Note: It's not the case that $|\vec{\mathbf{J}}| == J$. It's actually super fucking infuriating notation.

C.3 Qualitative Parameter Descriptions and Convention Compatibility

Appendix D

Comparing Notation between Holstein and JTW

This section provides several equations and tables intended to be used as a quick reference for comparing differences in notation, sign convention, and normalization between two different descriptions of the beta decay probability distribution.

The following equations provide a term-by-term comparison between the Holstein and JTW conventions, intentionally neglecting ROC terms.

$$\xi = G_v^2 \cos \theta_C f_1(E) \quad (\text{D.1})$$

$$a_{\beta\nu} = f_2(E) / f_1(E) \quad (\text{D.2})$$

$$\frac{\langle \vec{J} \rangle}{J} \cdot \frac{\vec{p}}{E} A_\beta = \Lambda_1 \hat{n} \cdot \frac{\vec{p}}{E} f_4(E) / f_1(E) \quad (\text{D.3})$$

$$\frac{\langle \vec{J} \rangle}{J} \cdot \frac{\vec{p}_\nu}{E_\nu} B_\nu = \Lambda_1 \hat{n} \cdot \vec{k} f_6(E) / f_1(E) \quad (\text{D.4})$$

$$\frac{\langle \vec{J} \rangle}{J} \cdot \frac{(\vec{p} \times \vec{p}_\nu)}{EE_\nu} D_{\text{TR}} = \Lambda_1 \hat{n} \cdot \left(\frac{\vec{p}}{E} \times \hat{k} \right) f_8(E) / f_1(E) \quad (\text{D.5})$$

$$\begin{aligned} & \left[\frac{J(J+1) - 3\langle (\vec{J} \cdot \hat{j})^2 \rangle}{J(2J-1)} \right] \left[\frac{1}{3} \frac{\vec{p} \cdot \vec{p}_\nu}{EE_\nu} - \frac{(\vec{p} \cdot \hat{j})(\vec{p}_\nu \cdot \hat{j})}{EE_\nu} \right] c_{\text{align}} \\ &= \Lambda_2 \left[(\hat{n} \cdot \frac{\vec{p}}{E})(\hat{n} \cdot \hat{k}) - \frac{1}{3} (\frac{\vec{p}}{E} \cdot \hat{k}) \right] f_{12}(E) / f_1(E) \end{aligned} \quad (\text{D.6})$$

Holstein	JTW	Thesis	Comments
k			Neutrino momentum 4-vector
	E_ν		Neutrino energy
\hat{k}	$\frac{\mathbf{p}_\nu}{E_\nu}$		3D Neutrino emission direction unit vector. Neutrinos are always treated as massless.
p			Beta momentum 4-vector, or sometimes the magnitude of the beta momentum 3-vector. Never the magnitude of the 4-vector.
E	E_e	E_β	Beta energy
\mathbf{p}	\mathbf{p}_e	\vec{p}_β	Beta momentum 3-vector
q			Recoil momentum 4-vector, or sometimes a magnitude.

Table D.1: A comparison of some kinematic terms in JTW [1] [2] and Holstein [39][59]. Bolding/italicization carries meaning.

Holstein	JTW	Comments
u	J	Initial state total nuclear angular momentum.
v	J'	Final state total nuclear angular momentum.
s	No equivalent	

Is it *really* true that there's no equivalent?? I think it must be, since it's an allowed approximation thing. I think.

Table D.2: A comparison of some angular momenta in JTW [1] [2] and Holstein [39][59].

Holstein	JTW	Thesis	Comments
$G_v^2 \cos \theta_C f_1(E)$	ξ	$\xi(E_\beta)$	Normalization. Proportional to the fractional decay rate.
\hat{n}	\mathbf{j}	$\hat{\mathbf{j}}$	Nuclear polarization unit vector. Also the axis of quantization.
J	J		Total nuclear angular momentum quantum number
$\langle M \rangle$	$ \langle \mathbf{J} \rangle $		Angular momentum projection along the axis of quantization
$\Lambda^{(1)} \hat{n} = \frac{\langle M \rangle}{J} \hat{n}$	$\frac{\langle \mathbf{J} \rangle}{J}$	$\Lambda_1 \hat{\mathbf{n}}$	Dipole element vector. Proportional to nuclear polarization.
$\Lambda^{(2)}$	$\frac{J(J+1)-3\langle(\vec{\mathbf{J}} \cdot \hat{\mathbf{j}})^2\rangle}{J(2J-1)} \frac{(2J-1)}{(J+1)}$	$T_{\text{align}}(\vec{\mathbf{J}}) \frac{(2J-1)}{(J+1)}$	Quadrupole element
$\Lambda^{(3)}$	No equivalent	Λ_3	Octopole element
$\Lambda^{(4)}$	No equivalent	Λ_4	Hexadecapole element

Table D.3: A comparison of terms relating to multipole elements and their normalizations in JTW [1] [2] and Holstein [39] [59].

Term	Integral
$f_1(E_\beta)$	$\leftrightarrow \int 1 d\hat{\Omega}_k = 4\pi$
$f_2(E_\beta)$	$\leftrightarrow \int \left(\frac{\vec{p}_\beta \cdot \hat{k}}{E_\beta} \right) d\hat{\Omega}_k = 0$
$f_3(E_\beta)$	$\leftrightarrow \int \left(\left(\frac{\vec{p}_\beta \cdot \hat{k}}{E_\beta} \right)^2 - \frac{1}{3} \frac{p_\beta^2}{E_\beta^2} \right) d\hat{\Omega}_k = 0$
$f_4(E_\beta)$	$\leftrightarrow \int \left(\hat{n} \cdot \frac{\vec{p}_\beta}{E_\beta} \right) d\hat{\Omega}_k = 4\pi \left(\hat{n} \cdot \frac{\vec{p}_\beta}{E_\beta} \right)$
$f_5(E_\beta)$	$\leftrightarrow \int \left(\hat{n} \cdot \frac{\vec{p}_\beta}{E_\beta} \right) \left(\frac{\vec{p}_\beta \cdot \hat{k}}{E_\beta} \right) d\hat{\Omega}_k = 0$
$f_6(E_\beta)$	$\leftrightarrow \int \left(\hat{n} \cdot \hat{k} \right) d\hat{\Omega}_k = 0$
$f_7(E_\beta)$	$\leftrightarrow \int \left(\hat{n} \cdot \hat{k} \right) \left(\frac{\vec{p}_\beta \cdot \hat{k}}{E_\beta} \right) d\hat{\Omega}_k = \frac{1}{3} 4\pi \left(\hat{n} \cdot \frac{\vec{p}_\beta}{E_\beta} \right)$
$f_8(E_\beta)$	$\leftrightarrow \int \hat{n} \cdot \left(\frac{\vec{p}_\beta \times \hat{k}}{E_\beta} \right) d\hat{\Omega}_k = 0$
$f_9(E_\beta)$	$\leftrightarrow \int \hat{n} \cdot \left(\frac{\vec{p}_\beta \times \hat{k}}{E_\beta} \right) \left(\frac{\vec{p}_\beta \cdot \hat{k}}{E_\beta} \right) d\hat{\Omega}_k = 0$
$f_{10}(E_\beta)$	$\leftrightarrow \int T_2(\hat{n}) : \left[\frac{\vec{p}_\beta}{E}, \frac{\vec{p}_\beta}{E} \right] d\hat{\Omega}_k = 4\pi T_2(\hat{n}) : \left[\frac{\vec{p}_\beta}{E}, \frac{\vec{p}_\beta}{E} \right]$
$f_{11}(E_\beta)$	$\leftrightarrow \int T_2(\hat{n}) : \left[\frac{\vec{p}_\beta}{E}, \frac{\vec{p}_\beta}{E} \right] \left(\frac{\vec{p}_\beta \cdot \hat{k}}{E} \right) d\hat{\Omega}_k = 0$
$f_{12}(E_\beta)$	$\leftrightarrow \int T_2(\hat{n}) : \left[\frac{\vec{p}_\beta}{E}, \hat{k} \right] d\hat{\Omega}_k = 0$
$f_{13}(E_\beta)$	$\leftrightarrow \int T_2(\hat{n}) : \left[\frac{\vec{p}_\beta}{E}, \hat{k} \right] \left(\frac{\vec{p}_\beta \cdot \hat{k}}{E} \right) d\hat{\Omega}_k = \frac{1}{3} 4\pi T_2(\hat{n}) : \left[\frac{\vec{p}_\beta}{E}, \frac{\vec{p}_\beta}{E} \right]$
$f_{14}(E_\beta)$	$\leftrightarrow \int T_2(\hat{n}) : \left[\hat{k}, \hat{k} \right] d\hat{\Omega}_k = 0$
$f_{15}(E_\beta)$	$\leftrightarrow \int T_2(\hat{n}) : \left[\hat{k}, \hat{k} \right] \left(\frac{\vec{p}_\beta \cdot \hat{k}}{E} \right) d\hat{\Omega}_k = 0$
$f_{16}(E_\beta)$	$\leftrightarrow \int T_2(\hat{n}) : \left[\frac{\vec{p}_\beta}{E}, \frac{\vec{p}_\beta}{E} \times \hat{k} \right] d\hat{\Omega}_k = 0$
$f_{17}(E_\beta)$	$\leftrightarrow \int T_2(\hat{n}) : \left[\hat{k}, \frac{\vec{p}_\beta}{E} \times \hat{k} \right] d\hat{\Omega}_k = 0$
$f_{18}(E_\beta)$	$\leftrightarrow \int T_3(\hat{n}) : \left[\frac{\vec{p}_\beta}{E}, \frac{\vec{p}_\beta}{E}, \frac{\vec{p}_\beta}{E} \right] d\hat{\Omega}_k = 4\pi T_3(\hat{n}) : \left[\frac{\vec{p}_\beta}{E}, \frac{\vec{p}_\beta}{E}, \frac{\vec{p}_\beta}{E} \right]$

Table D.4: Integrals of terms from Holstein's Eq. (51) [39] [59].

Appendix E

Derivation of the b_{Fierz} Dependence of the Superratio Asymmetry

Recall the integrated JTW probability distribution for outgoing beta particles from Eq. (C.13):

$$\begin{aligned} d^3\Gamma(E_\beta, \hat{\Omega}_\beta) dE_\beta d^2\hat{\Omega}_\beta &= \frac{2}{(2\pi)^4} F_{\mp}(Z, E_\beta) \xi p_\beta E_\beta (E_0 - E_\beta)^2 dE_\beta d^2\hat{\Omega}_\beta \\ &\times \left[1 + b_{\text{Fierz}} \frac{m_e c^2}{E_\beta} + A_\beta \left(\frac{\vec{J}}{J} \cdot \frac{\vec{p}_\beta}{E_\beta} \right) \right]. \end{aligned} \quad (\text{E.1})$$

We note that the only angular dependence remaining in this equation is the dot product between the direction of beta emission and the direction of nuclear spin-polarization. This allows us to pull out a further factor of 2π by choosing the axis of polarization as defining our coordinate system, and integrating over the “ ϕ_β ” coordinate. The result is a bit more friendly to work with:

$$d^2\Gamma(E_\beta, \theta) dE_\beta d\theta = W(E_\beta) \left[1 + b_{\text{Fierz}} \frac{m_e c^2}{E_\beta} + A_\beta \frac{v_\beta}{c} |\vec{P}| \cos \theta \right] dE_\beta d\theta, \quad (\text{E.2})$$

where θ is the angle between the beta emission direction and the polarization direction, and is the only angular dependence that remains. Here, we have grouped the overall energy dependence into $W(E_\beta)$, so that

$$W(E_\beta) = \frac{2}{(2\pi)^3} F_{\mp}(Z, E_\beta) \xi p_\beta E_\beta (E_0 - E_\beta)^2, \quad (\text{E.3})$$

where we note that the Fermi functions in the above make Eq. E.3 integrable only by numerical methods. Because it would be difficult to make this expression *more* challenging to work with, it is therefore easy enough to include in this expression any small corrections to overall energy dependence that might arise from e.g. recoil-order corrections, as described by Holstein [39].

In the TRINAT geometry with two polarization states (+/-) and two detectors (T/B) aligned along the axis of polarization, we are able to describe four different count rates, with different combinations of polarization states and detectors. Thus, neglecting beta scattering effects, we have:

$$r_{T+}(E_\beta) = W(E_\beta)\varepsilon_T(E_\beta)\Omega_T N_+ \left[1 + b_{\text{Fierz}} \frac{m_e c^2}{E_\beta} + A_\beta \frac{v}{c} |\vec{P}_+| \langle \cos \theta \rangle_{T+} \right] \quad (\text{E.4})$$

$$r_{B+}(E_\beta) = W(E_\beta)\varepsilon_B(E_\beta)\Omega_B N_+ \left[1 + b_{\text{Fierz}} \frac{m_e c^2}{E_\beta} + A_\beta \frac{v}{c} |\vec{P}_+| \langle \cos \theta \rangle_{B+} \right] \quad (\text{E.5})$$

$$r_{T-}(E_\beta) = W(E_\beta)\varepsilon_T(E_\beta)\Omega_T N_- \left[1 + b_{\text{Fierz}} \frac{m_e c^2}{E_\beta} + A_\beta \frac{v}{c} |\vec{P}_-| \langle \cos \theta \rangle_{T-} \right] \quad (\text{E.6})$$

$$r_{B-}(E_\beta) = W(E_\beta)\varepsilon_B(E_\beta)\Omega_B N_- \left[1 + b_{\text{Fierz}} \frac{m_e c^2}{E_\beta} + A_\beta \frac{v}{c} |\vec{P}_-| \langle \cos \theta \rangle_{B-} \right], \quad (\text{E.7})$$

where $\varepsilon_{T/B}(E_\beta)$ are the (top/bottom) detector efficiencies, $\Omega_{T/B}$ are the fractional solid angles for the (top/bottom) detector from the trap position, $N_{+/-}$ are the number of atoms trapped in each (+/-) polarization state, and $|\vec{P}_{+/-}|$ are the magnitudes of the polarization along the detector axis for each polarization state. $\langle \cos \theta \rangle_{T/B,+/-}$ is the average of $\cos \theta$ for *observed* outgoing betas, for each detector and polarization state combination. This latter term is approximately ± 1 as a result of our detector geometry, but contains important sign information. For a pointlike trap in the center of the chamber, 103.484 mm from either (DSSSD) detector, each of which is taken to be circular with a radius of 15.5 mm, we find that $\langle |\cos \theta| \rangle_{T/B,+/-} \approx 0.994484$, and is the same for all four cases. Note that a horizontally displaced trap will decrease the magnitude of $\langle |\cos \theta| \rangle$, but as it is an expectation value of an absolute value, all four will remain equal to one another. In the case of a vertically displaced trap, these four values will no longer all be equal, however it will still be the case that $\langle |\cos \theta| \rangle_{T+} = \langle |\cos \theta| \rangle_{T-}$, and $\langle |\cos \theta| \rangle_{B+} = \langle |\cos \theta| \rangle_{B-}$.

In the case of the present experiment, we note that $|\vec{P}_+| = |\vec{P}_-|$ is correct to a high degree of precision.

Does this even agree with whatever I wrote about the geometry in the other section?

Not quite true. Some strips are missing.

This is only true if we neglect (back-)scatter. This is not actually a good approximation. But we have pretty good simulations to give us the real numbers, anyway.

Is that definitely true, or is it only true to lowest order?

We define the ‘superratio’, s , to be:

$$s = s(E_\beta) := \frac{r_{T+} r_{B-}}{r_{T-} r_{B+}}, \quad (\text{E.8})$$

and the ‘superratio asymmetry’, A_{super} , as

$$A_{\text{super}} = A_{\text{super}}(E_\beta) := \frac{1 - \sqrt{s}}{1 + \sqrt{s}} \quad (\text{E.9})$$

$$= \frac{\sqrt{r_{T-} r_{B+}} - \sqrt{r_{T+} r_{B-}}}{\sqrt{r_{T-} r_{B+}} + \sqrt{r_{T+} r_{B-}}} \quad (\text{E.10})$$

This is explicitly an experimental quantity that is measured directly by the above combination of count rates, however it is obvious that it reduces, under appropriate limits, to be equivalent to a naive asymmetry. In particular, if we require that the physical conditions and relative detector positions and sensitivities are identical when the polarization is flipped, then we have $r_{T+}(E_\beta) = r_{B-}(E_\beta)$ and $r_{T-}(E_\beta) = r_{B+}(E_\beta)$. It follows that we can simplify the superratio asymmetry into a more intuitive quantity that we might use for a measurement with only a single polarization state, e.g.,

$$A_{\text{super},+} \rightarrow \frac{r_T - r_B}{r_T + r_B}. \quad (\text{E.11})$$

While Eq. E.11 is conceptually encouraging, the assumptions that gave rise to that expression are too simplifying. We will introduce some more limited assumptions for what follows, along with shorthand notation for improved readability. First, we require that the magnitude of the polarization vector is the same for both polarization states, and also that the average of the magnitude of $\cos \theta$ for a given detector does not change when the polarization is flipped (equivalent to a requirement that the trap position doesn’t change when the polarization is flipped). Then:

$$P := |\vec{P}_+| = |\vec{P}_-| \quad (\text{E.12})$$

$$\langle |\cos \theta| \rangle_T := \langle |\cos \theta| \rangle_{T+} = \langle |\cos \theta| \rangle_{T-} \quad (\text{E.13})$$

$$\langle |\cos \theta| \rangle_B := \langle |\cos \theta| \rangle_{B+} = \langle |\cos \theta| \rangle_{B-}, \quad (\text{E.14})$$

and we can further define

$$c = \langle |\cos \theta| \rangle := \frac{1}{2} (\langle |\cos \theta| \rangle_T + \langle |\cos \theta| \rangle_B) \quad (\text{E.15})$$

$$\Delta c = \Delta \langle |\cos \theta| \rangle := \frac{1}{2} (\langle |\cos \theta| \rangle_T - \langle |\cos \theta| \rangle_B) \quad (\text{E.16})$$

and

$$\tilde{A} = \tilde{A}(E_\beta) := A_\beta \frac{v}{c} \quad (\text{E.17})$$

$$\tilde{b} = \tilde{b}(E_\beta) := b_{\text{Fierz}} \frac{mc^2}{E_\beta}, \quad (\text{E.18})$$

$$\tilde{r} = \tilde{r}(E_\beta) := 1 + \tilde{b}. \quad (\text{E.19})$$

With this new set of variables defined, we can re-write Eqs. (E.4-E.7) as

$$r_{T+}(E_\beta) = W(E_\beta) \varepsilon_T(E_\beta) \Omega_T N_+ [\tilde{r} + \tilde{A}P(c + \Delta c)] \quad (\text{E.20})$$

$$r_{B+}(E_\beta) = W(E_\beta) \varepsilon_B(E_\beta) \Omega_B N_+ [\tilde{r} - \tilde{A}P(c - \Delta c)] \quad (\text{E.21})$$

$$r_{T-}(E_\beta) = W(E_\beta) \varepsilon_T(E_\beta) \Omega_T N_- [\tilde{r} - \tilde{A}P(c + \Delta c)] \quad (\text{E.22})$$

$$r_{B-}(E_\beta) = W(E_\beta) \varepsilon_B(E_\beta) \Omega_B N_- [\tilde{r} + \tilde{A}P(c - \Delta c)], \quad (\text{E.23})$$

and the superratio becomes

$$s = \frac{(\tilde{r} + \tilde{A}Pc)^2 - (\Delta c)^2}{(\tilde{r} - \tilde{A}Pc)^2 - (\Delta c)^2} \quad (\text{E.24})$$

where all factors of $W(E_\beta)$, $\varepsilon_{T/B}(E_\beta)$, $\Omega_{T/B}$, and $N_{+/}$ have been cancelled out entirely.

For simplicity we take $\Delta c = 0$ in what follows. Although this is not strictly accurate within the present experiment, this assumption greatly simplifies the expressions that follow. Then, absent other corrections (*e.g.* backscattering, unpolarized background, ...), it is clear that if $\tilde{b} = 0$ as in the Standard Model,

$$A_{\text{super}} = \tilde{A}Pc = A_\beta \frac{v}{c} |\vec{P}| \langle |\cos \theta| \rangle \quad (\text{E.25})$$

In the case where $\tilde{b} \neq 0$, we find that

$$A_{\text{super}} = \frac{\tilde{A}Pc}{1 + \tilde{b}} \quad (\text{E.26})$$

$$\approx \tilde{A}Pc(1 - \tilde{b} + \tilde{b}^2), \quad (\text{E.27})$$

where we have utilized the assumption that $\tilde{b} \ll 1$. Thus, to leading order in terms of \tilde{b} ,

$$A_{\text{super}} \approx A_\beta \frac{v}{c} |\vec{P}| \langle |\cos \theta| \rangle \left(1 - b_{\text{Fierz}} \frac{mc^2}{E_\beta} \right). \quad (\text{E.28})$$